THE ONSET OF FREE CONVECTIVE FLOW PATTERNS AND THEIR EFFECTS ON THE HEAT TRANSFER IN ANNULAR FLUID LAYERS

A Thesis

Presented to

the Faculty of the Graduate School

The University of Manitoba

In Partial Fulfillment

of the Requirements for the Degree

Master of Science in Engineering

---

by

Harvey Dale Pettapiece

March 1969

ABSTRACT

This work was undertaken to observe the onset of free-convective fluid flow in annular spaces and to study its effect on the heat flow. The study was concerned with examining the affect of the fluid-layer thickness to length ratios and the attitude of the layer on the point at which convection starts.

The apparatus consisted of two concentric cylinders. The layer thickness was varied by using outer cylinders of different diameters. The thickness to length ratios used were 124 and 280. Tests were conducted with the annular axis in the horizontal, vertical and 45 degree positions to determine the affects on the onset of free convection. Glycerine was used for most of the studies but supporting work was carried out with water and air.

A temperature gradient was induced across the annular fluid layer by heat from an electrical heater in the inner cylinder. Motion was detected by visual observation of aluminum dust particles and polystyrene beads. Recommendations for dimensionless parameters suitable for specifying the onset of free convection were made, but the accuracy was not intended to be sufficient for an exact evaluation of the heat transfer and therefore only preliminary observation of the general trends were made.

ACKNOWLEDGEMENTS

The author wishes to express his sincere thanks to Professor R. E. Chant, my advisor, for his guidance and encouragement throughout the project. Also, the auther is indebted to the technicians in the Department of Mechanical Engineering for their time and suggestions.

TABLE OF CONTENTS

PAGE

LIST OF FIGURES

LIST OF TABLES

NOMENCLATURE

SYMBOL	DEFINITION
A	Cross-sectional area
c_p	Constant pressure specific heat
d	Characteristic length
D_o	Outer cylinder diameter
D_i	Inner cylinder diameter
g_c	Local acceleration of gravity
H	Length of fluid layer
h	Coefficient of heat transfer between a surface and a fluid
I	Electrical current (Amperes)
K	Thermal conductivity of fluid
Ke	Equivalent thermal conductivity
L	Thickness of fluid layer (dimension in the direction of heat flow)
Q	Heat flow
t_o	Surface temperature of outer cylinder
t_i	Surface temperature of inner cylinder
t	Temperature at any point
T	Time
U	Velocity component parallel to the x-axis
V	Electrical potential (Volts)
Z	Fluid property $\equiv \frac{g_c \beta}{\nu^2} \times \frac{\mu c_p}{K}$
N_{GR}	Grashof number $\equiv \frac{g_c \beta \Delta t\, d^3}{\nu^2}$
N_{GRL}	Grashof number (based on layer thickness)
N_{NU}	Nusselt number $\equiv hd/K$

SYMBOL	DEFINITION
N_{PR}	Prandtl number
N_{RAY}	Rayleigh number $\equiv N_{GR} \times N_{PR}$

GREEK SYMBOLS

α	Coefficient of thermal diffusivity
β	Coefficient of volumetric expansion
ϵ	Emissivity
γ	Constant of proportionality
ϕ	Constant of proportionality
Δt	Temperature difference across fluid layer
δ	Boundary-layer thickness
θ	Dimensionless temperature ratio
μ	Dynamic viscosity
ν	Kinematic viscosity
ρ	Fluid density
ω	Error function
λ	Dimensionless number
Π	Dimensionless number
σ	Stefan-Boltzmann constant

SUBSCRIPTS

C	Concentric
E	Eccentric
i	Inner
L	Large

SYMBOL	DEFINITION
M	Mean
o	Outer
r	Radiation
S	Small

THE ONSET OF FREE CONVECTIVE FLOW PATTERNS AND THEIR EFFECTS ON THE HEAT TRANSFER IN ANNULAR FLUID LAYERS

INTRODUCTION

1.1 General Introduction

The use of fluid layers for insulating purposes has been a long established engineering practice. Heat is transferred by conduction alone until some critical condition, which is often referred to as the convection point, is reached. At this point the fluid begins to circulate and some additional heat is transferred by free convection. The criteria for this point is very important in order to ensure that the maximum insulating effect is being achieved.

The approach, that has been established over the years, for calculating the transfer of heat from a surface to a fluid whether by free or forced convection has been to express the heat transfer in terms of the Nusselt number, hd/K. Thus for any convective heat transfer calculation, the fluid thermal conductivity must be known and since to date theoretical calculations of thermal conductivity have been unreliable it must be determined experimentally. Any experimental measurement of the thermal conductivity of a fluid must eliminate convection heat transfer; therefore, the convection point for the apparatus must be ascertained.

The University of Manitoba Mechanical Engineering Department uses a constant heat flux across an annular layer to measure thermal conductivity.

This experimental investigation was done to find the point at which the fluid could be expected to move via free convection in the previously mentioned apparatus and also to find the effect of various inclinations. This point, the convection point, was determined by visual inspection and the flow patterns noted. Also, since this point is seen in the heat transfer measurements, it was indirectly checked by doing a heat balance. The apparatus was an enlargement on the conductivity cell used by the University of Manitoba with emphasis on visual flow inspection with only a preliminary design for heat transfer measurements.

1.2 Nature of Free Convection

When a fluid is being heated by contact with a hotter surface it becomes lighter and is displaced upward by the pressure of the surrounding denser fluid, carrying away heat in the stream of warm fluid or "convection currents" thus produced. If the surface is colder than the fluid the reverse is true, but the same laws apply in either case. This motion is called free convection. The extent of the motion and thus of the heat transfer is a function of the fluid properties and the temperature gradients. These quantities have been grouped together to form a dimensionless number called the Rayleigh number.

Free convection motion can be divided into different classifications depending upon its flow patterns. When the motion is uniform with no mixing, the movement is called laminar flow. In this regime, the heat transfer appears to be a function of the 1/4 power of the Rayleigh number, N_{RAY}. As the N_{RAY} increases a transition zone appears which extends over a relatively long range. A

further increase in N_{RAY} brings a new regime characterized by a a completely disorderly pattern which is constantly shifting. This movement is called turbulent flow and the corresponding heat transfer appears to be a function of the 1/3 power of N_{RAY}.

In this work the velocities are extremely small. Some investigators have given this a special classification[1*] of its own even though it does resemble the laminar region in most respects. Because the heat transfer is so closely connected to the flow modes, heat transfer regimes can be classified by specific flow patterns. Eckert and Carlson[2] classified the low velocity regimes by temperature considerations, as the conduction regime and as the thermal boundary layer regime; each regime having a definite flow pattern and definite temperature distribution.

The rate at which heat is transferred by free convection between a fluid and a solid surface is indicated by the convective film coefficient, h. When two surfaces are close to each other (the boundary layer is no longer small in comparison with the dimensions of the fluid space) the development of the flow is often strongly influenced by the shape of the boundaries and the problem is quite different from that of free convection. The process of heat transfer includes radiation between the two surfaces and conduction through the fluid layer. The extent to which radiation and conduction affect the total rate of heat transfer between the two surfaces depends upon their temperatures, the width of the fluid space, and other factors[3]. W. J. King[4] states, that if the fluid is a liquid, the convection currents normally dissipate all of the heat

---

* See Bibliography

lost by the surface, but if it is a gas the exchange of radiant heat between the two surfaces must be taken into account.

Since the heat flow is based on the combined rate of heat transfer by conduction, convection, and radiation, some investigators use a term called the apparent thermal conductivity, defined by the conductive heat transfer that is applicable to the geometry. Mull and Reiher[5] used an equivalent thermal conductivity, Ke, which combined the effect of convection and radiation.

The transition from conduction to convection, that is the convection point, is followed by an abrupt increase in the apparent thermal conductivity due to the added heat transferred by convection.

THEORETICAL CONSIDERATIONS AND LITERATURE REVIEW OF FREE CONVECTION IN ENCLOSED SPACES

2.1 Convection Flow Patterns and Flow Instability Point

Convection flow patterns will be discussed under two main headings: geometry, that is plane layers and annular layers; and layer orientation, that is vertical or horizontal. The fundamental equations of fluid motion for all theoretical analysis begins with a differential element, Figure 1, and are the following:

1. Continuity equation derived from the conservation of mass on an elemental volume

$$0 = \frac{\partial \rho}{\partial T} + \frac{\partial(\rho V)}{\partial Y} + \frac{\partial(\rho u)}{\partial X} + \frac{\partial(\rho w)}{\partial Z}$$

2. Navier-Stokes equation derived from the conservation of momentum on an elemental volume

$$\frac{\partial u}{\partial T} + \frac{u\partial u}{\partial X} + \frac{v\partial u}{\partial Y} + \frac{w\partial u}{\partial Z} = -\frac{1}{\rho}\frac{\partial P}{\partial X} + g_c\left(\frac{\rho-\rho_0}{\rho_0}\right) + \nu\left(\frac{\partial^2 u}{\partial X^2} + \frac{\partial^2 u}{\partial Y^2} + \frac{\partial^2 u}{\partial Z^2}\right)$$

with similar equations for the y and z directions.

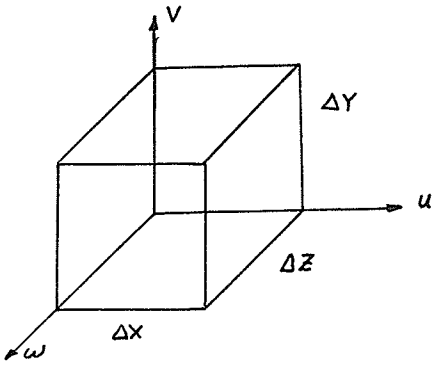

FIGURE 1 Differential Element

3. Heat balance of the elemental volume

$$\frac{1}{\alpha}\left[\frac{\partial t}{\partial T} + \frac{u\partial t}{\partial x} + v\frac{\partial t}{\partial Y} + w\frac{\partial t}{\partial z}\right] = \frac{\partial^2 t}{\partial X^2} + \frac{\partial^2 t}{\partial y^2} + \frac{\partial^2 t}{\partial Z^2}$$

This equation is developed from an energy balance on the differential element, Figure 1, and is thus a three-dimensional case because the energy flow has been accounted for in the X, Y, and Z directions. Internal heat generation has been neglected because it is not applicable in this case and the equation has been further simplified by assuming that the thermal conductivity is uniform throughout the system; that is, the material is assumed to be homogeneous.

Because an exact solution using these equations is difficult without making more simplifying assumptions the usual practice is to use logical grouping of the governing factors into dimensionless parameters. The most important parameter is the Grashof number, N_{GR}. It represents the ratio of the buoyancy and inertia forces to the viscous or drag forces. The other very important dimensionless parameter is the Prandtl number, N_{PR}. This parameter is a measure of the molecular diffusivity of momentum to the molecular diffusivity of heat and is therefore a function of fluid properties only. There are many more parameters applicable to natural convection fluid flow and heat transfer, but in general they contain the same terms that are expressed in the Grashof and Prandtl numbers.

In order to prevent confusion arising from the term convection point pertaining to both the heat flow and the fluid flow, the following discussion on fluid flow will use the analogous term 'instability point' in lieu of the fluid convection point.

Horizontal Plane Layers Heated From Below

The earliest and the most extensive study of the convection point or point of thermal instability was done on horizontal layers heated from below. In 1901, Benard observed a clearly defined flow pattern at the onset of free convective flow. This cellular motion, now called Benard cells, circulated in hexagonal prisms with the warmer liquid ascending at the middle and the cooler liquid descending along the sides.

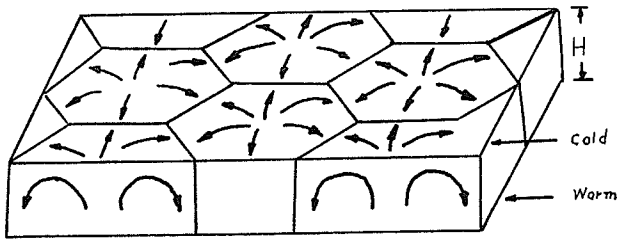

FIGURE 2 Benard Cells

Many experimenters followed Benard's work with both theoretical and experimental investigations. Lord Rayleigh[6] and H. Jeffreys[7] showed mathematically that a fluid layer was in stable equilibrium even if its density increased upwards provided

its viscosity was sufficient. They found also that equilibrium conditions were governed by $\lambda = \frac{g\beta \Delta t H^3}{\alpha \nu^2}$ * where H is the thickness of the fluid layer. H. Jeffreys obtained a detailed solution for several boundary conditions; for two rigid boundaries, an enclosed space, he found the equilibrium criterion of λ = 1709. This result has been confirmed many times, (8, 9, 10, 11, 12). In particular, it was found that λ was the sole parameter determining stability and was independent of cell shape. This number which is the product of the Prandtl number and Grashof number is now called the Rayleigh number.

Chandra[13] followed up the work on the stability point with a detailed examination of the convective flow patterns in air. He found that the flow patterns varied with the thickness of the layer and the temperature difference, giving two distinct groups:

1. With a thickness greater than 0.4 inches the polygonal prismatic cell was the basic form (Benard Cell). The pattern did not remain fixed; cells joined into long rolls in an irregular manner. The diameter of the cells and the widths of the rolls increased with depth and temperature difference.

2. When the thickness is less than 0.25 inches there is no longer any prismatic cells.

The results confirmed Jeffreys' theory for the appearance of cellular motion for all depths down to 0.28 inches but at shallower depths another type of motion appears at a Rayleigh

---

* Symbols defined in Nomenclature

number less than 1700. This is seen in Figure 3 where Chandra's curve differs from Jeffrey's curve at layers less than 0.28 inches for the chosen instability parameter.

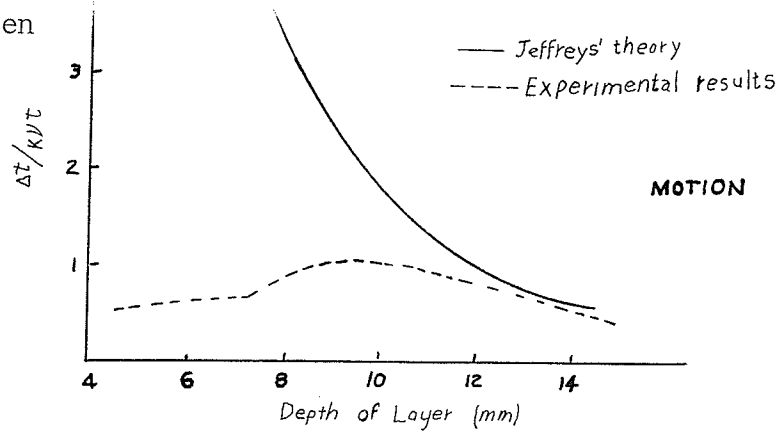

FIGURE 3 Instability Parameter vs Layer Depth for Jeffreys' Theory and Chandra's Exerimental Results (Ref. 13)

Schmidt and Silveston[1] postulated that the assumption of constant fluid properties within the layer made by Rayleigh and Jeffreys was inaccurate in the shallow layers.

Horizontal Plane Layers Heated From Above

Free convection currents are non-existent in horizontal plane layers when the fluid is heated from above, (14, 15). The difference between the fluid weight and buoyancy force of the gravitational field is caused by the temperature gradient, but the net force tends to stabilize motion since it is outward at the boundaries as compared to the net force in the horizontal layer heated from below, which is inward at each boundary. Some evidence of convection can be seen at the edges which causes some cellar motion.

Vertical Plane Layers

The first systematic experimental investigation of heat transfer in plane vertical layers was reported by Mull and Reiher. Later Jakob[5] simplified and generalized their results dividing the convective-flow regions into two regimes, the laminar flow region and the turbulent flow region. Jakob postulated that the enclosed vertical boundary layer was similar to that for the single vertical plate and that the exponent in the heat transfer equation $N_{NU} = \Phi N_{RAY}^{n}$ was dependent on the flow. From the experimental data the exponent (n) was found to change from 1/4 for laminar to 1/3 for turbulent at N_{RAY} of 2×10^5 where the characteristic dimension in the Grashof number is the layer thickness as compared to N_{RAY} of 10^9 for the vertical plate where the plate length is the characteristic dimension in N_{GR}. FIGURE 4 shows the type of boundary layer conditions that were found experimentally in laminar flow over a heated vertical plate.

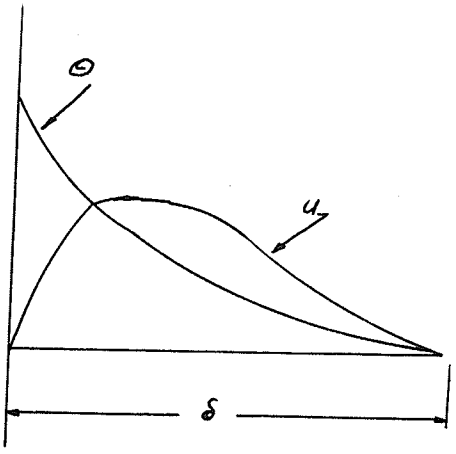

FIGURE 4 Boundary Layer in a Vertical Plane Layer

In 1953, Van Der Held and De Graaf[16] published a paper on convection heat transfer in enclosed plane air layers. These authors felt that the nature of the convective flow had a definite influence on the heat transfer; thus, any study of the heat flow must include a study of the mass flow. Both an optical method, using the principle based on the change of the index of refraction with density change, and smoke visualization were used. With the optical method numerous disturbances were visible, all running downward as soon as the layer inclination was increased past 10^{o}. With the smoke the disturbances became visible as motion in the form of rolls with their axes perpendicular to the layer axis. The air spiraled upwards along the circumference of the rolls and came back along the centre. This motion only existed in the laminar region, $2000 < N_{RAY} < 40{,}000$. At 70^{o} inclination to the vertical, a laminar circulation appeared as long as N_{RAY} was smaller than 40,000.

An analytical examination of fluid flow by free convection was made by Batchelor[17] in 1954. He established several ranges of the N_{RAY} for different H/L values which were the criteria for stability of his different flows. For large values of H/L, the boundary layers on the two walls were assumed to overlap in the centre of the enclosed space. This regime Batchelor called the asymptotic state. The flow is purely vertical with the temperature and velocity profiles being as follows:

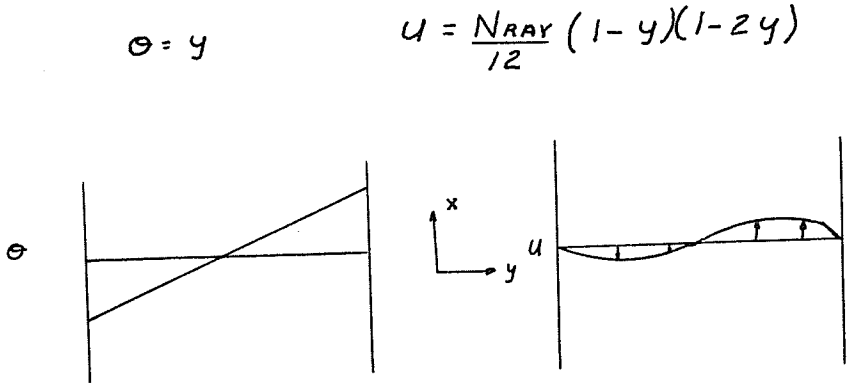

FIGURE 5 The Asymptotic State

The criteria for this asymptotic state was that $H/L > \frac{N_{RAY}}{500}$. However, some horizontal convective flow would be present at the top and the bottom.

In discussing the criteria for the flow to be laminar, Batchelor postulated that two equations must be satisfied: first, the criterion for laminar flow on a single vertical flat plate, $N_{RAY}\ (H/L)^3 < 10^9$; and second, in the asymptotic flow found in large H/L ratios, the laminar flow breakdown would occur when the maximum velocity difference gave the critical Reynolds number for the laminar breakdown on an isolated plate. The resulting criterion being $N_{RAY} = 18{,}700\ N_{PR}$. The governing factors for laminar flow in vertical layers is thus much more complex than for the horizontal layers and the criterion for the convection point in the vertical layer is probably more complex than the single N_{RAY} used in the horizontal layer and will possibly follow the same general pattern as the laminar to turbulent curve, FIGURE 6.

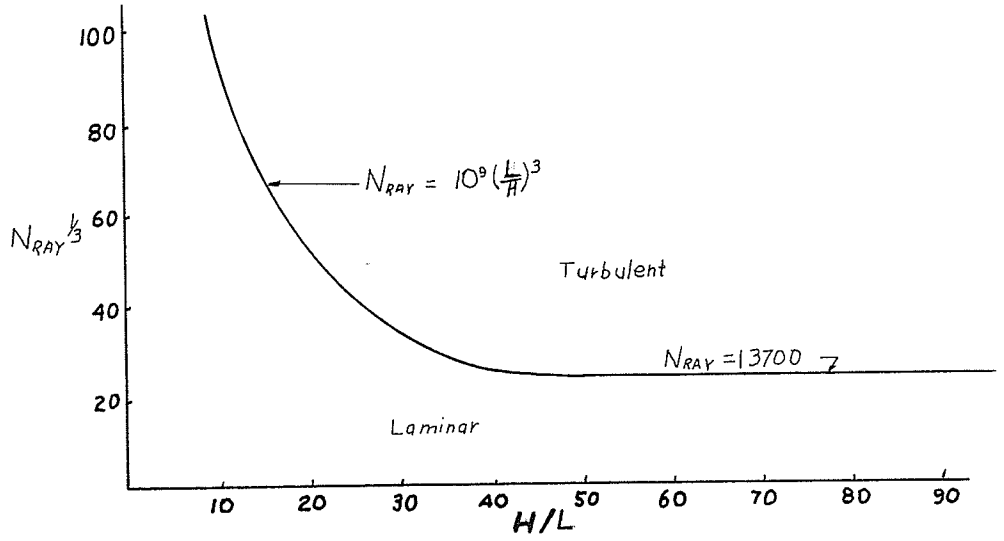

FIGURE 6 Critical Relations Governing Laminar Flow in Vertical Plane Layers (For Air Ref. 17)

W. Carlson[18] conducted a detailed study of the boundary layer profile and convective flow phenomena in vertical air layers using a Zehnder-Mach interferometer. His experimental results indicated that the flow in vertical gas layers is complex and not a function of N_{GR} only and that convective flow takes place at all gas-layer thickness and gap temperature differences. He defined four different convective-flow regimes:

1. For $N_{GR} < 124\ N_{PR}^{-2}\ (\frac{20}{21} + N_{PR})\ H/L$ there exists laminar flow, up at the hot plate and down at the cold plate. Linear temperature profiles are characteristic of this regime.

2. For $N_{GR} > 124\ N_{PR}^{-2}\ (\frac{20}{21} + N_{PR})\ H/L$ and $0.5 < \delta/L < 1$ convective flow predominates and temperature profiles are no longer linear. Fluctuations in the flow occur in the central core of the

---

δ - boundary layer thickness

layer,but separate boundary layers do not exist. A temperature gradient along the centre line exists, increasing from the bottom to the top.

3. For $\delta/L < 0.5$ separate boundary layers form and the flow is similar to that of a single vertical plate.

4. For $N_{GR} > 10^9$ turbulent flow will exist at the plate surfaces.

The first regime has one governing factor: the linear temperature profile. The profile can only be linear if the fluid velocity is very slow; therefore, the dimensionless number N_{GR} which is a measure of convective fluid flow will be the governing factor. In the second case the velocity has increased enough to form a temperature boundary layer which introduces the second condition which insures that the gap thickness is large enough to form a boundary layer on each enclosing plane and small enough that the boundary layers are related. In cases three and four, the gap thickness is wide enough that two separate boundary layers form with the transition from laminar to turbulent convective flow occurring at $N_{GR} = 10^9$.

Horizontal and Vertical Annular Layers

The first experimental investigation of free convection in an annular space with a horizontal axis was done by Beckmann in 1931. Jakob[19] reported his results, stating that free convection flow rates decreased with the difference in diameters and in air

became negligible when the difference was less than 1/4 inch. The flow in the annulus was reported as the now characteristically known kidney shape, FIGURE 7.

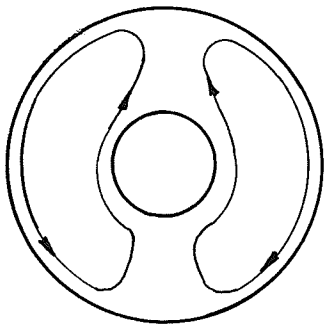

FIGURE 7 Free Convection Flow in a Horizontal Annulus

A very detailed study of the flow field and types of flow instabilities was done on a horizontal annulus (axis in the horizontal plane) by Liu, Mueller and Landis[20]. For large gap sizes the flow was relatively insensitive to the geometry with instabilities near the top and sides developing with increasing N_{RAY}. With small gap sizes the geometrical effects become predominant. The fluid moved rapidly in a thin layer near the cylinders' vertical surface remaining practically stationary in the centre gap. The velocities in the vertical flow varied from 5 to 50 ft/hr at $N_{RAY} = 10^4$. At N_{RAY} below 1600 the flow was nearly stagnant at the top and bottom regions with a greatly reduced kidney-shaped boundary layer flow at the sides. At a N_{RAY} of 1700 cellular flow started near the top and extended for an angle of 25^{o} on either side of the vertical centre line. Both geometry and fluid properties appeared

to affect the flow pattern when the gap size is small, FIGURE 8.

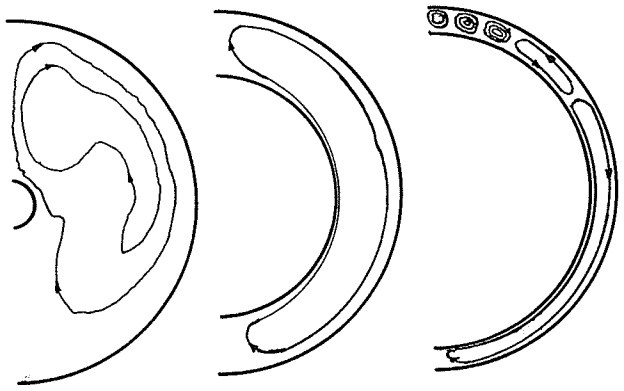

FIGURE 8 Horizontal Annular Flow Patterns as a Function of D_o/D_i and Δt ($t_i > t_o$)

In 1962 Crawford and Lemlich[21] did a theoretical study of free convection between horizontal concentric cylinders using the steady-state momentum, energy and continuity equations which they converted to finite difference equations and solved on a computer. The stream function showed the characteristic two kidney-shaped circulation patterns as mentioned before. The centres of rotation were located above the horizontal axis with the velocity lowest near the centres of rotation and the bottom of the annulus.

Very little work has been done on vertical annular layers. For small D_o/D_i ratios it would seem reasonable to assume that the vertical plane layer would exhibit similar flow patterns since the principle flow is vertical and is not affected by the wall curvature but only by height and gap thickness.

Experiments performed on rotating coaxial vertical cylinders have shown cellular motion to be set up in the annular space[22].

Taylor[22] did a mathematical analysis of this system using analogous equations to Rayleigh for motion in the horizontal layer. The instability point was again 1700 for the cellular motion which is now called Taylor vortices, FIGURE 9.

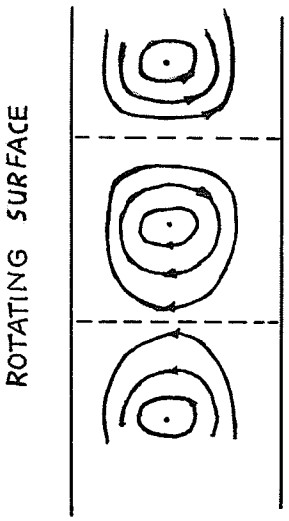

FIGURE 9 Taylor Vortices (One Surface Rotating)

Walowit, Tsao, and Di Prima[23] found that the flow stability between rotating concentric cylinders is effected by a radial temperature gradient. Temperature has at least a secondary effect on the couette type of flow between rotating cylinders and this type of flow may be expected to appear in vertical spaces on flow due to free convection only.

Summary of Flow Conditions

1. For all but very narrow gaps between plane surfaces, the instability point for free convection flow in horizontal layers

heated from below is well defined at $N_{RAY} = 1700$.

2. For horizontal layers heated from above the fluid layer is stable.

3. The instability point for vertical layers is a complex problem being a function of Δt, L, and H. The characteristic flow in vertical cylindrical layers is independent of D_o/D_i.

4. Horizontal cylindrical layers contain three different types of flow. The instability point is a function of the following three types:

vertical layers

horizontal layer heated from below

horizontal layer heated from above.

The stability point is probably a function of D_o/D_i, Δt, and L.

2.2 Heat Transfer Equations

Dimensionless Parameters

The complete mathematical analysis of the thermal boundary layer is a very involved problem and is in fact impossible without some simplifying assumptions. The early heat transfer equations were obtained by fitting experimental data to dimensionless groups which appeared to be the governing parameters for the situation considered. The Rayleigh Algebraic Method[2.4] was used to derive the applicable dimensionless groups for enclosed spaces (Appendix A).

$$N_{NU} = \Phi\ (N_{GR},\ N_{PR},\ H/L,\ D_i/L) \quad \ldots\ldots\ldots\ldots\ 2.1$$

The result obtained by applying dimensional analyses is limited by the validity and completeness of the assumptions as to the governing

parameter made prior to the analysis. The derived equation is in general agreement with all free convection experimental determinations, namely $N_{NU} = \Phi\ (N_{RAY}$, geometry), and will be presumed to be a starting point.

Equivalent Thermal Conductivity for an Annular Space

The heat flow in this experimental work was calculated using Ke, the equivalent thermal conductivity where Ke is defined by the heat conduction equation for annular spaces. (See Appendix B for derivation and assumptions).

$$Ke = \frac{Q}{L} \times \frac{\ln\ (D_o/D_i)}{2\ \pi\ (t_i - t_o)} \quad \ldots\ldots\ldots\ldots\ldots\ldots \quad 2.2$$

The early practise in the convective heat transfer field was to use the convective film coefficient in the dimensionless number N_{NU} to define the heat flow. Lately, the ratio Ke/K has been used extensively. By equating the heat transferred across an enclosed gap using Ke and h, it can be shown that $Ke/K = N_{NUx}$

$$Q' = \frac{Ke\ \Delta t}{X} = h\ \Delta t$$

$$\frac{Ke}{K} = \frac{hX}{K} = N_{NUx} \quad \ldots\ldots\ldots\ldots\ldots\ldots \quad 2.3$$

Q' - heat flux, energy flow per unit area

X - dimension in the direction of the heat flow

Plane Layers

In 1946 Jakob[5] evaluated the dimensionless heat flow formuli from Mull and Reiher's results for enclosed plane air layers and compared his equations with other data. He defined three regimes for both the horizontal and the vertical layer:

Conduction

$Ke/K \longrightarrow 1$ when $N_{GRL} \longrightarrow 0$ 2.4

Laminar Convection

$Ke/K = \Phi\ (N_{GRL}^{1/4})$ when $10^4 < N_{GRL} < 2 \times 10^5$ 2.5

Turbulent Convection

$Ke/K = \Phi\ (N_{GRL}^{1/3})$ when $2 \times 10^5 < N_{GRL} < 10^7$ 2.6

For horizontal layers with heat flow upward it was shown that the heat flow was dependent only on the layer thickness, but for vertical layers it was found that the heat flow was dependent on the layer height to width ratio for values from 3 to 42. Although, there was no published data below $N_{GRL} = 10^4$, Jakob postulated the general form of the heat flow equations for the vertical and horizontal layers on their respective graphs as seen in FIGURE 10 and 11.

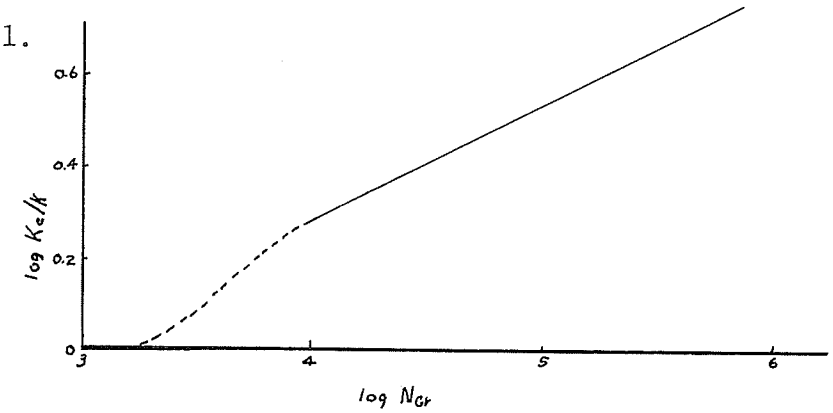

FIGURE 10 Jakob's Correlation for Horizontal Air Layers

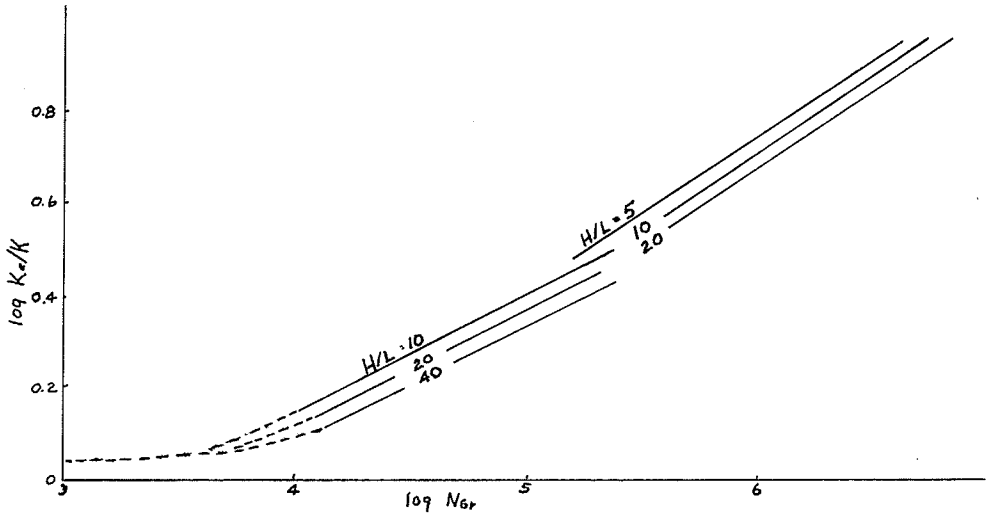

FIGURE 11 Jakob's Correlation for Vertical Air Layers

Jakob modified his results for fluids other than diatomic fluids by multiplying by $(N_{PR}/0.72)^n$ with n = 1/4 for laminar flow and 1/3 for turbulent. The laminar case, the one of interest, is given below:

Horizontal layer - $Ke/K = 0.212\ (N_{PR} \times N_{GRL})^{\frac{1}{4}}$, $10^4 < N_{GRL} < 2 \times 10^5$ . . . 2.7

Vertical layer - $Ke/K = 0.195\ (N_{PR} \times N_{GRL})^{\frac{1}{4}} (H/L)^{-1/9}$, $10^4 < N_{GRL} < 2 \times 10^5$. 2.8

Also included in the data was a result for inclination of the air layer at 45^o which confirmed that for angles from 0 - 90^o linear interpolation between the equation for horizontal and vertical layer would give reasonable results.

The next major work on enclosed spaces was done by De Graaf and Van Der Held[16] using air layers. They concluded that heat transfer is independent of height for the vertical layer using narrow air layers, but did find that heat transfer was a function of layer inclination in the convection region.

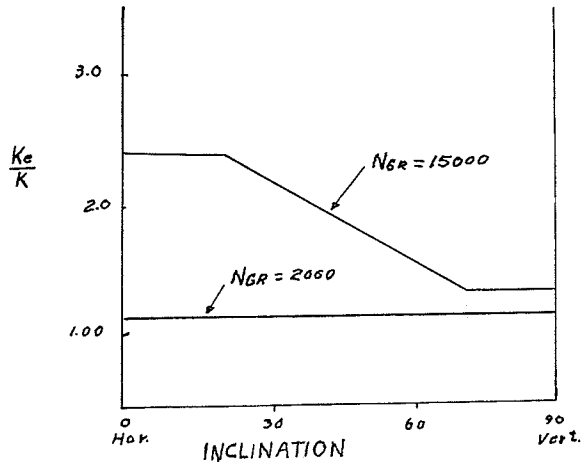

FIGURE 12 Heat Transfer in Air Layers as a Function of Inclination

Their experimental results can be summarized as follows:

horizontal - 20^{o} $N_{NU} = 1$ $(N_{GR} < 2 \times 10^{3})$ 2.9

$N_{NU} = 0.0507\ N_{GR}^{0.4}$ $(2 \times 10^{3} < N_{GR} < 5 \times 10^{4})$ 2.10

70^{o} to vertical $N_{NU} = 1$ $(N_{GR} < 6 \times 10^{3})$ 2.11

$N_{NU} = 0.0384\ N_{GR}^{0.37}$ $(10^{4} < N_{GR} < 8 \times 10^{4})$ . . 2.12

Interpolation between the horizontal to the vertical being possible between the 20^{o} to 70^{o} positions.

Batchelor[17], in the examination of the vertical enclosed layer also did a mathematical analysis of the heat transfer problem. For $N_{RAY} < 10^{3}$ a first approximation of N_{NU} gave:

$$N_{NU} = H/L + \gamma_1^{*} (N_{RAY})^{2} \quad . . . . . \quad 2.13$$

The second regime was defined by asymptotic flow as discussed in section 2.1; that is, flow in which the boundary layers

---

* - Constant

from each surface occupy the entire layer thickness and in which the flow is slow enough that the temperature gradient is a straight line. A second criteria for this heat transfer equation to be valid is $H/L > N_{RAY}/500$.

$$N_{NU} = H/L + \frac{(2\gamma_2 - 1)}{720} N_{RAY} \quad \ldots\ldots\ldots\ldots\ldots\ldots 2.14$$

$$1/2 < \gamma_2 < 1$$

The third regime has a uniform core temperature. Fluid and temperature boundary layers are present at both surfaces with a uniform temperature core section separating the temperature boundary layers.

$$N_{NU} = \gamma_3 N_{RAY}^{1/4} (H/L)^{3/4} \quad \ldots\ldots\ldots\ldots\ldots\ldots 2.15$$

$\gamma_3 = 0.3$ gives good correlation with experimental data.

Using interferometer studies of temperature profiles in vertical layers Carlson and Eckert[18] proposed heat flow equations using the temperature profiles as their criteria.

1. Conduction Regime - the temperature profiles are straight lines indicating heat is transported by conduction on the central part. The fluid may not be completely at rest but no heat transfer is connected with the flow. Distortion of the temperature field near the corners indicates some convective heat flow taking place.

For air with a term added for the corner effects the heat flow can be approximated by

$$N_{NU} = 1 + 0.00166\ L/H\ (N_{GR})^{0.9} \quad \ldots\ldots\ldots\ldots\ldots 2.16$$

2. Boundary Layer Regime - the distinguishing feature is a

central core with a constant horizontal temperature profile and a thermal boundary layer on each surface.

$$N_{NU} = 0.119\ (N_{GR})^{0.3}\ (L/H)^{0.1} \quad \ldots\ldots\ldots\ldots\ 2.17$$

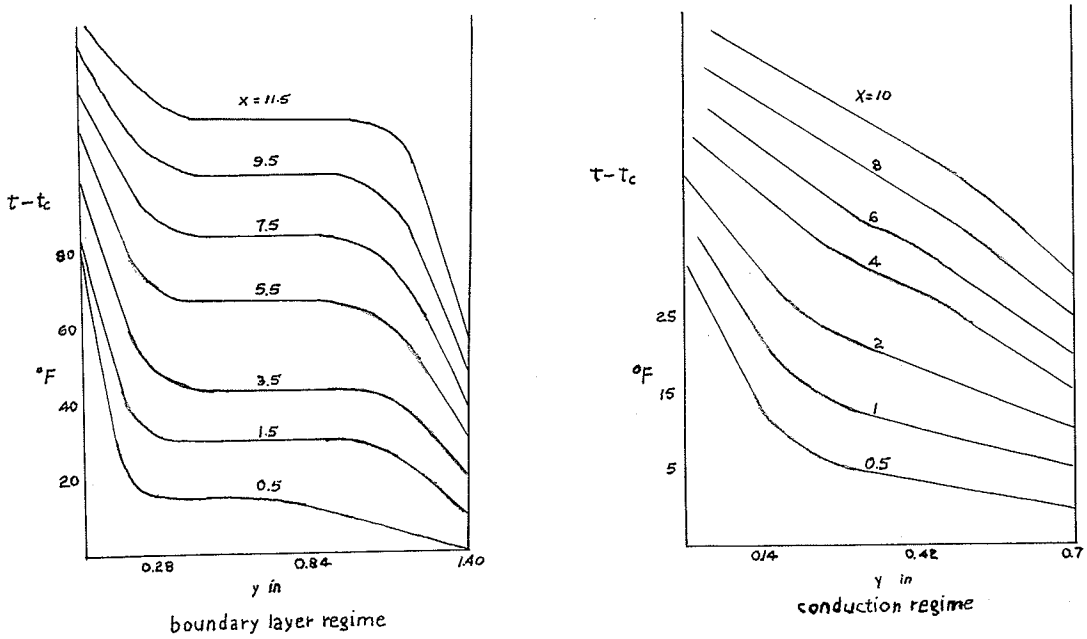

FIGURE 13 Temperature Fields in a Vertical Air Layer

The test results were insufficient to determine the limits of the conduction regime but it was found to be a function of N_{GR} and height. However, Batchelor's estimation that $N_{RAY} = 500\ H/L$ is the limit for conduction appeared conservative.

The latest work published on vertical layers is by Emery and Chu[25] in which an equation is derived using the velocity and temperature profiles found on a single plate

$$N_{NU} = 0.280\ (N_{RAY})^{1/4}\ (H/L)^{-1/4} \qquad 10^3 < N_{RAY} < 10^7 \quad \ldots\ 2.18$$

Schmidt and Silveston[1] did a detailed study of the heat

transfer in horizontal liquid layers at the convection point. Fluid convection flow appears at $N_{RAY} = 1700 \pm 3\%$ with an accompanying abrupt increase in apparent thermal conductivity. In the region immediately after convection appears, the velocities are very small, and the region was called the creeping region. The Nusselt number was found to be nearly proportional to the Rayleigh number.

$$N_{NU} = 0.0012 \ (N_{RAY})^{0.9}, 1700 < N_{RAY} < 3000 \quad . \ . \ . \ . \ . \ . \quad 2.19$$

The convection laminar heat flow equation ($N_{RAY}^{1/4}$) was applicable after $N_{RAY} = 3000$.

$$N_{NU} = 0.24 \ (N_{RAY})^{1/4} \ , \quad 3000 < N_{RAY} < 8000 \ (N_{PR})^{0.2} \quad 2.20$$

The maximum deviation for five different liquids with a range of N_{PR} from 3 to 4000 was 7%.

Although no work has been done on horizontal plane layers heated from above the heat flow is presumed to be by conduction only since there is no convection currents (radiation excluded). The temperature profile would thus be linear with the fluid temperature constant on any horizontal plane.

Annular Layers

In 1931 Beckmann[19] did experiments on horizontal annular gas layers and found the heat transfer was related to D_o/D_i ratio, FIGURE 14.

Kraussold[19,26] correlated Beckmann's and his own results for horizontal annular layers using the conventional dimensionless numbers of free convection heat transfer and the gap thickness as

the characteristic dimension in N_{GR}.

$$Ke/K = 1 \qquad \log_{10} N_{RAY} < 3 \quad \ldots\ldots\ldots\ldots\ldots \quad 2.21$$

$$Ke/K = 0.11 \, (N_{RAY})^{0.29} \qquad 3.8 < \log_{10} N_{RAY} < 6 \quad \ldots\ldots \quad 2.22$$

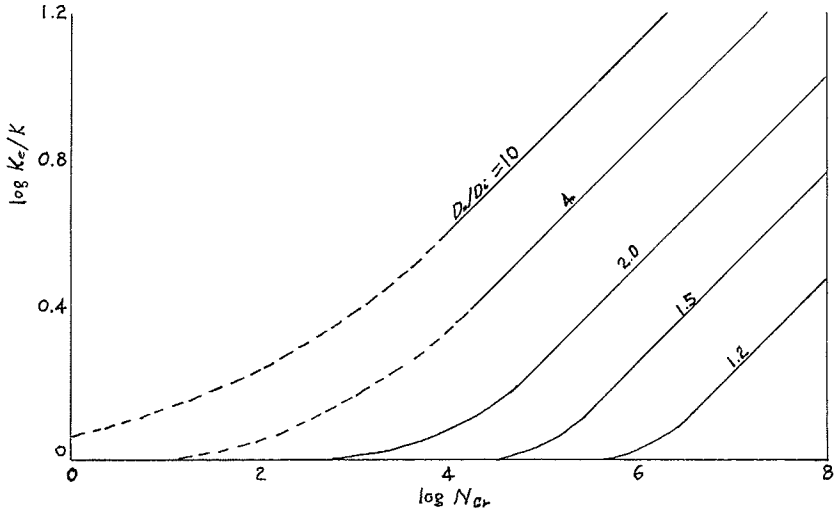

FIGURE 14 Heat Flow Between Coaxial Horizontal Tubes

Although some experiments were performed with vertical annular layers no quantitive conclusions were drawn, and Jakob[19] and Kreith[27] recommend the use of the formuli for vertical plane layers rather than horizontal cylindrical layers.

A later investigation of natural convection in horizontal annuli was performed by Lui, Mueller and Landis[20]. The temperature profiles were found to be similar to that found by Eckert and Carlson: the pure conduction distribution below $N_{RAY} = 6000$ and the isothermal gap peculiar to convection at N_{RAY} above this. The temperature profiles showed a dependence on angular position.

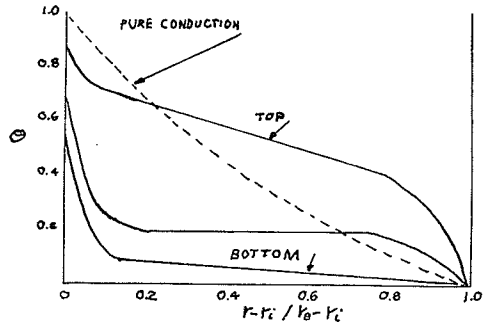

FIGURE 15 Dimensionless Temperature Profiles in Horizontal Annuli

For the range of gap thickness to diameter ratios tested (3.25 to 0.077), the maximum deviation was 4%; therefore, the geometry effects appear negligible.

Their results were correlated with the following relationships with a deviation of ±20%.

$$Ke/K = 0.135\left(\frac{N_{PR}^{2}\, N_{GR}}{1.36 + N_{PR}}\right)^{0.278} \quad \ldots\ldots\ldots\ldots \quad 2.23$$

$$3.5 < \log_{10}\left(\frac{N_{PR}^{2}\, N_{GR}}{1.36 + N_{PR}}\right) < 8 \qquad 0.25 < L/D_i < 3.25$$

$$Ke/K = 1 \qquad \log_{10}\left(\frac{N_{PR}^{2}\, N_{GR}}{1.36 + N_{PR}}\right) < 3.0 \quad \ldots\ldots\ldots \quad 2.24$$

L. Cox[28] used the abrupt rise in Ke/K to define the convection point. He found that for H/L of 115 convection effects became appreciable at N_{RAY} = 1100 ±40% for the vertical annuli. The resulting curve after the convection point was steeper than the curve proposed

by Eckert and Carlson. This result is in agreement with Tyrrel[29], who states that below N_{RAY} = 1000 convection is insignificant in horizontal coaxial cylinders and that in any steady state apparatus with horizontal temperature gradient the tendency for convection currents should be less - N_{RAY} = 1000 is then an upper safe limit.

Summary of Applicable Equations

The applicable equations are summarized by the plots of $Ke/K = \Phi\ (N_{RAY}, N_{PR}, \text{geometry})$ in FIGURE 16. The postulated curves of Mull and Reiher for fluid layers at low N_{RAY}, FIGURES 10 and 11, appear to be correct. The curves of Schmidt and Silveston verify the horizontal case and the curve of Eckert and Carlson verifies the vertical case.

Horizontal layers

$$N_{NU} = 0.0012\ (N_{RAY})^{0.9} \qquad 1700 < N_{RAY} < 3000 \quad . \quad . \quad . \quad . \quad . \quad 2.19$$

$$N_{NU} = 0.24\ (N_{RAY})^{0.24} \qquad \text{laminar} \quad . \quad . \quad . \quad . \quad . \quad . \quad . \quad . \quad . \quad . \quad . \quad 2.20$$

Vertical layers

$$N_{NU} = 1 + 0.00166\ (L/H)\ (N_{GR})^{0.9} \qquad N_{RAY} < 500\ H/L \quad . \quad . \quad 2.16$$

The curves by Kraussold's and Mueller, Lui and Landis' formuli are the only applicable equations for the horizontal annuli although they are not valid at low N_{RAY}.

$$N_{NU} = 0.11\ (N_{RAY})^{0.29} \qquad N_{RAY} > 10^{3.8} \quad . \quad . \quad . \quad . \quad . \quad . \quad . \quad . \quad 2.22$$

$$Ke/K = 0.135 \left[\frac{N_{PR}^{\ 2}\ N_{GR}}{1.36 + N_{PR}} \right]^{0.278}, \quad \frac{N_{PR}^{\ 2}\ N_{GR}}{1.36 + N_{PR}} > 10^{3.5} \quad . \quad . \quad 2.23$$

Since the flow patterns in vertical coaxial cylinders of small D_o/D_i ratios are similar to vertical plane layers, the heat transfer equations should also be similar[19,27]. The only applicable

heat transfer equation is that by Eckert and Carlson, namely equation 2.16. Also, the criteria for the linear temperature profiles should apply to both cases; $N_{GR} < 124\ N_{PR}^{-2}\ (\frac{20}{21} + N_{PR})\ H/L$ proposed by Carlson and $N_{RAY} < 500\ H/L$ proposed by Batchelor. They are very similar although Carlson's experimental results are more conservative than Batchelor's theoretical predictions.

The large errors introduced from extrapolating curves to below $N_{RAY} = 4000$ when the curves were tabulated from results taken above $N_{RAY} = 10^4$ can be seen in Figure 16. For the horizontal layer case, the steep initial curve that Schmidt and Silveston obtained from tests at low Rayleigh numbers does not agree with the extrapolated curve of Graaf and Van Der Held. The opposite error appears in the vertical layer data when comparing the extrapolated curves of Emery and Chu and Mull and Reiher to the curve that Eckert and Carlson have published. The extrapolated curves, for the vertical layer case, intersecting the Ke/K = 1.00 line well above $N_{RAY} = 3000$, indicate falsely that there is no convective heat transfer below $N_{RAY} = 3000$.

In conclusion, it would seem that there is a distinct type of heat transfer and correspondingly a distinct type of motion that is associated with low Rayleigh numbers ($N_{RAY} < 3000$), and that an accurate prediction of the convection point is not possible by extrapolation of curves derived from data taken at large Rayleigh numbers.

FIGURE 16

HEAT TRANSFER EQUATIONS FOR ENCLOSED SPACES

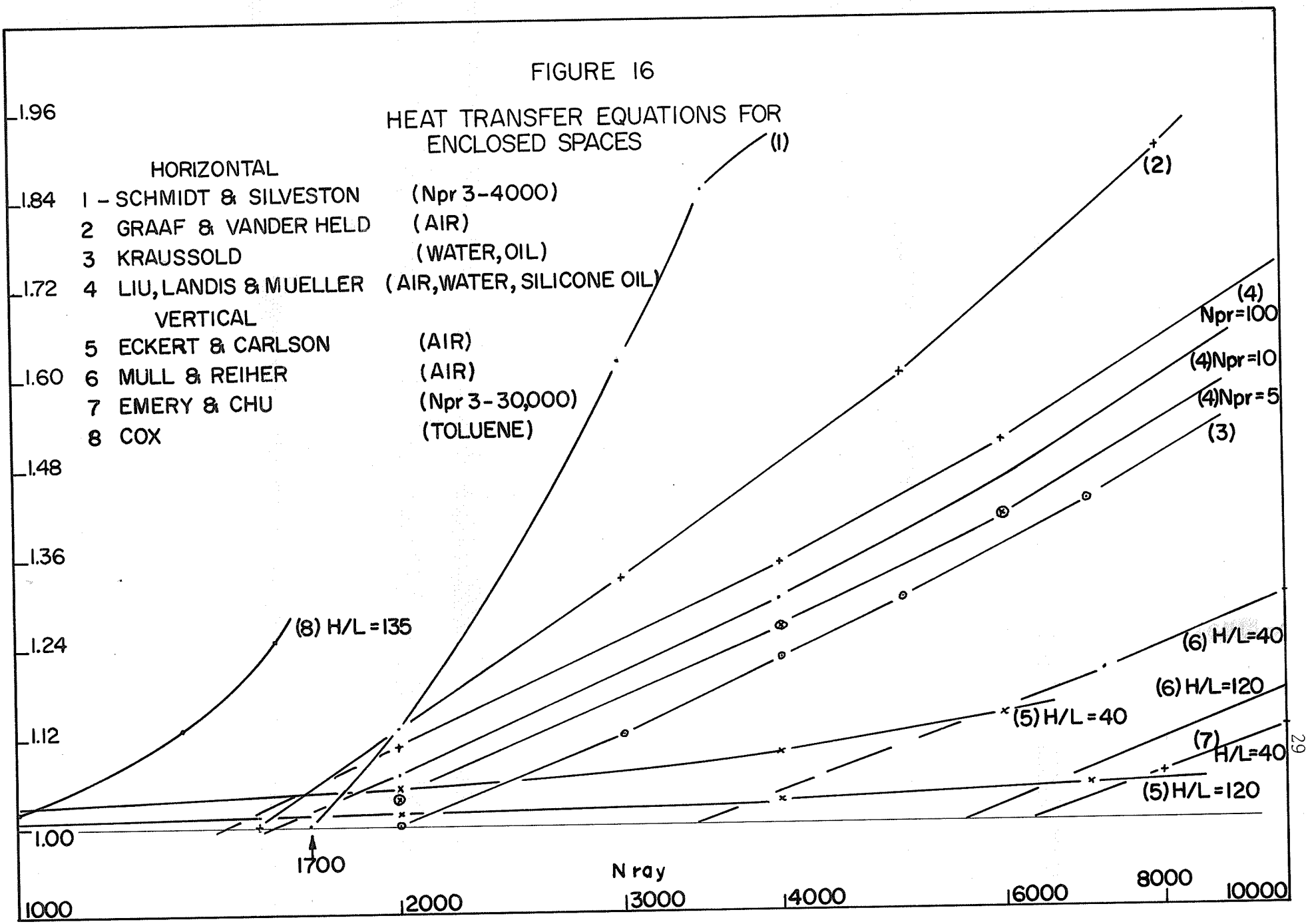

TEST APPARATUS CONSTRUCTION AND INSTRUMENTATION

The literature review and the dimensionless analysis (equation 2.1) show that the heat flow and thus also the flow patterns are very dependent on geometry. The test model was made of coaxial cylinders; the outer cylinder being changeable in order to vary gap width, D_o/D_i, and H/L. The model was mounted on a stand which would allow the cylinder axis to be rotated from the vertical to the horizontal or any degree between, FIGURES 17, 18, and 19. The two annular layers are shown in the cross-sectional views in Figure 20.

Inner Cylinder

The inner cylinder consisted of a tubular electric heater and an enclosing sheath which held the temperature sensing thermistors. The heater proper was a coil of electrical wire packed in magnesium oxide and contained in 0.500 inch inconel tubing. The overall wire resistance was 11 ohms with a maximum power rating of 1800 watts.

The enclosing sheath was made of 2 concentric fitting 304 stainless steel tubes which were cut between the test section and the ends,stabilizing sections, in order that insulating teflon washers could be inserted to reduce the end heat leak, see Appendix C. The inner enclosing tubing was split axially and served as a spacer holding the thermistors and the thermistor wires. The outer enclosing tubing contained the thermistor positioning holes. The inner spacer tubing was machined such that the outer cylinder could be pressed on over the heater and spacers and the spacers would provide enough interference to hold the outer tubing in position.

The thermistors were then placed accurately in the spacer grooves via the positioning holes in the outside tubing and cemented to the heater casing with thermon cement. The holes in the outside tubing were sealed with silicone phenolic lacquer. FIGURE 21 shows the thermistor orientation on the heater.

The heating section was 35-1/8 inches long and the inner cylinder overall length was 35-13/16 inches with the diameter 0.750 $\pm$0.004 inches and the eccentricity $\pm$0.02 inches. The cylinder was broken down into an 18-3/16 inch test section with an 8-5/8 inch stabilizing section at each end.

Outer Cylinder

The outer cylinder was made of glass tubing. Cylinders of 1.000 $\pm$.002 inches and 1.31 $\pm$.01 inches were used to give gap widths of 0.125 and 0.28 inches. On the larger cylinder, the thermistors were mounted on the outside with rubber cement and insulated from the surrounding air with an 1/8 inch covering of asbestos paste. In order to measure the temperature drop across the glass, one thermistor (No. 9) was mounted on the inside surface via an 1/8 inch hole in the glass. The orientation is shown in FIGURE 21. On the smaller cylinder, the thermistors were all mounted on the inside glass surface by cementing them into holes in the tubing, orientation in FIGURE 21.

Since the temperature sensing elements were 0.040 inches in diameter their "center" was placed on the inner surface. They were

positioned by means of the shadow cast from a light source set on the tube axis. By using a slight angle between the light rays and the tube axis, the shadow cast showed an exaggerated movement as compared to the thermistor movement giving better positioning accuracy.

Mounting Apparatus

The inner and the outer cylinders were mounted on plastic end plates, see Appendix C. The inner cylinder "cold" ends were positioned in centering holes which allowed the thermistor and heater wires to pass through. One end of the inner cylinder was clamped permanently at the end plate while the other end was left free for movement on expansion.

The outer cylinder was positioned in grooves with rubber o-ring seals. The end plates were held together by three tie-rods which also kept enough tension on the outside cylinder to provide a seal at the end plates. The whole apparatus was then mounted on an arm that could rotate 90^{o} - from the horizontal to the vertical position.

Power Supply

The heater power source was 115 V, single phase, AC, with a step-down power transformer to regulate the supply, FIGURE 22. The circuit diagram for the power transformer is shown in FIGURE 23. The power output was determined by a wattmeter at high outputs and

an ammeter and voltmeter at low outputs. Calibration data for the measuring instruments is shown in Appendix D.

Temperature Sensing Devices

Thermistors were used as the temperature sensing device. These are semi-conductors with a negative coefficient of resistivity, resistance being a function of absolute temperature, FIGURE 24. Because of their high resistance and high sensitivity (approximately 2% per ^{o}F) large potentials and low currents eliminate the necessity of complicated circuitry and sensitive measuring equipment.

The thermistors used were of the bead and probe type, FIGURE 25. Each contained a 0.043 inch resistance element and were glass covered. The beads were used on the heater, because of their compactness, and the probes on the tubes. For thermistor characteristics and construction technique, see Appendix E.

The thermistors were calibrated in a constant temperature bath with a temperature fluctuation not greater than $\pm 0.01^{o}$F. The resistance reading was made within $\pm 0.2\%$ which is better than $\pm 0.1^{o}$F.

Thermistor Bridge

A wheatstone bridge consisting of three variable resistance boxes was used to take the thermistor resistance readings. The circuitry, FIGURES 26, 27, and 28, was such that the resistance of any one thermistor on either the heater cylinder or the outside cylinder could be read alone or the difference in resistance between

a heater cylinder thermistor and an outside cylinder thermistor could be read. The variable resistance branch of the bridge could be varied from 0 to 9999.9 ohms in steps of 0.1 ohms. The other two resistance boxes were used to form the 5000 ohm permanent resistance branches of the bridge. The variable resistance boxes had an absolute accuracy of 0.025% above 100 ohms giving an overall accuracy of 0.075%. Two test resistors of 900 ohms and 1900 ohms showed the bridge reading error to be less than 0.2%.

A Leeds and Northrup null detector was used to detect the bridge unbalance. A single pen recorder was used to monitor the bridge unbalance via the null detector output. The recorder arrangement was used to determine steady state conditions only.

FIGURE 17

TEST APPARATUS

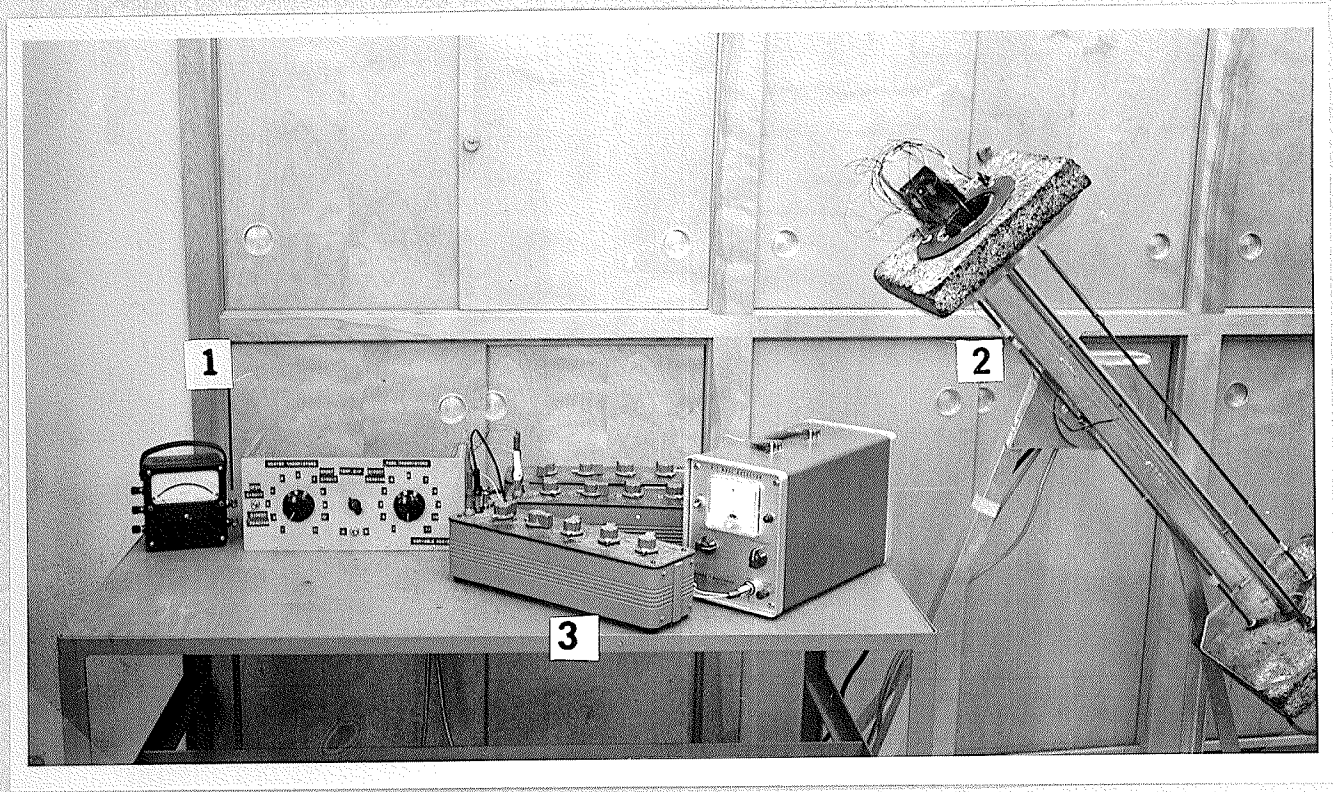

1 POWER METER

2 CONCENTRIC CELL

3 THERMISTOR SWITCH AND BRIDGE

FIGURE 18

CONCENTRIC CELL (HORIZONTAL)

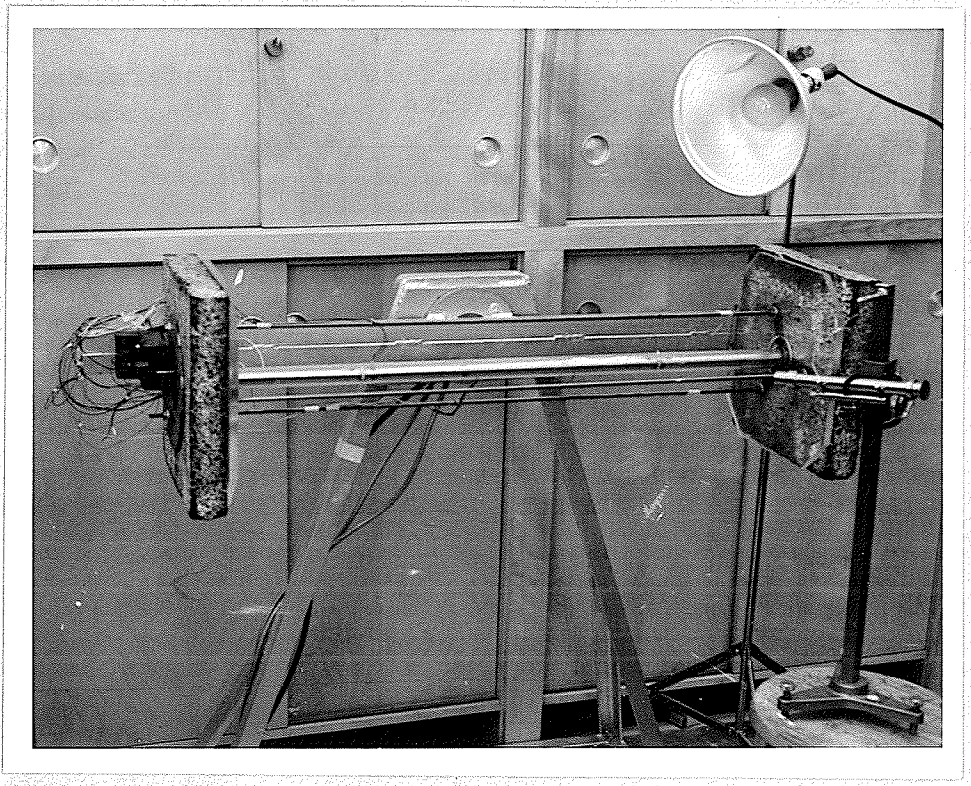

FIGURE 19

CONCENTRIC CELL (VERTICAL)

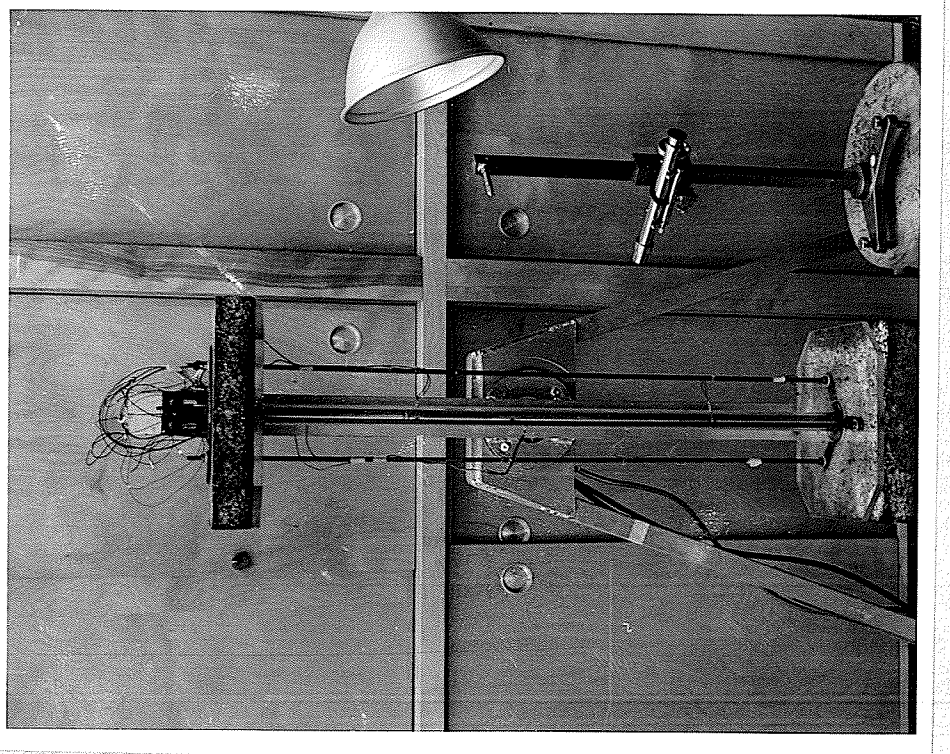

FIGURE 20

ANNULAR CROSS-SECTIONS

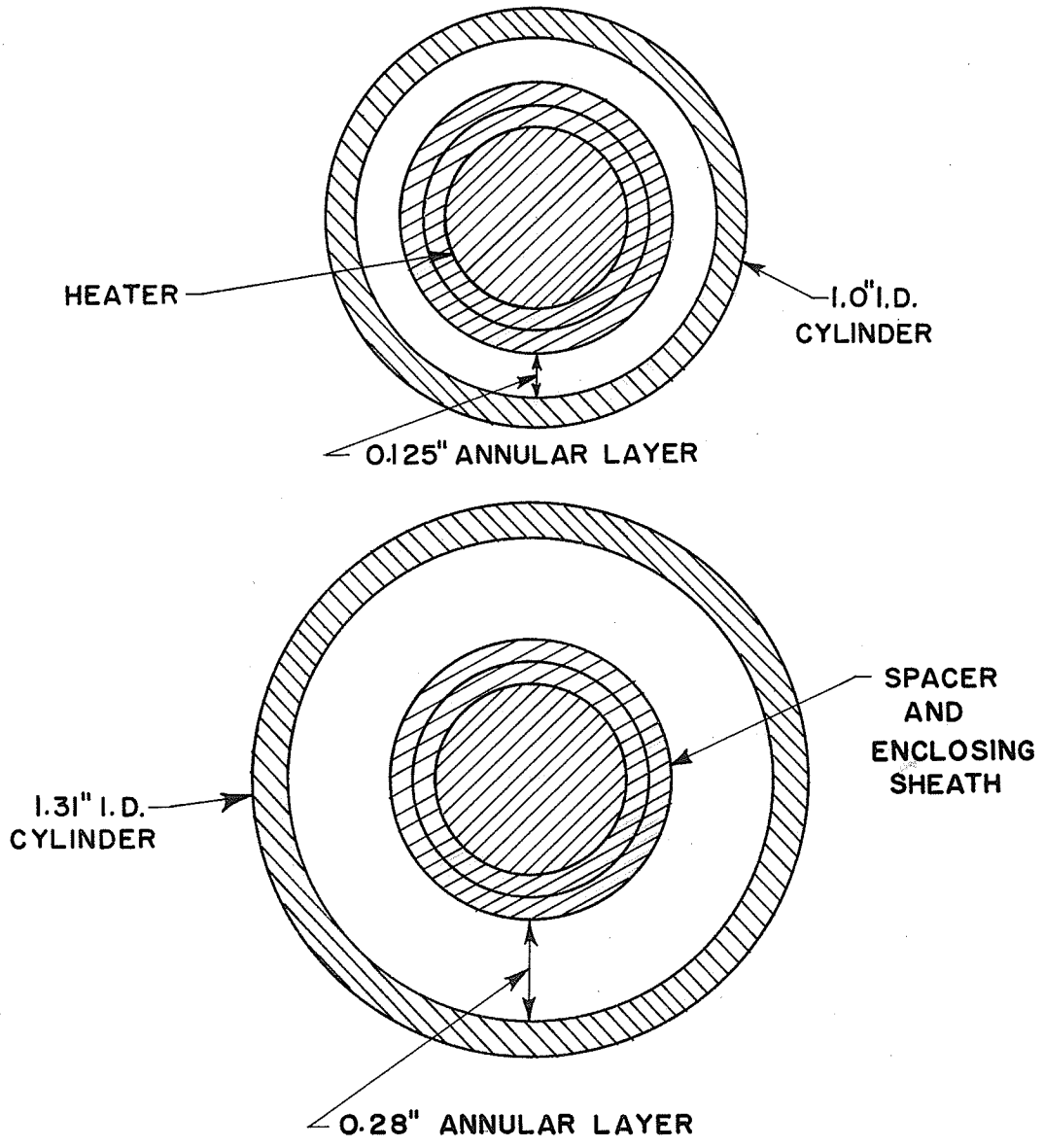

FIGURE 21

THERMISTOR ORIENTATION ON THE INNER CYLINDER

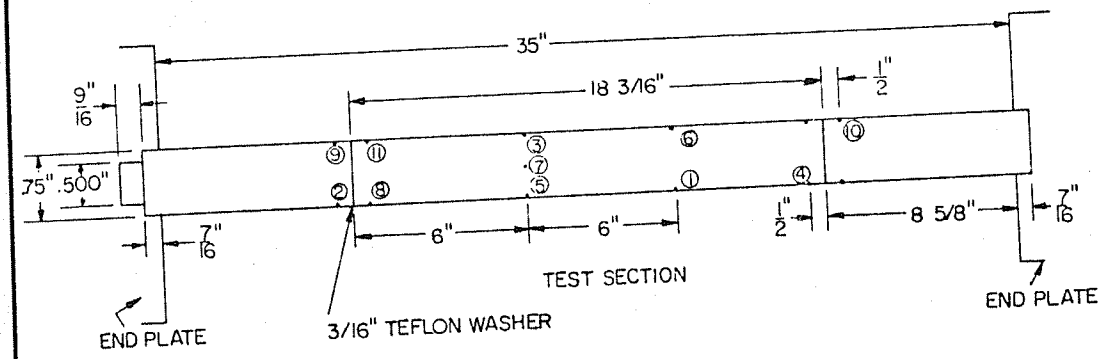

THERMISTOR ORIENTATION ON THE OUTER GLASS CYLINDERS

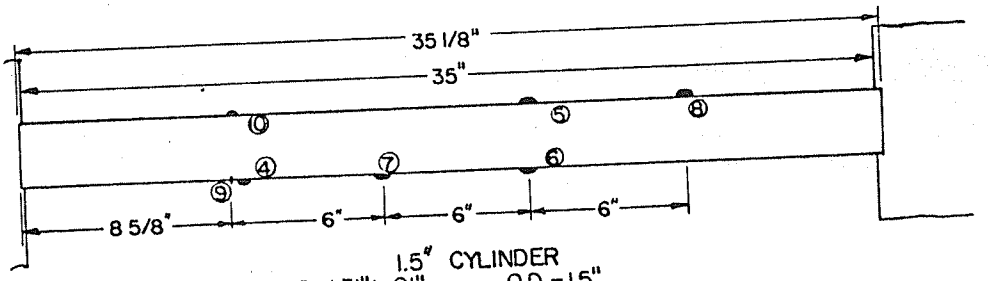

1.5" CYLINDER
I.D.-1.31" ± .01" O.D.-1.5"

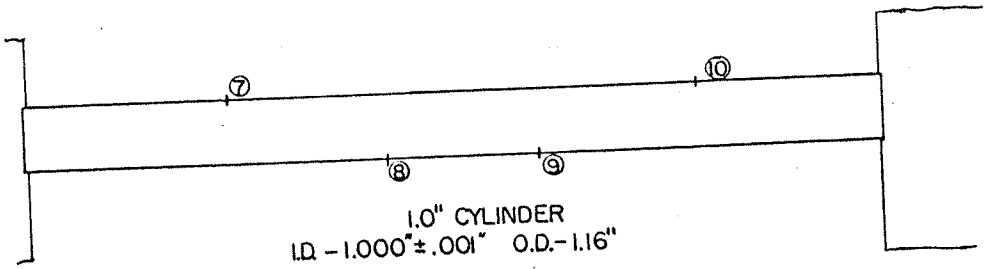

1.0" CYLINDER
I.D. - 1.000" ± .001" O.D.- 1.16"

FIGURE 22

Power Supply

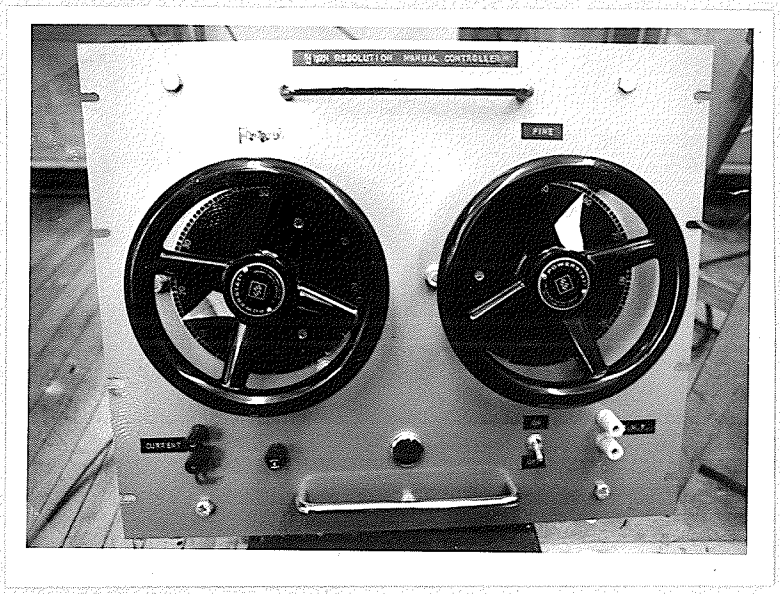

FIGURE 23

Power Supply Circuitry

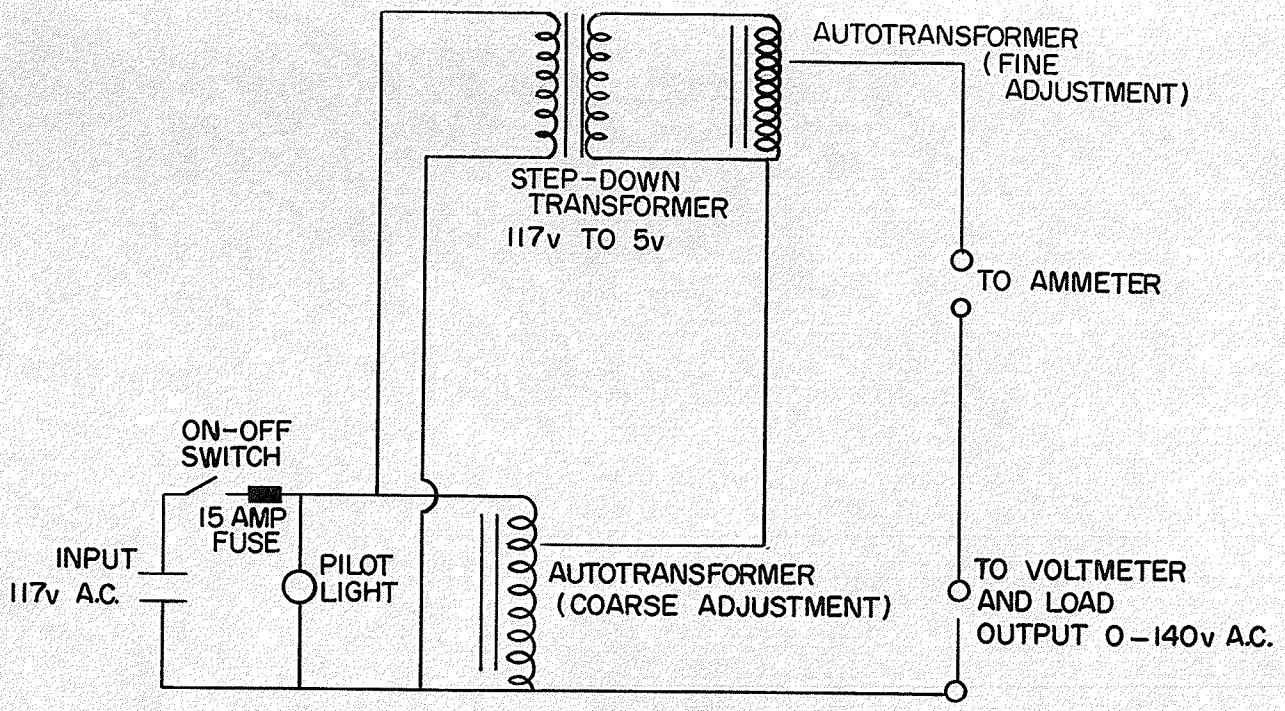

FIGURE 24

TYPICAL THERMISTOR CURVE

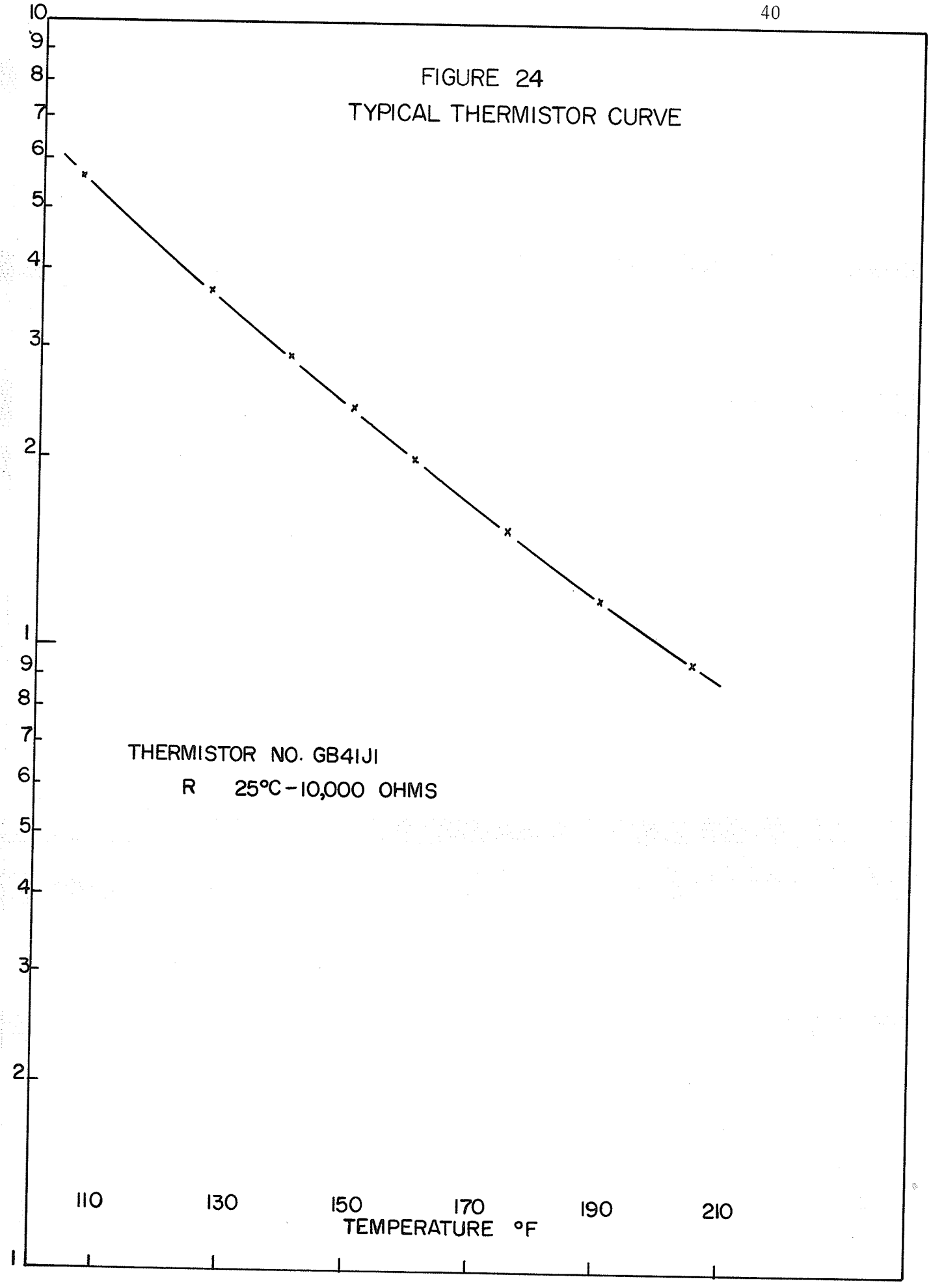

FIGURE 25

BEAD AND PROBE THERMISTORS

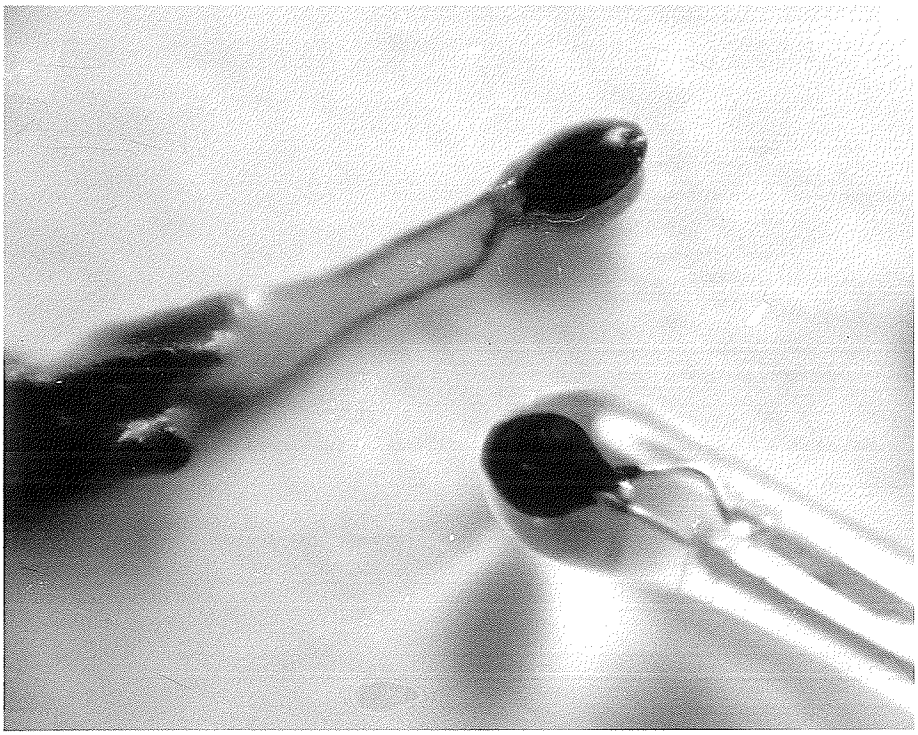

FIGURE 26

THERMISTOR SWITCH BOX

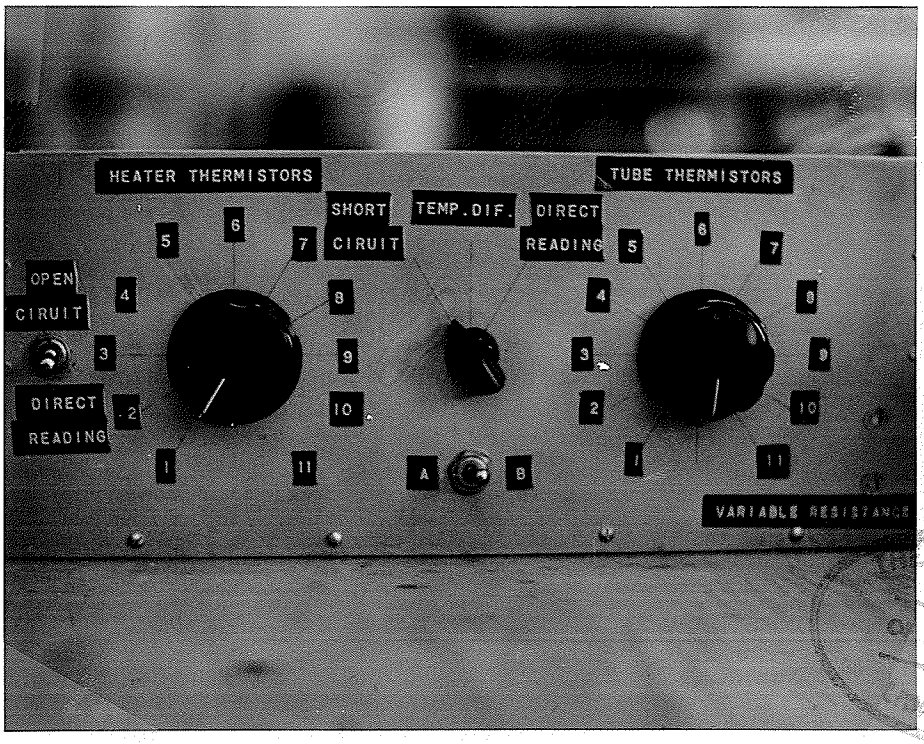

FIGURE 27

THERMISTOR INSTRUMENTATION

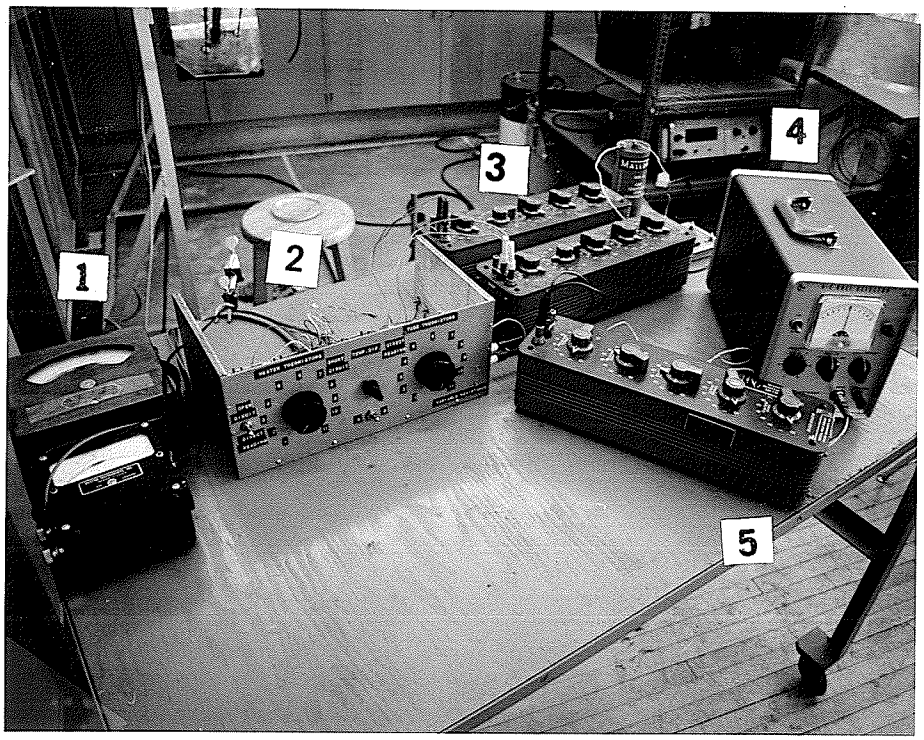

1 POWER METERS
2 SWITCH BOX
3 5000 OHM PERMANENT RESISTANCE ARMS
4 NULL DETECTOR
5 VARIABLE RESISTANCE ARM

FIGURE 28

THERMISTOR BRIDGE CIRCUITRY

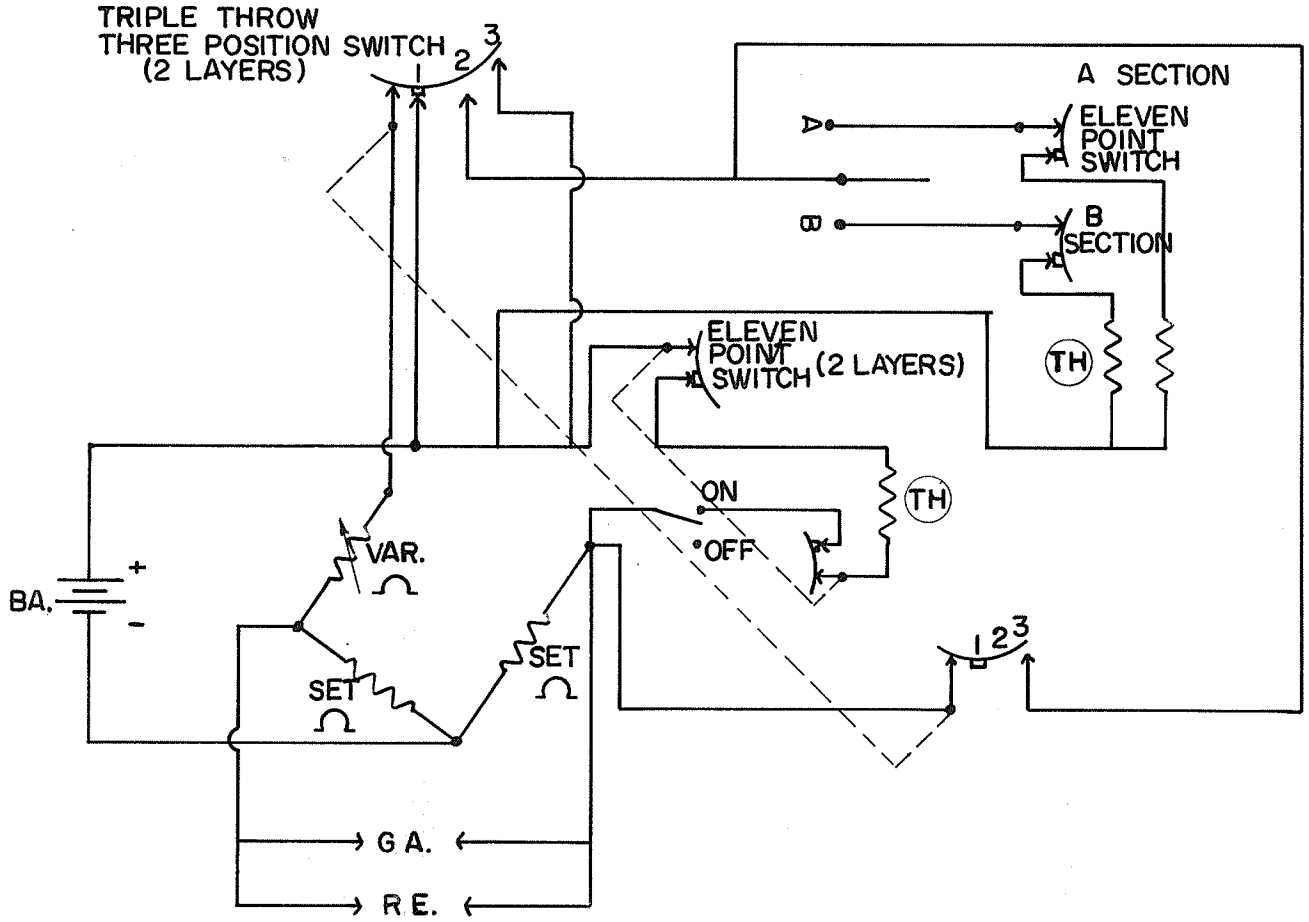

EXPERIMENTAL PROCEDURE

The apparatus was assembled in a temperature controlled room; the control being $\pm 1.0^{o}F$ from $65^{o}F$ to $85^{o}F$. The temperature range was used to vary the outside surface temperature of the glass, outer cylinder which in turn varied the temperature throughout. Because of the temperature limitations of the material, low room temperatures were used at high heat inputs to reduce the maximum temperature. Also the temperature control was used to vary the fluid mean temperature. The temperature set point variance, $\pm 1.0^{o}F$, was necessary to insure steady state conditions.

For any particular test, the annuli axis was set in one of the three positions; horizontal, vertical, or 45^{o} to the vertical, and the heat input set. Low velocity air was forced over the outside cylinder to increase the heat transfer from its surface and to maintain a more uniform temperature distribution along the cylinder. When steady state temperature conditions were reached, the heat flow characteristics and the flow patterns, if any, were observed. In order to vary the Rayleigh number and thus go from non fluid flow to fluid flow, successive tests were taken varying the temperature difference across the gap by varying the heat input.

The heat transfer properties for any test were measured by recording each thermistor resistance reading and the heat input.

The flow patterns were observed in two ways. In order to see the general flow pattern, dye was introduced into the annular space via a 0.040 inch O.D. plastic tube and a syringe. Small

particles were used to time the fluid motion and to determine the point of initial motion. In the glycerine, aluminum powder with an average dimension of 0.001 inches was used. The particles were observed by illuminating them with a floodlight and viewing them through an exstenometer which had a magnification power of 10 times. When the apparatus was in the vertical position, the particle speed was also noted. In the water, polystyrene beads (Montopore fines manufactured by the Monsanto Chemical Company) having a specific gravity of 1.04 and an average diameter of 0.010 inches were used and viewed with the naked eye. 'Merian red' was the dye used in the glycerine and in the water while smoke was used in the air layer.

With the 0.28 inch gap, glycerine was the only fluid used since it alone had the Rayleigh number range that covered the region from pure conduction heat transfer to conduction and convection. With the 0.125 inch gap; air, water and glycerine were the fluids used. In filling the cell, air was trapped in the liquids, glycerine and water. The air bubbles were removed from the glycerine by introducing a partial vacuum on the top of the cell when it was in the vertical position and were removed from the water by boiling when in the cell.

CALCULATIONS AND ANALYSES OF RESULTS

The heat transferred under any particular conditions was studied by determining the value of Ke/K and plotting this ratio vs N_{RAY}.

The equivalent thermal conductivity was calculated from:

$$Ke = \frac{Q}{L} \frac{\ln(D_o/D_i)}{2\pi(t_i - t_o)} \quad \ldots\ldots\ldots\ldots\ldots\ldots\ldots \quad 2.2$$

The value of the thermal conductivity, K, was taken from applicable references[14,24].

5.1 Sample Calculations for the 0.28" Annular Layer

Calculation of Ke

Test No. 105B (Horizontal Series)

$$\Delta t_{bottom} = \left[\Delta t(1^*-6) + \Delta t(5^*-7) + \Delta t(2^*-4)\right] \div 3$$

$$= 22.7^{\circ}F$$

$$\Delta t_{top} = \left[\Delta t(6^*-5) + \Delta t(11^*-10) + \Delta t(10^*-8)\right] \div 3$$

$$= 18.9^{\circ}F$$

$$\Delta t_{glass} = \Delta t\ 9\text{-}4 = 3^{\circ}F$$

$$\therefore \Delta t_{average} = \frac{(22.7 + 18.6)}{2} - 3 = 17.8^{\circ}F$$

Power Input = corrected volts x corrected amperes

= 14.5 x 1.82

= 26.39 watts

---

*Heater Cylinder Thermistor Number

$$Ke = \frac{Q}{L} \frac{\ln(D_o/D_i)}{2\pi(t_i - t_o)}$$

$$= \frac{Q}{35.1/12} \times 3.413 \times \frac{\ln(\frac{1.315}{0.750})}{2(3.142)} \times \frac{1}{(t_i - t_o)}$$

$$= \frac{Q}{(t_i - t_o)} \times (0.104) \quad \ldots\ldots\ldots\ldots\ldots\ldots \quad 5.1$$

Q - total power input in watts

$(t_i - t_o)$ - degrees fahrenheit

$$Ke = \frac{26.39}{17.8} \times 0.104 = 0.1545$$

Eccentricity correction from Appendix B, FIGURE 1

$$\frac{\Delta t_L - \Delta t_S}{\Delta t_M} = \frac{3.8}{17.8} = .213$$

Ke error = 1.06

Ke actual = 1.06 x 0.1545 = 0.164

$$Ke/K^* = \frac{0.164}{0.168} = 0.975 = 0.98$$

Calculation of N_{RAY}

Test No. 105B (Horizontal Series)

$$N_{RAY} = (g \beta \mu c_p / V^2 K) \quad (t_i - t_o) \left(\frac{D_o - D_i}{2}\right)^3$$

$$= Z^{**} (t_i - t_o) \left(\frac{D_o - D_i}{2}\right)^3 \quad \ldots\ldots\ldots \quad 5.2$$

$$= Z(t_i - t_o) \left(\frac{1.315 - 0.750}{2}\right)^3$$

$$= Z(t_i - t_o) \quad 22.5 \times 10^{-3} \quad \ldots\ldots\ldots \quad 5.3$$

K^* = 0.168 @ 109°F ±2% (Appendix F, FIGURE F-2)

Z^{**} = fluid properties and constants evaluated at the mean temperature (Appendix F, FIGURE F-1)

$$N_{RAY} = 2.5 \times 10^{3} \times 17.8 \times 22.5 \times 10^{-3}$$
$$= 1000$$

5.2 Sample Calculation for the 0.125" Annular Layer

Calculation of Ke

The calculations for Ke for the 0.125" annular layer differed in three ways from the calculations for Ke for the 0.28" annular layer.

1. In calculating the average Δt only three Δt's were used -

$$\Delta t_{average} = \left[\Delta t\ (1^{*}, 6^{*} - 9) + \Delta t(5^{*}, 7^{*}-8) + \Delta t(10^{*}-10)\right] \div 3$$

Since the thermistors on the outer cylinder were on the inner surface, no correction was needed for the Δt across the glass.

2. The formula was modified for the change in the outer diameter -

$$Ke = \frac{Q}{(t_i - t_o)} \times (0.0534) \quad \ldots\ldots\ldots\ldots\ldots \quad 5.4$$

3. The error due to temperature eccentricity was ignored because the smaller gap reduced the error and because of calculation difficulties due to the heater eccentricity. However, a correction was applied to the results for air to compensate for the heat transferred by radiation.

Calculation of N_{RAY}

This calculation was also similar to that for the 0.28" annular layer except the basic formula was changed, as indicated in

*Heater Cylinder Thermistor Number

formula 5.5 because of the change of the outer diameter.

$$N_{RAY} = Z(t_i - t_o)\ 1.953 \times 10^{-3} \quad \ldots\ldots\ldots\ldots\ldots\ldots\ 5.5$$

5.3 Results for the Horizontal Position

The results for the concentric cylinders in the horizontal position are shown in FIGURE 29. The general shape of the curve follows closely the shape of the reference lines by Graaf and Van Der Held and Kraussold (No. 2.10 and 2.22). The scatter of the experimental points was very good, $\pm$3%, except for a few points.

All the points for the 0.125" annular layer were higher than the 0.28" annular layer with all the points for water, at the high Rayleigh numbers, high by 10% as compared to the trend set by the remainder of the results.

The main discrepancy was the fact that the readings are low by 4% at the low Rayleigh number. Convective heat flow should not be present at this point and thus Ke/K should be one.

Visual observation of the test fluids during the tests showed that convective fluid motion appeared before the Rayleigh number of 1700 cited as the point of instability for the horizontal plane layers heated from below. Motion in the 0.28"annular layer was fully developed by a Rayleigh number of 1000; however, motion was not observed in the 0.125"annular layer at Rayleigh numbers below 300. The fluid motion was the characteristic kidney shape, FIGURE 7, as reported by previous investigators. A "dead" spot was noted on the top of the heater cylinder as the aluminum

particles settled out of the glyerine at this point.

For this case, free convection heat transfer became important as soon as fluid flow began as seen by the abrupt increase of Ke/K at approximately the same Rayleigh number as the fluid motion first appeared.

5.4 Results for the Vertical Position

The results for the concentric cylinders in the vertical position are shown in FIGURE 30. The general shape of the curve is as expected, following closely the shape of the reference line given by Eckert and Carlson (No. 2.16). The scatter of the experimental points was small, $\pm 6\%$, except for the points from the tests with water which appear high by 10% as in the horizontal case. Also the curve goes below Ke/K = 1 at the low Rayleigh numbers; this time the error is quite significant, 10%.

Convective fluid motion was observed to start at different Rayleigh numbers depending upon the geometry. Motion began at a Rayleigh number of 400 in the 0.28" annular layer and 150 in the 0.125" annular layer. However, a slight creeping action was detected when dye was placed in the glycerine and it was suspected that convective flow was present almost all the time.

The fluid motion formed the same pattern for every test, and did not at any time show resemblance to the cellular motion as reported for the flat plate. The motion was always upward along the heater cylinder and downward along the outside cylinder with a

stagnant layer between the two motions as seen in FIGURE 31.

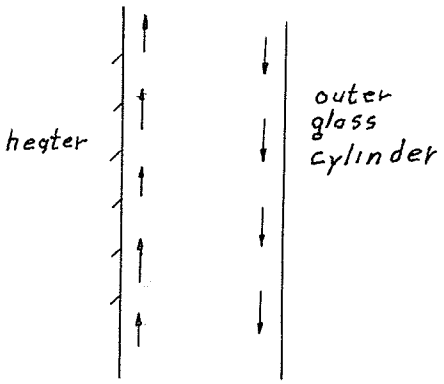

FIGURE 31 Motion in Vertical Annular Layers

There was never a breakdown of this motion into a cellular motion similar to the Taylor vortices. With increasing Rayleigh number the fluid velocity was observed to increase, however; at the onset of free convection, the fluid velocity was estimated to be 0.14 mm/sec $\pm$0.05 mm/sec while at large Rayleigh numbers, 3000, the velocity was 0.3 mm/sec .

As can be seen in FIGURE 30, there is no sudden increase in the Ke/K ratio, and thus in the equivalent thermal conductivity, when motion begins as in the horizontal case. The curve indicates that free convection heat transfer makes up only a small percentage of the overall heat transfer up to a Rayleigh number of 2000 for H/L ratios greater than 100.

5.5 Results for the 45^{o} to the Vertical Position

The results for the concentric cylinders in the 45^{o} position are shown in FIGURE 32. Because of the absence of reliable literature

on this case, the reference line has been omitted. The general shape is similar to the two previous cases. In fact, the 45^{o} position appears to be a compromise between the vertical and the horizontal cases as can be seen in FIGURE 33 which shows all three cases.

The scatter was $\pm 5\%$ with the results from the 0.125" annular layer being high by 10%. In this case the results at the low Rayleigh number appear slightly low.

Convective fluid motion appeared to be present at all Rayleigh numbers in the 0.28" annular layer, and was definitely present above a Rayleigh number of 300. Motion appeared at a Rayleigh number of 100 in the 0.125" annular layer.

The fluid motion had a very definite pattern which followed the general geometry of the cell, FIGURE 34. The flow patterns, in the 0.28" annular layer, were observed to develop in stages to attain fully developed flow. The first motion to appear was upward along the heater cylinder. At a Rayleigh number of 250 (0.28" annular layer) the upward motion was very pronounced with some very slow downward motion on the underside of the heater. The motion became quite rapid; approximately 0.3 mm/sec at $N_{RAY} = 1000$ which is comparable to the speed in the vertical position at a Rayleigh number of 2000 or 3000.

A secondary motion was observed to move perpendicular to the cylinder axis although it was not pronounced until a Rayleigh number of 1000 and then was very slow. It was always in an upward direction along the sides of the heater, FIGURE 34. By a Rayleigh

number of 3000, temperatures on the cylinder surfaces were very unstable, ± 5 to $10^{o}F$, presumably reflecting unstable motion.

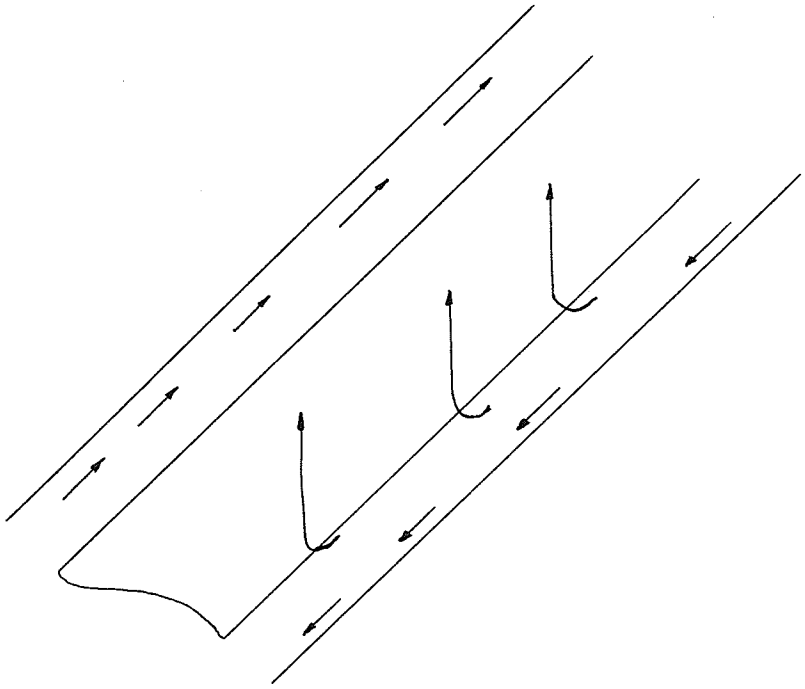

FIGURE 34 Motion in an Annular Layer at 45^{o} to the Vertical

The next section contains a detailed description of the results and a complete discussion of the errors involved. The results are listed separately for each different test condition with the absolute error, expected error, and probable reasons for the errors listed for each case discussed.

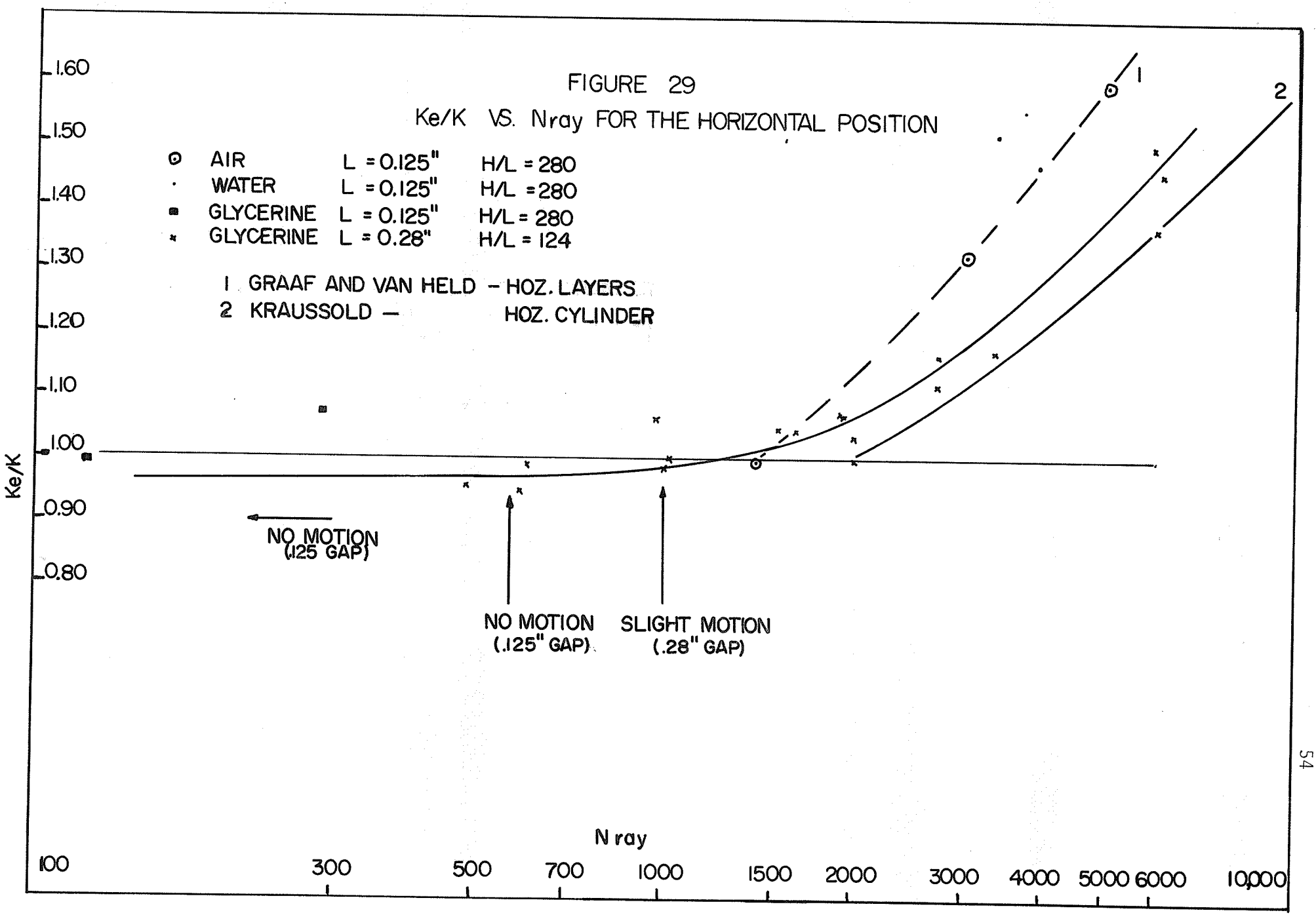
FIGURE 29
Ke/K VS. Nray FOR THE HORIZONTAL POSITION
AIR L = 0.125" H/L = 280
WATER L = 0.125" H/L = 280
GLYCERINE L = 0.125" H/L = 280
GLYCERINE L = 0.28" H/L = 124
1 GRAAF AND VAN HELD – HOZ. LAYERS
2 KRAUSSOLD – HOZ. CYLINDER
1
2
Ke/K
1.60
1.50
1.40
1.30
1.20
1.10
1.00
0.90
0.80
NO MOTION (.125 GAP)
NO MOTION (.125" GAP)
SLIGHT MOTION (.28" GAP)
N ray
100
300
500
700
1000
1500
2000
3000
4000
5000
6000
10,000

FIGURE 30

Ke/K VS Nray FOR THE VERTICAL POSITION

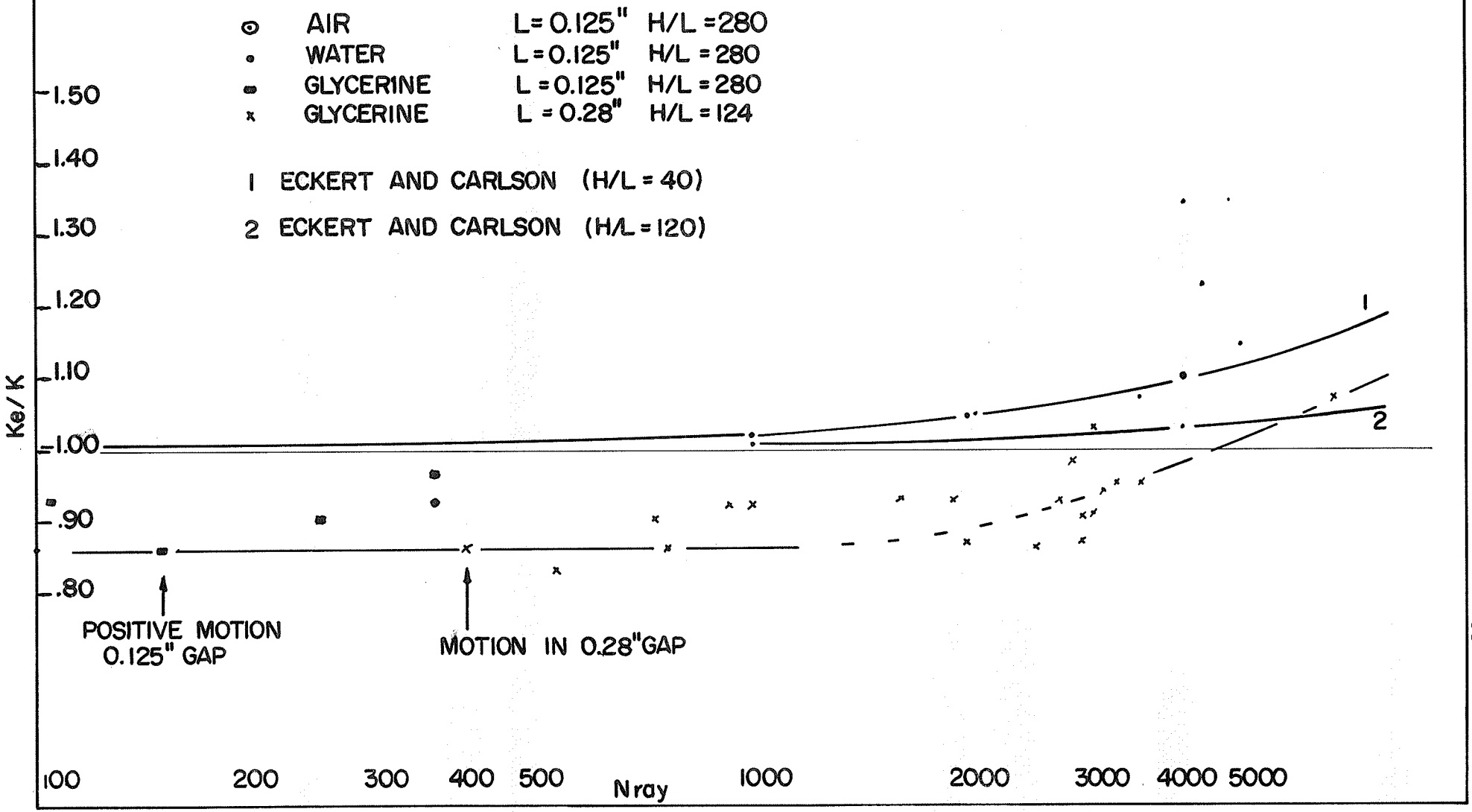

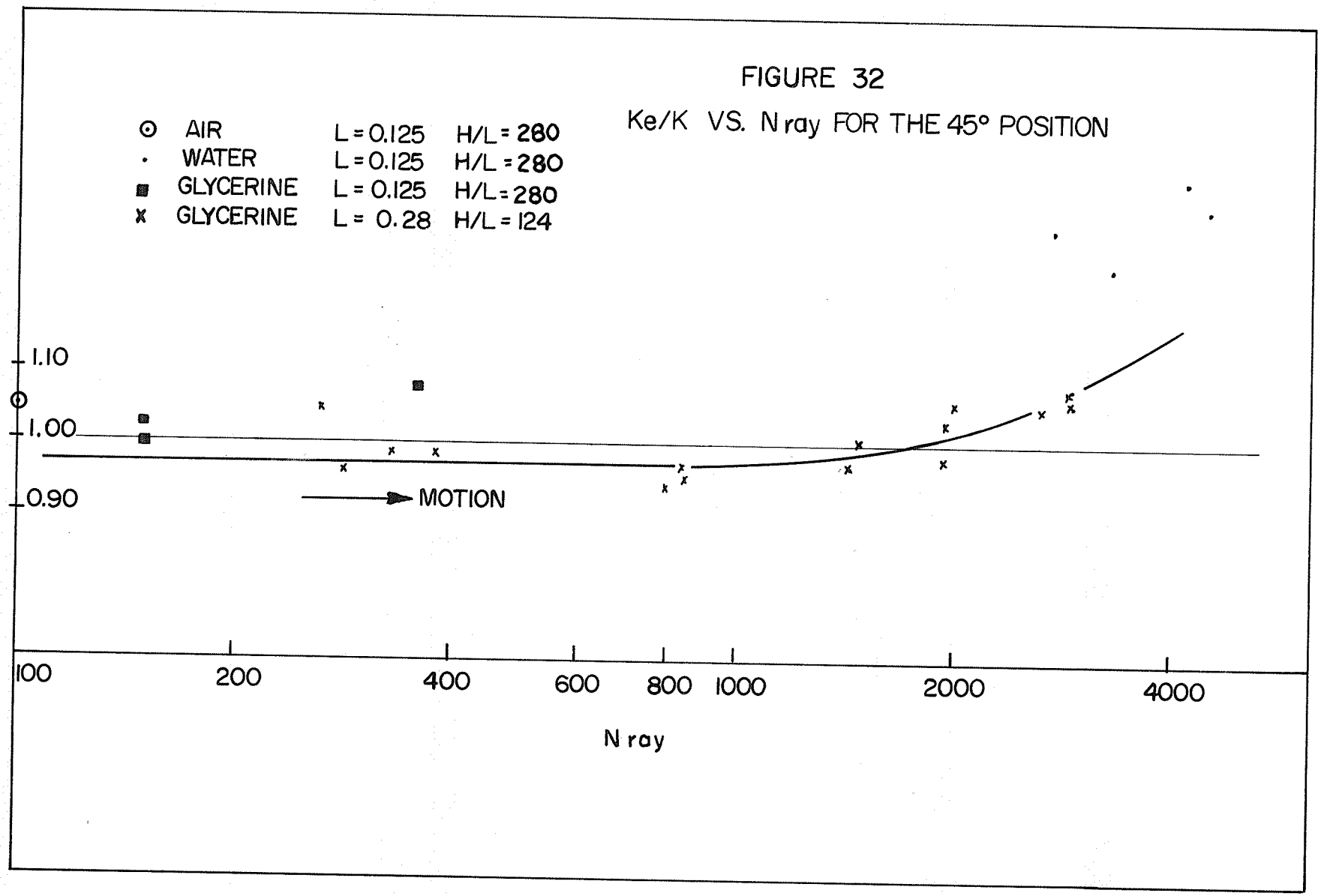
FIGURE 32
Ke/K VS. N ray FOR THE 45° POSITION
AIR L = 0.125 H/L = 280
WATER L = 0.125 H/L = 280
GLYCERINE L = 0.125 H/L = 280
GLYCERINE L = 0.28 H/L = 124
Ke/K
1.10
1.00
0.90
MOTION
100
200
400
600
800
1000
2000
4000
N ray

FIGURE 33

Ke/K V.S. RAYLEIGH NUMBER

FOR FLUIDS IN AN ANNULAR LAYER AT VARIOUS INCLINATIONS

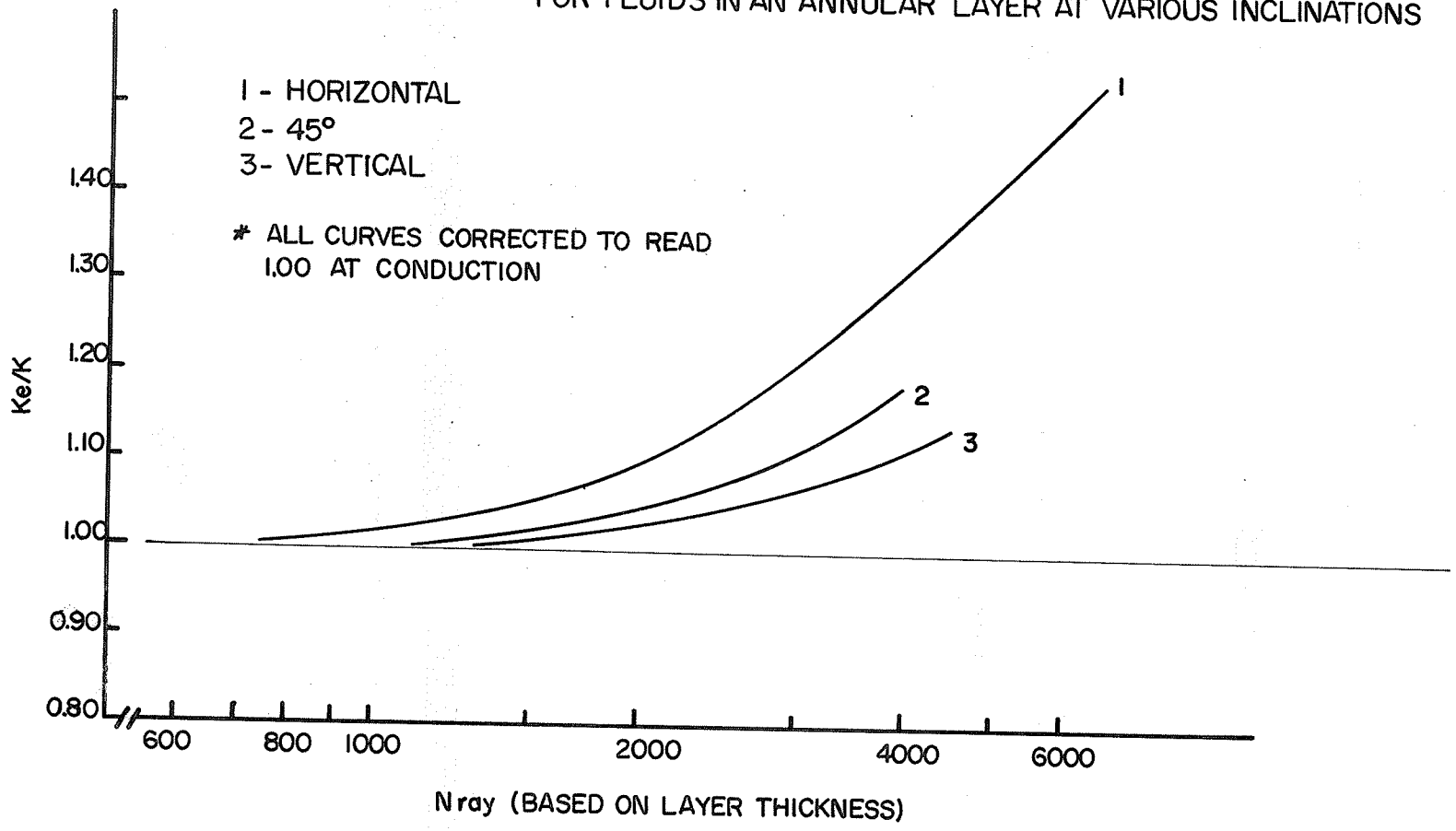

DISCUSSION OF RESULTS AND ERRORS

6.1 Annular Layer 0.28" Thick

The most significant results were obtained with glycerine in the 0.28" annular layer. These results covered the pertinent Rayleigh number range, 400 - 3,000, where the effect of convection and heat flow was first noticeable. The Rayleigh number was varied in two ways. Firstly, the heat input was varied which in turn changed the temperature difference across the fluid layer (Δt changed from $10^{o}F$ to $30^{o}F$). Since the Rayleigh number is directly proportional to the Δt, this changed the Rayleigh number by a factor of three. Secondly, the value of the fluid properties, Z, varied with the change in the mean temperature of the fluid layer (Z changed from 2.0 to 5.0). This method varied the Rayleigh number by 2.5 times. Therefore, the Rayleigh number for glycerine in this gap could be changed by a factor of 7.5 times by temperature and heat input control.

The error in the calculation of the Rayleigh number and the equivalent thermal conductivity (90 % certainty) was $\pm$15.7% and $\pm$11.8% respectively (Appendix G). The significant error, sometimes called precision, is an indication of the scatter likely to be found in the results, and for the equivalent thermal conductivity calculation was $\pm$4.7%. The absolute error in the thermal conductivity calculation can be reduced to the significant error by calibrating the apparatus with a liquid whose thermal conductivity is known. It may be noted here, that several different means of

obtaining the temperature difference were tried. That is, instead of averaging all the temperatures on each surface, different combinations of thermistor readings were tried. The value of the equivalent thermal conductivity calculation was dependent on the thermistor combination, but the resulting curves showed the same trends. For example, the value in the vertical position was always 10% lower than the 45° position in the conduction regime.

Horizontal Position

The most significant problem encountered in this position was the poor temperature distribution, FIGURE 35. The temperature distribution on the heater cylinder was quite uniform on any particular circumference, but the outer glass cylinder temperature was not uniform. As was expected the top surface of the glass cylinder was hotter than the bottom because of the characteristic flow in horizontal annular layers, FIGURE 7. The fluid is warmed as it rises past the heater surface towards the top of the glass cylinder and then moves downward along the glass cylinder. Finally, the cooled liquid comes to the bottom which leads to the cooler glass surface temperature at the bottom. A fan system was necessary to increase the heat transfer from the outside surface of the glass cylinder, and it was altered to offset this radially eccentric temperature distribution by increasing the heat transfer from the glass cylinder on the warmer portion. The situation was impossible to correct completely. This problem will always be inherent in a

system such as this in which the cylinders do not have enough heat capacity to form a heat sink and thus prevent temperature gradients.

Because a concentric temperature distribution was assumed in the derivation of the conduction heat transfer equation used to calculate the equivalent thermal conductivity (Appendix B), a correction was applied to allow for temperature eccentricity (Appendix B).

An axial temperature gradient was also encountered, FIGURE 35. Because guard heaters were omitted from the stabilizing end sections, the absolute temperature and the temperature difference across the gap were expected to decrease at the ends due to heat being lost by conduction through the end plates. This situation was true for one end, but at the other end, the absolute temperature remained constant or increased and the temperature difference increased. It was presumed that the heater was not uniformly wound with a smaller coil pitch at the constant temperature end than at the end where the temperature decreased. The effect of the axial gradient on the flow patterns and on the equivalent thermal conductivity was assumed to be small in the test section for the horizontal case.

Below a Rayleigh number of 600 convective motion disappeared and the heat transfer must therefore be by conduction alone. The Ke/K ratio should be one but FIGURE 29 indicates the curve to be low by 4%. One possible explanation for the results being low by 4% is that the heater output was not uniform as was discussed previously. In calculating Ke, the heat flux was calculated by dividing the

total heat input by the length; if the heater output, on an average, was higher in the test section than in the stabilizing end sections, a higher temperature difference would occur producing a lower equivalent thermal conductivity. Tests were conducted using a thermocouple probe to verify that lower temperatures were present toward the ends but it was not known if this result was due to lower heat outputs at the end sections or heat losses through the end plates.

If it is assumed that all the points for glycerine in the 0.28" layer are low by 4% and if 4% is added to all the results the resultant curve would show the abrupt increase from Ke/Ke = 1, at approximately N_{RAY} = 1000. This is the same Rayleigh number at which motion was first detected visually. Convective motion became quite significant at a Rayleigh number of 3000. The heat transfer by convection is 22% (4 + 18) of the heat transfer by conduction alone.

Vertical Position

Again as in the horizontal position, poor temperature distribution was the main problem, FIGURE 36. The fan system and the eccentricity of the heater cylinder produced a radially eccentric temperature distribution for which the application of a correction factor was considered necessary in calculating Ke (Appendix B). However, because of the limited number of thermistors in a single circumferential plane a complete radial temperature distribution could not be determined (temperatures measured on one diameter only).

This unsymmetrical temperature distribution was assumed to have little effect on the fluid flow, but a temperature rise along the vertical axis was thought to have a marked effect on the flow.

The air cooling system was set up to combat the higher temperatures at the top but even with a uniform axial temperature on the outside cylinder, the inside heater cylinder temperature increased with height. Although this rise of temperature is normal for vertical layers, the situation was aggrevated because the heater had a higher heat output at the upper end (as discovered by the temperature distribution in the horizontal case). The effect of the temperature rise would be to reduce the rate of acceleration of the upward flow adjacent to the surface of the inner cylinder.

The Rayleigh number at which free convection has a significant affect on the heat flow is not clearly defined. At a Rayleigh number of 3000 the Ke/K value is at least 10% above the value at N_{RAY} = 400 and it would appear then that 10% of the heat is being transferred by convection. FIGURE 30 shows an increase of Ke/K at a Rayleigh number of 1000 and then a decrease up to a Rayleigh number of 2500. It is felt that the accuracy of the equivalent thermal conductivity measurement is not sufficient to justify any statement of this trend since the variance is only at most 6% and the scatter is $\pm$6%.

The low values of Ke/K (0.90 instead of 1.00) at the low Rayleigh number shows the inaccuracy of the equipment for heat transfer determinations. As discussed in this problem for the

horizontal position, non-uniform heater output may be the problem with the situation being aggravated with the apparatus in the vertical position. Also a possible error may be the eccentric temperature distribution which could not fully be explored because of the limited number of temperature sensing devices.

Inclination 45^{o} to the Vertical Position

The temperature distribution for this position was very difficult to ascertain. Because of the inclination, the thermistors were not on any one plane and the temperature distribution could not be analyzed. The inclination of the heater appeared to offset the eccentricity problem encountered in the other two positions, and the temperature differences showed very little error due to eccentricity. In fact, the error was so small that it was neglected. The Ke/K ratio was very close to one which appears to confirm the theory that the eccentricity problem was largely responsible for the Ke/K ratio being low in the horizontal and vertical positions.

Motion was always present in this case but convective heat transfer did not become appreciable until a Rayleigh number of 1000.

6.2 Annular Layer 0.125" Thick

The Rayleigh number range investigated by use of water and glycerine did not cover the pertinent portion of the curve as well as glycerine for the 0.28" layer. However, the results verify the trends shown earlier.

The error in the calculation of the Rayleigh number and the equivalent thermal conductivity was ±25.2% and ±12.5% respectively (Appendix G). The significant error was calculated to be ±5.7%.

Horizontal Position

With glycerine, motion was non-existent up to the maximum Rayleigh number attained (300). The value of Ke/K checked closely with the accepted value of one for conduction except at very high heat input (60 watts) which showed values high by 9%. The Ke/K values for water in this annular layer were also tested at a high power input (80 watts) in order to give a readable Δt, and the corresponding Ke/K values also appeared high (10%) as compared to the results from the 0.28" annular layer.

Vertical Position

Convective fluid motion was found to occur in the 0.125" layer in the vertical position. The motion began at a Rayleigh number of 150. It would appear that the Rayleigh number based on layer thickness is not the criterion for motion in vertical annular layers since motion appeared in the same fluid at two different Rayleigh numbers in two different layer thicknesses. In fact, the ratio of the layers ($\frac{0.28}{0.125} = 2.2$) is approximately the same as the ratio of the Rayleigh numbers at which motion began in their respective annular layers ($\frac{400}{150} = 2.7$). By modifying the Rayleigh numbers by $(H/L)^{1.25}$, a new dimensionless number is formed having

approximately the same absolute value when motion begins in either the 0.28" or the 0.125" annular layer. Therefore, for a vertical annular layer the dimensionless parameter for the onset of convective fluid motion would appear to be $\Phi\left(\frac{g_c \beta \Delta t L^3}{\nu^2} \times \frac{\mu C_p}{K} (H/L)^n\right)$ where $0 < n < 3$. This parameter would likely also govern the heat transfer in this region.

The heat transfer property Ke/K followed the trend of the 0.28" annular layer of being 10% low, and the results for water as in the horizontal case appear 10% higher than the other results.

Inclination 45° to the Vertical Position

The 45° position appears to be a compromise between the two previous cases. Fluid motion began at a Rayleigh number of 300 indicating this position shows some dependence on the layer height as in the vertical position, but because the motion has been partially suppressed by the small layer thickness, a more probable dimensionless number to indicate the point of convective fluid motion is $\Phi\left(\frac{g_c \beta \Delta t L^3}{\nu^2} \times \frac{\mu C_p}{K} (D_o/D_i)^p (H/L)^r\right)$. As before, the high heat input tests have increased the Ke/K ratio by 10%.

6.3 Air in the 0.125" Thick Annular Layer

Air was used in the 0.125" annular layer in an attempt to study the temperature distribution. Because of air's low thermal conductivity, large temperature differences across the layer were possible with low heat inputs. Although no evidence of movement

was seen when smoke was introduced into the layer ($N_{RAY} < 90$), the temperature distribution changed with position. The Δts were smallest for the horizontal case and largest for the vertical case. It was concluded that the distribution was not, therefore, a function of the fluid motion but of the cell position only. Also, the Ke/K values were all higher than the other results, which was assumed to be due to the added heat transfer by radiation. A correction factor was applied (Appendix B), and the corrected results followed the trends set by the other fluids.

6.4 Summary of Results

Convective heat transfer in the vertical and the 45^{o} position is not as dependent on the Rayleigh number as the horizontal case. Convective motion in the vertical and in the 45^{o} position began before the horizontal position, but the convective heat flow became appreciable at the same Rayleigh number (1000). Also, the curve of Ke/K rose much more quickly in the horizontal case, see FIGURE 33, which indicates a more rapid increase in the percentage of heat transferred by convection in the horizontal position.

For the horizontal case, convective fluid motion and convective heat transfer began simultaneously at $N_{RAY} = 1000$. The error in the absolute value of this Rayleigh number is large ±25%, and the difference in the Rayleigh number for convective fluid motion and for convective heat transfer is of similar magnitude. The error in determining the point of convection from FIGURE 29 being ±300 or ±30%.

Convective fluid flow for the vertical and for the 45^{o} position do not appear to be solely dependent on the Rayleigh number. In fact, the following dimensionless numbers appear more realistic:

vertical $\quad N_{GRL} \times N_{PR} \, (H/L)^{n}$

45^{o} position $\quad N_{GRL} \times N_{PR} \, (D_o/D_i)^{p} \, (H/L)^{r}$

FIGURE 35
TEMPERATURE DISTRIBUTION IN
0.28 ANNULAR HORIZONTAL LAYER
TEST NO. 105 B
Nray = 1700 Ke/K = 0.99

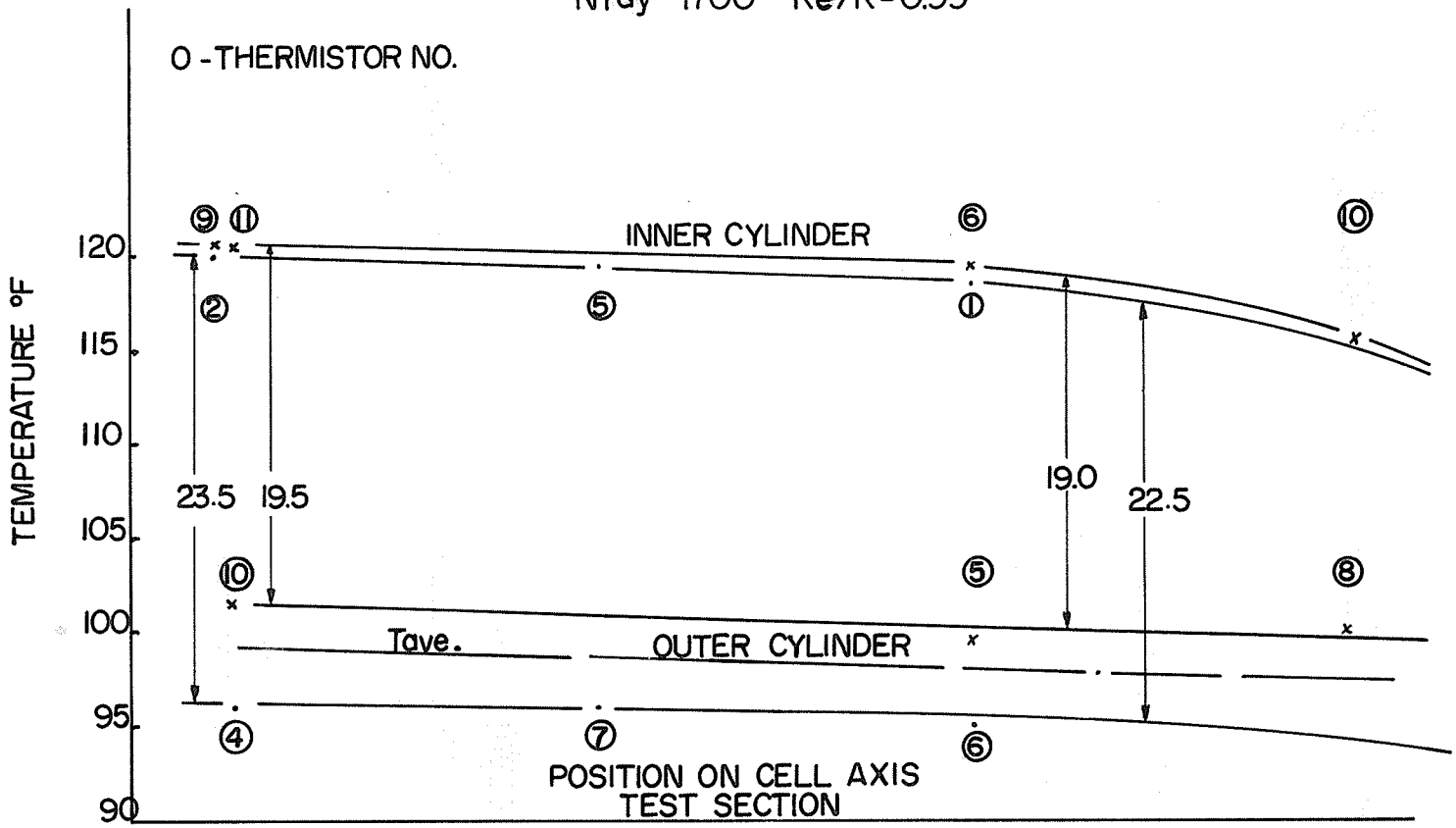

FIGURE 36

TEMPERATURE DISTRIBUTION IN 0.28" ANNULAR VERTICAL LAYER

TEST NO. 6B

Nray = 2800 Ke/k = 0.93

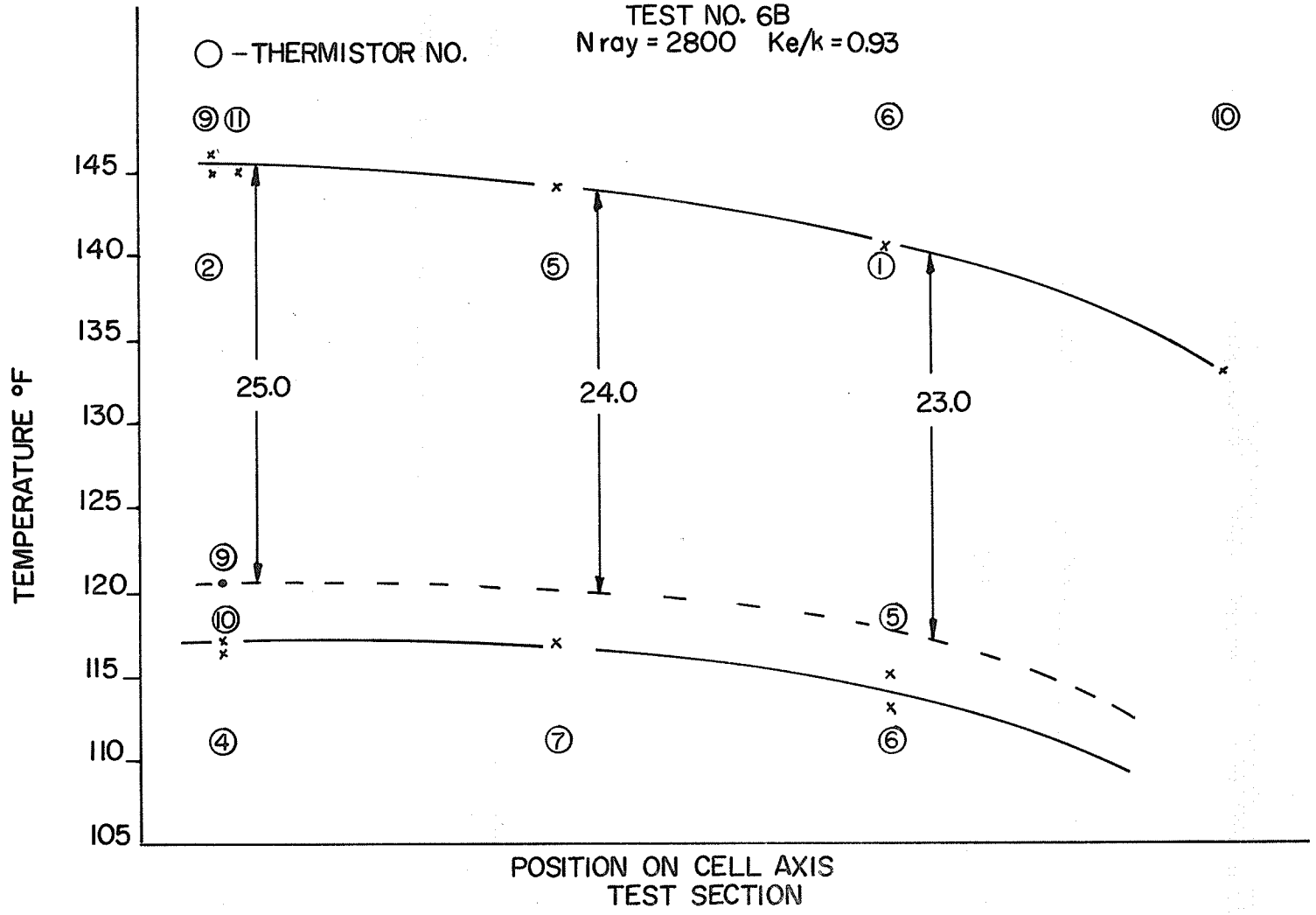

CONCLUSIONS AND RECOMMENDATIONS

7.1 Conclusions

For horizontal concentric cylinders the Rayleigh number based on the layer thickness is a suitable parameter for the convection point - the point of convective fluid flow and the point of convective heat flow.

For horizontal concentric cylinders, both convective heat flow and convective fluid flow begin at the same Rayleigh number, ($\pm$30% because of the inaccuracies in the calculation of the Ke/K ratio). The Rayleigh number for convective fluid flow being 1000 $\pm$25%, (by observation).

For vertical concentric cylinders and any angle to the vertical, the Rayleigh number based on the layer thickness is not a reliable parameter for convective fluid flow when the H/L ratio is large (over 100). The layer length must be considered. The equations for heat transfer proposed by Eckert and Carlson, and Batchelor (No. 2.16, 2.13, 2.14 and 2.15) for vertical plane layers use the Rayleigh number based on the layer thickness and modify it with an H/L ratio. This experimentation would indicate this approach for the fluid flow convection point also.

7.2 Recommendations

In order to ascertain the effect of fluid flow on the heat transfer more detailed studies must be undertaken. For example, in the vertical position the sensitivity must be $\pm$1% or better since

the increased heat transfer by convection is very small (3% from conduction to N_{RAY} of 2000), and also because a discrepancy was found in that the apparent thermal conductivity decreased when convection appeared (N_{RAY} of 1500).

It is recommended that for better accuracy larger cylinder diameters should be used. The diameter accuracy would be the same but the increased metal on the inner cylinder would give more stiffness reducing the eccentricity error and would reduce the temperature gradients. The outer cylinder's temperature stability could be increased and temperature gradients could be decreased by a surrounding clear liquid layer. The liquid, such as water, would allow visual observation but would form a heat sink. Also by obtaining a liquid of the correct index of refraction, the problem of taking pictures through curved surfaces is reduced.

For the measurement of thermal conductivity using an annular layer, the recommendations depend on the accuracy required. For results within 5%, the vertical axis position is preferred since the heat transfer by convection is well within the accuracy of the results for Rayleigh numbers up to 2000. For very accurate results in which all convection must be eliminated the horizontal case is recommended. The fluid convection point in the horizontal case is more distinct and thus convective heat transfer can be entirely avoided by keeping the Rayleigh number below this point.

The maximum Rayleigh number in the horizontal case is much less than the 2000 of the vertical case, however, the onset of convection is more clearly defined for this case. The curve for the horizontal case meets the Ke/K = 1.00 line sharply while the curve for the vertical case is asymptotic to the Ke/K = 1.00.

BIBLIOGRAPHY

1. Schmidt, E., and Silveston, P. L., "Natural Convection In Horizontal Liquid Layers", Chemical Engineering Progress Symposium Series, Heat Transfer Section, Chicago, No. 29, Vol. 55, p. 163.

2. Eckert, E. R. G., and Carlson, W. O., "Natural Convection In An Air Layer", International Journal Of Heat Transfer, Vol. 2 (1961), p. 106.

3. Hsu, S. T., Engineering Heat Transfer, D. Van Nostrand Co., Princeton, 1963.

4. King, W. J., "The Basic Laws And Data Of Heat Transfer", Mechanical Engineering, Vol. 54 (1932), p. 347.

5. Jakob, M., "Free Convection Through Enclosed Plane Gas Layers", Transactions Of The A.S.M.E., Vol. 68 (1946), p. 189.

6. Rayleigh, Lord, "On Convection Currents In A Horizontal Layer Of Fluid When The Higher Temperature Is On The Underside", Philosophical Magazine, Vol. 32 (1916), p. 529.

7. Jeffreys, H., "Some Cases Of Instability In Fluid Motion", Proceedings Of The Royal Society (London), A118 (1928), p. 195.

8. Low, A. R., "On The Criterion For The Stability Of A Layer Of Viscous Fluid Heated From Below", Proceedings Of The Royal Society, A125 (1929), p. 180.

9. Ostrach, S., "Convection Phenomena In Fluid Heated From Below", Transactions Of The A.S.M.E., Vol. 79 (1957), p. 299.

10. Saunders, O. A., and Schmidt, R., "On The Motion Of A Fluid Heated From Below", Proceedings Of The Royal Society, A165 (1938), p. 216.

11. Sutton, O. A., "On The Stability Of A Fluid Heated From Below", Proceedings Of The Royal Society, A204 (1951), P. 297.

12. Malkus, O., "Discrete Transitions In Turbulent Convection", Proceedings Of The Royal Society, Vol. 225 (1954).

13. Chandra, K., "Instabilities Of Fluids Heated From Below", Proceedings Of The Royal Society, A164 (1938), p. 231.

14. Eckert, E. R. G., and Drake, R. M., Introduction To The Transfer Of Heat And Mass, McGraw-Hill, second edition, 1959.

15. Fishenden, M., and Saunders, O. A., An Introduction To Heat Transfer, Clarendon Press, 1950.

16. De Graaf, J. G. A., and Van Der Held, E. F. M., "Relation Between Heat Transfer And Convection Phenomena In Enclosed Plane Air Layers", Applied Scientific Research, A3, No. 6 (1953), p. 393.

17. Batchelor, G. K., "Heat Transfer By Free Convection Across A Closed Cavity Between Vertical Boundaries At Different Temperatures", Quarterly Of Applied Mathematics, Vol. 12 (1954), p. 209.

18. Carlson, W. O., "Interferometer Studies Of Convective Flow Phenomena In Vertical, Plane Enclosed Air Layers", Ph.D. Thesis, University of Minnesota, 1956.

19. Jakob, M., Heat Transfer, John Wiley and Sons, 1949.

20. Liu, C., Mueller, W. K., and Landis, F., "Natural Convection Heat Transfer In Long Horizontal Cylindrical Annuli", International Developments In Heat Transfer, Boulder, 1961, p. 976.

21 Crawford, L., and Lemlich, R., "Natural Convection In Horizontal Concentric Cylindrical Annuli", Industrial And Engineering Chemistry Fundamentals, No. 1 (1962), p. 260.

22. Taylor, G. I., "Stability Of A Viscous Fluid Contained Between Two Rotating Cylinders", Philosophical Transactions Of The Royal Society (London), 223A (1923), p. 289.

23. Walowit, J., Tsao, S.,and Di Prima, R. C., "Stability Of Flow Between Arbitrarily Spaced Concentric Cylindrical Spaces Including The Effect Of A Radial Temperature Gradient", Transactions Of The A.S.M.E., Vol. 86 (1964), p. 585.

24. McAdams, W. H., Heat Transmission, McGraw-Hill, third edition, 1954.

25. Emery, A., and Chu, N. C., "Heat Transfer Across Vertical Layers", Transactions Of The A.S.M.E., Vol. 87 (1965), p. 111.

26. Kraussold, H., "Warmeabgabe Von Zylinderischen Flussigkeits", Forschung Auf Gebiete Ingenieurwesens, Vol. 5 (1934), p. 186.

27. Kreith, F., Principles Of Heat Transfer, International Textbook Co., Scanton, 1958.

28. Cox, L., "An Experimental Investigation Of The Onset Of The Effects Of Natural Convection On Heat Transfer Through Vertical Annular Layers Of Liquid", M.Sc., Thesis, University Of Manitoba, 1966.

29. Tyrrel, H. I. V., Diffusion And Heat Flow In Liquids, Butterfield Press, London, 1961.

APPENDIX A

DIMENSIONAL ANALYSIS OF HEAT TRANSFER IN AN ENCLOSED ANNULAR SPACE

APPENDIX A

DIMENSIONAL ANALYSIS OF HEAT TRANSFER IN AN ENCLOSED ANNULAR SPACE

Variables	Symbol	Dimensions (MLΘT)*
Total heat flow	Q	ML^2/Θ^3
Temperature difference	Δt	t
Layer thickness	L	L
Layer height	H	L
Inside diameter	D_i	L
Coefficient of expansion	β	$1/t$
Viscosity	μ	$M/L\Theta$
Density	ρ	M/L^3
Specific heat	c_p	$L^2/\Theta^2 t$
Thermal conductivity	K	$ML/\Theta^3 t$
Acceleration of gravity	g_c	L/Θ^2
Proportionality constant	ϕ	None
Dimensionless group	Π	None
Constant	π	None

---

* M - mass
L - length
Θ - time
t - temperature

$$Q = \Phi \left[\Delta t^a,\ L^b,\ H^c,\ D_i{}^d,\ \beta^e,\ \mu^f,\ \rho^g,\ c_p{}^h,\ K^i,\ q_c{}^j \right]$$

$$\frac{ML^2}{\Theta^3} = \Phi\left[t^a,\ L^b,\ L^c,\ L^d,\ \frac{1}{t^e},\ \frac{M^f}{L^f\Theta^f},\ \frac{M^g}{L^{3g}},\ \frac{L^{2h}}{\Theta^{2h}t^h},\ \frac{M^iL^i}{\Theta^{3i}t^i},\ \frac{L^j}{\Theta^{2j}} \right]$$

ΣM - $1 = f + g + i$

ΣL - $2 = b + c + d - f - 3g + 2h + i + j$

$\Sigma \Theta$ - $-3 = -f - 2h - 3i - 2j$

Σt - $0 = a - e - h - i$

$f = 1 - g - i$

$j = 3/2 - f/2 - h - 3i/2 = 3/2 - 1/2 + g/2 + i/2 - h - 3i/2$

$= 1 + g/2 - h - i$

$e = a - h - i$

$b = 2 - c - d + f + 3g - 2h - i - j$

$$Q = \Phi \left[L^2\ (H/L)^c\ (D_i/L)^d\ (\beta\Delta t)^a \left(\frac{L^{3/2}\rho q_c^{1/2}}{\mu}\right)^g \left(\frac{c_p}{L\beta q_c}\right)^h \left(\frac{K}{L\beta\mu q_c}\right)^i \mu q_c \right]$$

Dimensionless Groups

$$\Pi_1 = L^2 \mu q_c$$

$$\Pi_2 = \beta \Delta t$$

$$\Pi_3 = H/L$$

$$\Pi_4 = D_i/L$$

$$\Pi_5 = \frac{L^{3/2}\rho q_c^{1/2}}{\mu}$$

$$\Pi_6 = \frac{c_p}{L\beta q_c}$$

$$\Pi_7 = \frac{K}{L\beta\mu q_c}$$

$$\Pi_5^2 \times \Pi_2 = \frac{L^3 g_c \rho^2}{\mu^2} \times \beta \Delta t \equiv N_{GRL}$$

$$\frac{\Pi_6}{\Pi_7} = \frac{C\rho}{L\beta g_c} \times \frac{L\beta\mu g_c}{K} \equiv N_{PR}$$

$$\Pi_1 \times \Pi_2 \times \Pi_3 \times \Pi_4 \times \Pi_7 = L^2 \mu g_c \times \beta \Delta t \times H/L \times D_i/L \times K/L\beta\mu g_c$$

$$= \frac{K \Delta t}{L} \times \frac{H D_i 2\pi}{2\pi}$$

New Grouping of Dimensionless Groups

$$Q = \frac{\Phi}{2\pi} \overset{*}{\int} \left[N_{GRL}, N_{PR}, \frac{K \Delta t}{L}, H D_i 2\pi, \frac{H}{L}, \frac{D_i}{L} \right]$$

$$\frac{Q L}{K \Delta t \times 2\pi H D_i} = \Phi \int \left[N_{GRL}, N_{PR}, \frac{H}{L}, \frac{D_i}{L} \right]$$

$$\frac{hL}{K}^{**} = N_{NU} = \Phi \int \left[(N_{GRL}) \quad (N_{PR}) \quad \left(\frac{H}{L}\right) \left(\frac{D_i}{L}\right)^r \right]$$

---

* Symbol for "mathematical expression of"

** $h = \frac{Q}{\Delta t \ 2\pi \ HD_i}$, for concentric cylinders where h is the coefficient of heat transfer between a surface and a fluid.

APPENDIX B

DERIVATION OF THE STEADY STATE CONDUCTION HEAT TRANSFER EQUATION IN AN ANNULAR SPACE

APPENDIX B

DERIVATION OF THE STEADY STATE CONDUCTION HEAT TRANSFER EQUATION IN AN ANNULAR SPACE

The heat flow in this experimental work was calculated using Ke, the equivalent thermal conductivity, where Ke is defined by the applicable heat conduction equation. The heat conduction equation for annular spaces will be derived and all assumptions and errors explained.

1. The general heat conduction equation in cylindrical co-ordinates without internal heat generation is stated as follows:

$$\frac{1}{r}\frac{\partial}{\partial r}\left(\frac{r\partial t}{\partial r}\right) + \frac{1}{r^2}\left(\frac{\partial^2 t}{\partial \Theta^2}\right) + \frac{\partial^2 t}{\partial Z^2} = \frac{1}{\alpha}\frac{\partial t}{\partial T}$$

Z - direction perpendicular to radius
r - radius

t - temperature

T - time

Θ - angular position

α - coefficient of thermal diffusivity

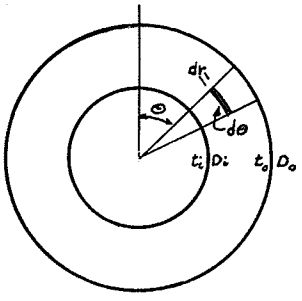

ANNULAR ELEMENT

If the temperature at D_i and D_o are kept at t_i and t_o respectively and if the temperature is constant axially irrespective of annular position; the solution for the temperature is the following:

$$t = \frac{t_i \ln(D_o/2r) + t_o \ln(2r/D_i)}{\ln(D_o/D_i)} \qquad D_i < r < D_o$$

Using the Fourier Law for heat flow and assuming a constant K:

$$Q = - KA \frac{dt}{dx} = - 2\pi r L K \frac{dt}{dr} = \frac{2\pi L K (t_i - t_o)}{\ln(D_o/D_i)}$$

A - area perpendicular to the temperature gradient

x - dimension parallel to the temperature gradient

L - element length

2. Non-uniform Surface Temperature Correction

In order to ascertain the error expected due to a non-uniform temperature distribution several flux plots were drawn with varying surface temperatures. The following diagram is an example of one of these plots.

$$\frac{Q}{A} = K \frac{N}{M} \Delta t$$

N - number of flow lanes

M - equal temperature increments

Δt - temperature difference across the fluid layer

Concentric Flux Plot

Eccentric Flux Plot

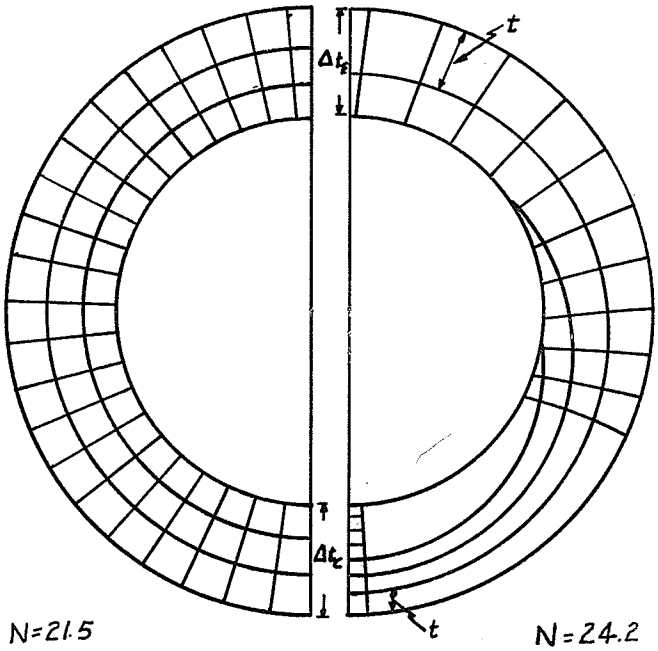

Concentric and Eccentric Temperature Profile Flux Plots

For the concentric temperature case

$$Q_C = K_C \frac{21.5}{3} \times \Delta t_C$$

For the eccentric temperature case

$$Q_E = K_E \frac{24.2}{2} \times \Delta t_E$$

Making the Δt across the concentric case (Δt_C) equal to the mean Δt across the eccentric case (Δt_E), that is $\Delta t_C = \frac{2t + 7t}{2} = 4.5t$, and setting the amount of heat transferred equal, the error in the thermal conductivity calculated on the concentric case using the eccentric mean temperature can be calculated:

$$\frac{Q_C}{Q_E} = 1 = \frac{K_C}{K_E} \times \frac{7.13}{12.1} \times \frac{4.5t}{2t}$$

$$K_C/K_E = 1.33 = K_{error}$$

The parameter for this case was taken as the difference between the large $\Delta t(\Delta t_L)$ and the small $\Delta t(\Delta t_S)$ divided by the mean $\Delta t(\Delta t_M)$.

$$\frac{\Delta t_L - \Delta t_S}{\Delta t_M} = \frac{7t - 2t}{4.5t} = 1.1$$

These calculations were repeated for several different eccentric temperature distributions using the appropriate flux plot for each case. FIGURE B-1 shows the resulting curve (approximated by a straight line) of the correction factor, K_{error}, versus the temperature ratio parameter. This curve then provided a simple method for correcting the thermal conductivity of the eccentric temperature distribution case when it was calculated on the mean temperature difference across the annual gap.

3. Radiation Correction

A radiation correction is necessary if the fluid in the cell is a gas, i.e. air. The equation for radiation heat flow between concentric cylinders is as follows:

$$Q_r = \frac{\sigma}{1/\epsilon_i + A_i/A_o(1/\epsilon_o - 1)} \times \left(t_i^4 - t_o^4\right)$$

t - °R

ϵ_o - glass = 0.90

ϵ_i - stainless steel $\approx$ 0.10

A_i/A_o - ≈ 1

σ - Stefan-Boltzmann constant

$$Q_r = \frac{0.173}{1/.90 + 1/0.10 - 1} \times \left[\left(\frac{t_i}{100}\right)^4 - \left(\frac{t_o}{100}\right)^4\right] \frac{BTU}{hr.\ ft^2}$$

FIGURE B-2 shows the heat transferred by radiation (calculated from the above equation) versus the temperature difference across the fluid layer. This value was subtracted from the total heat input to

give the heat transferred by conduction alone (for the case using air only). Because the radiation correction was small, at most the radiation heat transfer was 13% of the total heat transfer, the correction was not studied too extensively; therefore, the boundary surface emissivities were taken from tables in reference 14.

FIGURE B-1

ECCENTRIC TEMPERATURE DISTRIBUTION CORRECTION

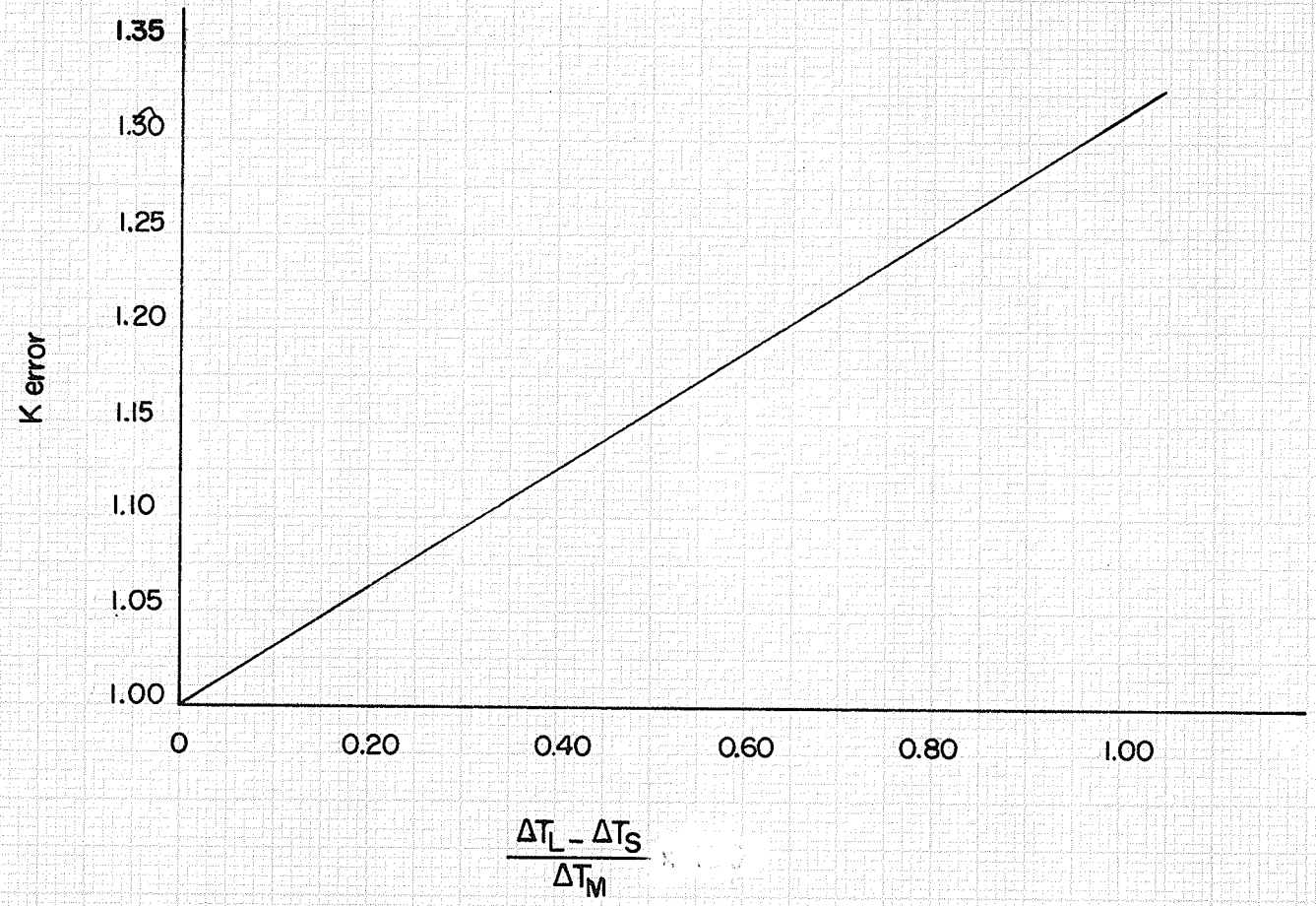

FIGURE B-2
RADIATION CORRECTION

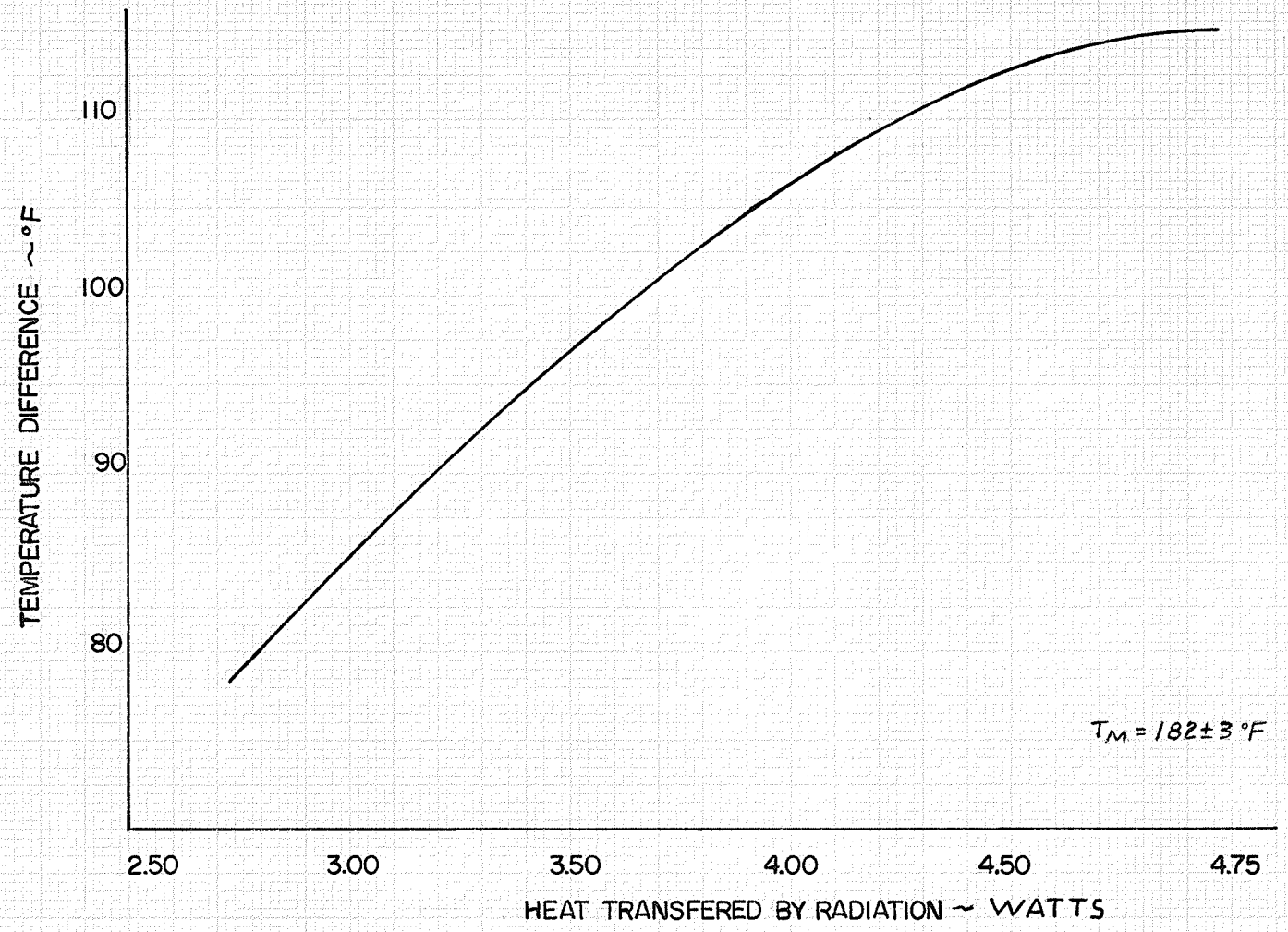

APPENDIX C

APPARATUS CONSTRUCTION DETAILS

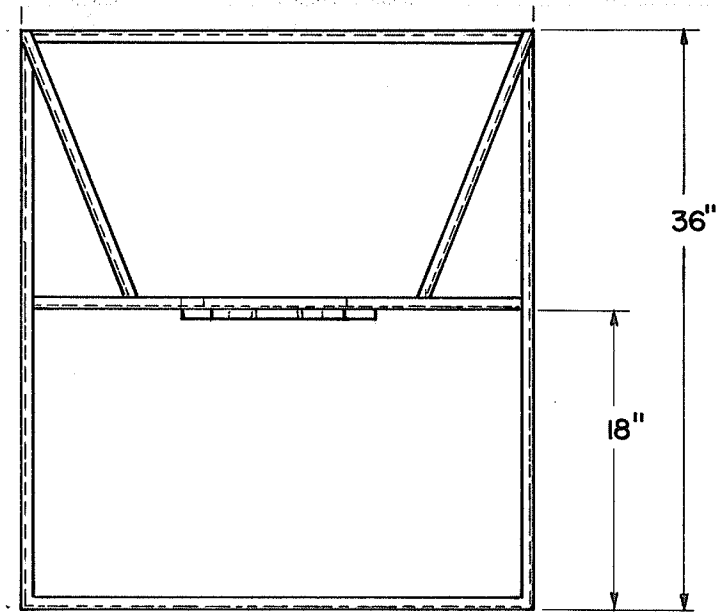

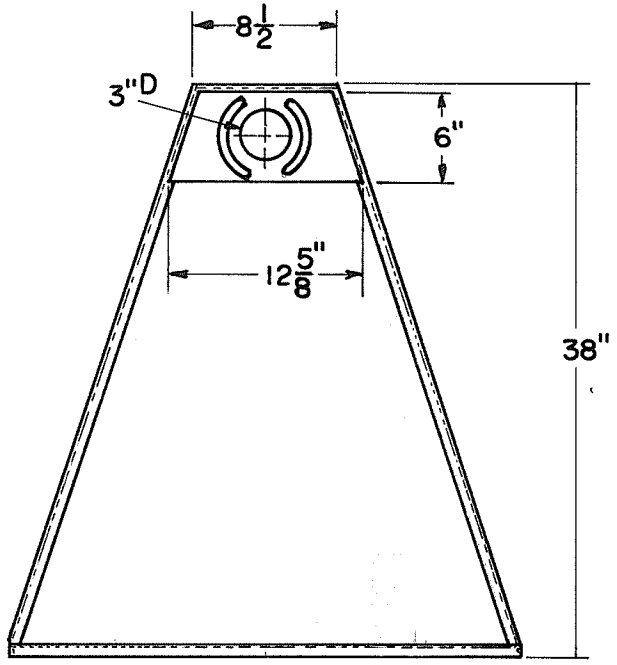

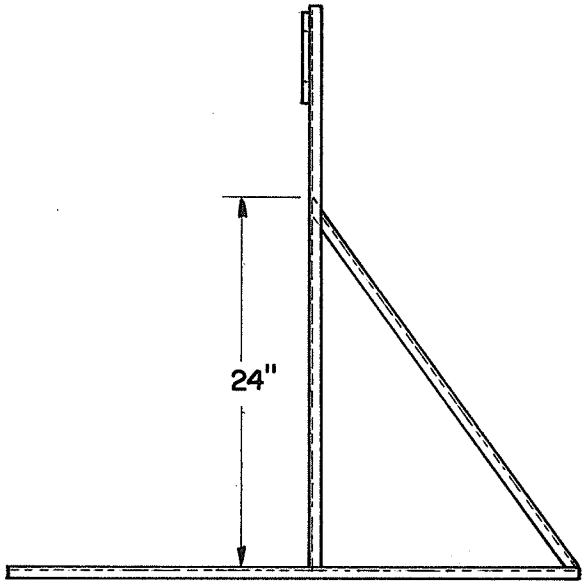

FIGURE C-1
STAND DETAILS

MATL: 2"x2"x1/4" ANGLE IRON
SCALE: 1" = 12"

FIGURE C-2 ROTATING HEAD DETAILS

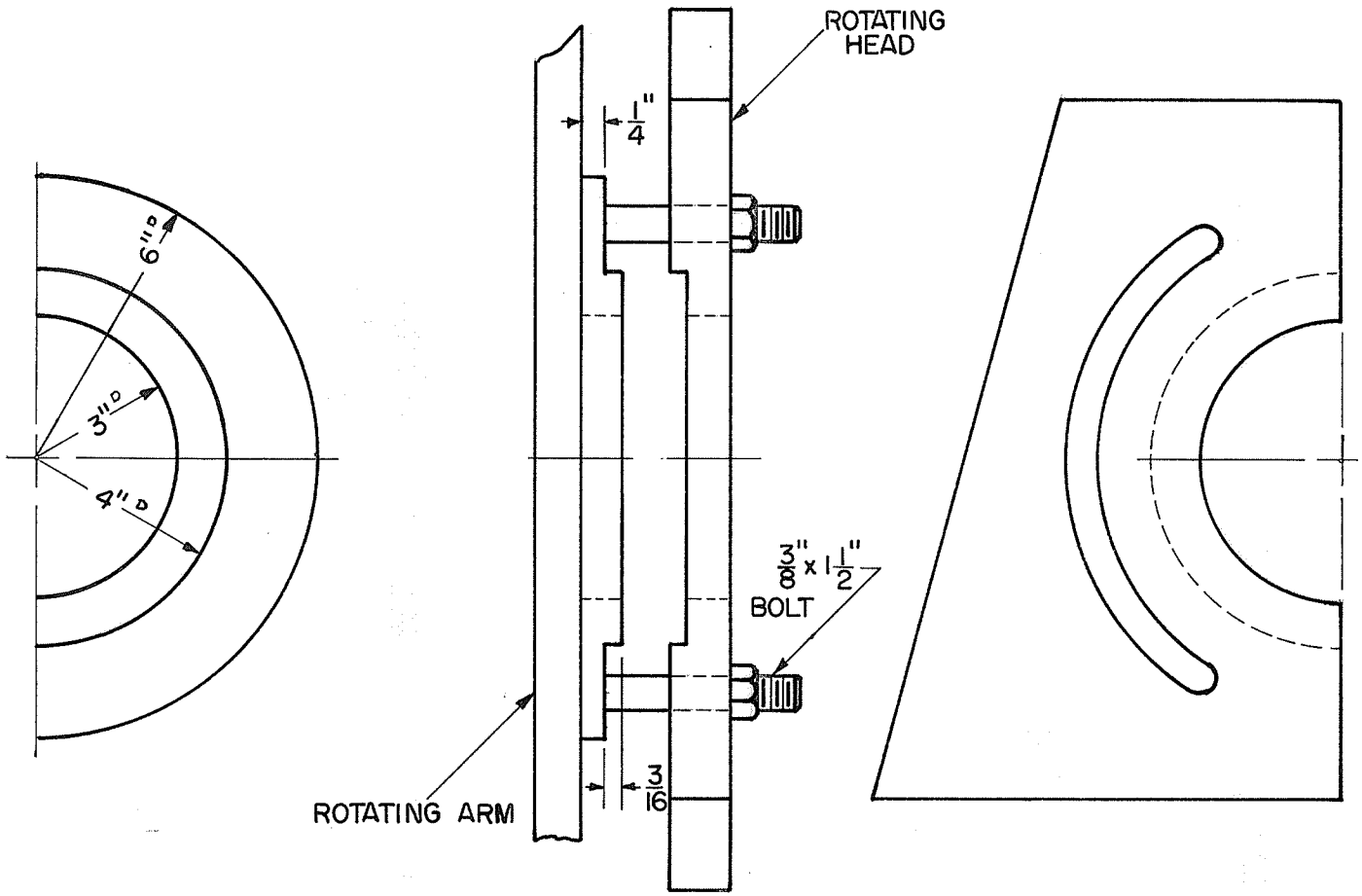

FIGURE C-3
HEATER DETAILS

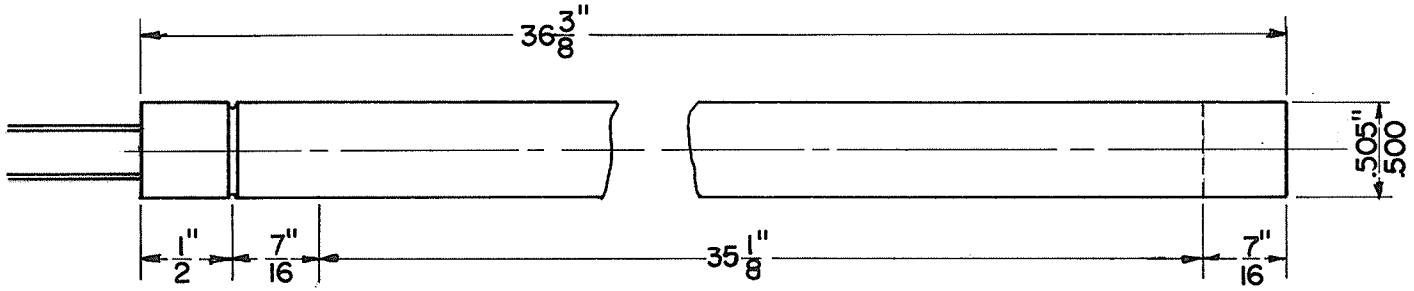

SHEATH — INCONEL .032" WALL
MAGNESIUM OXIDE INSULATION
HEATED LENGTH — 35 1/8" ± 1/8"

FIGURE C-4

END PLATE CONSTRUCTION

MOVABLE END

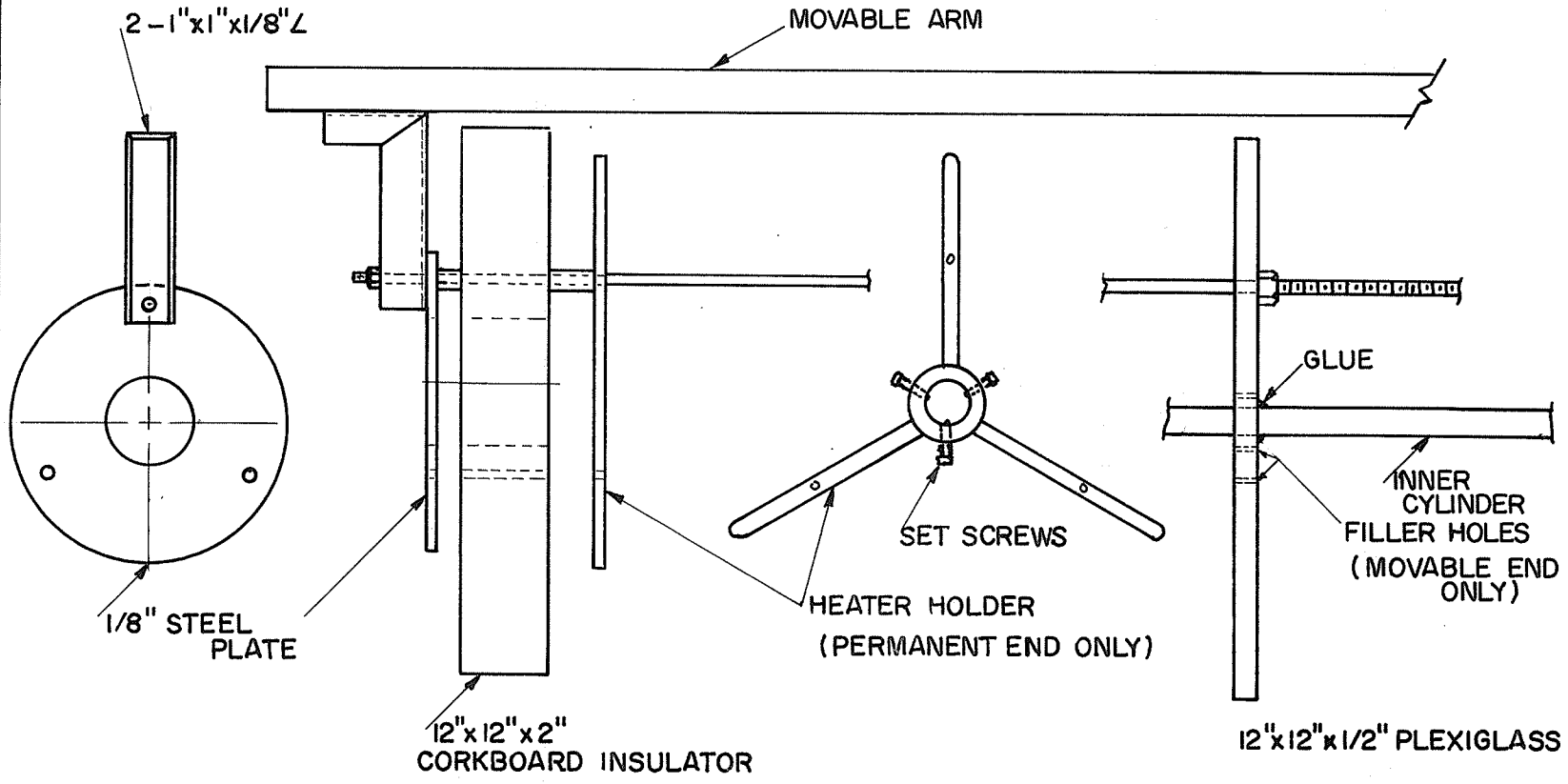

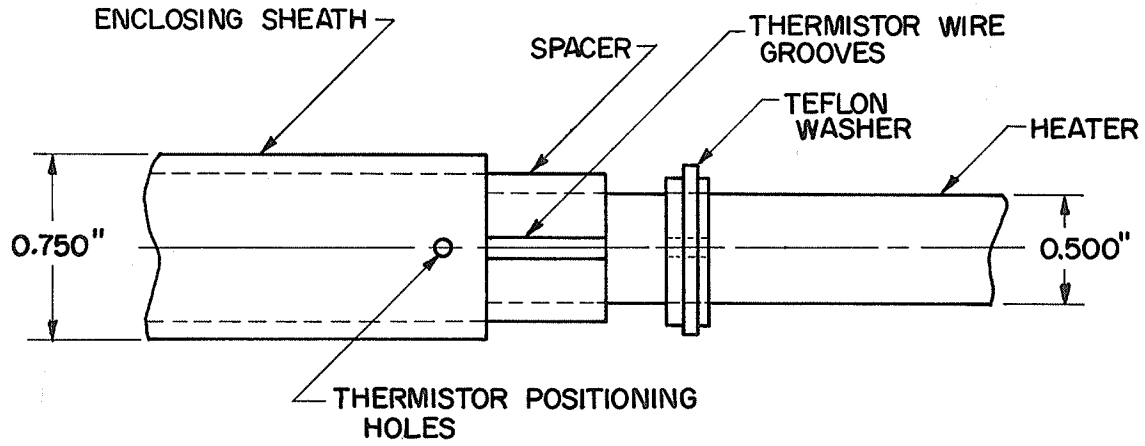

FIGURE C-5
INNER CYLINDER CONSTRUCTION

FIGURE C-6 GUARD SECTION DETAILS

ENCLOSING SHEATHS

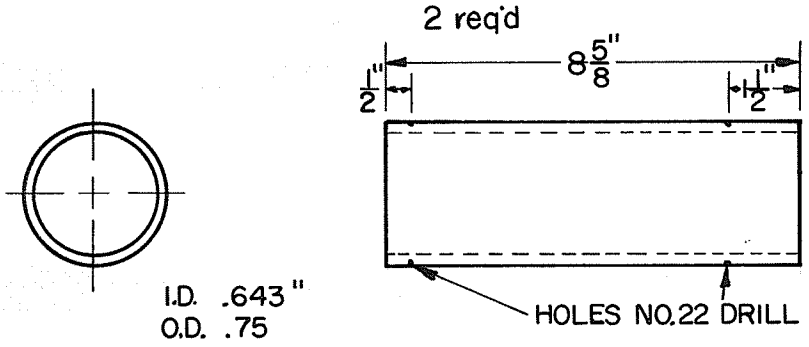

SPACERS

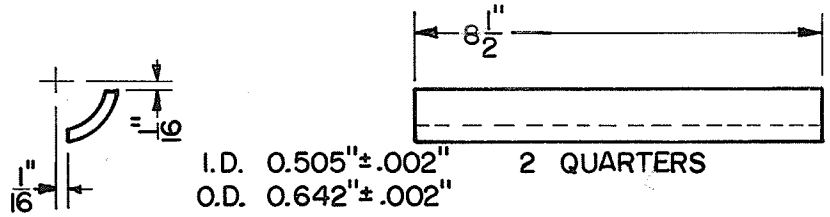

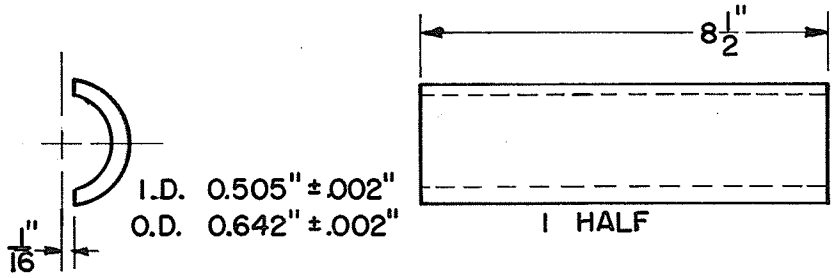

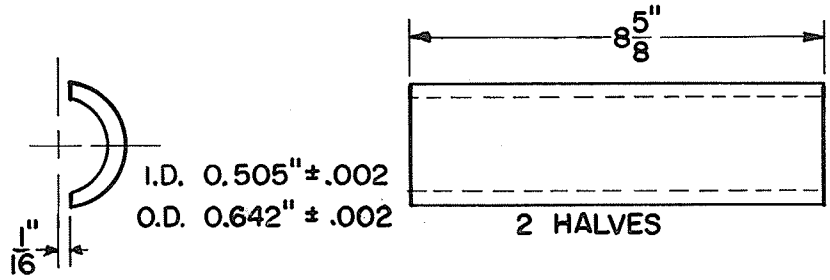

FIGURE C-7

TEST SECTION DETAILS

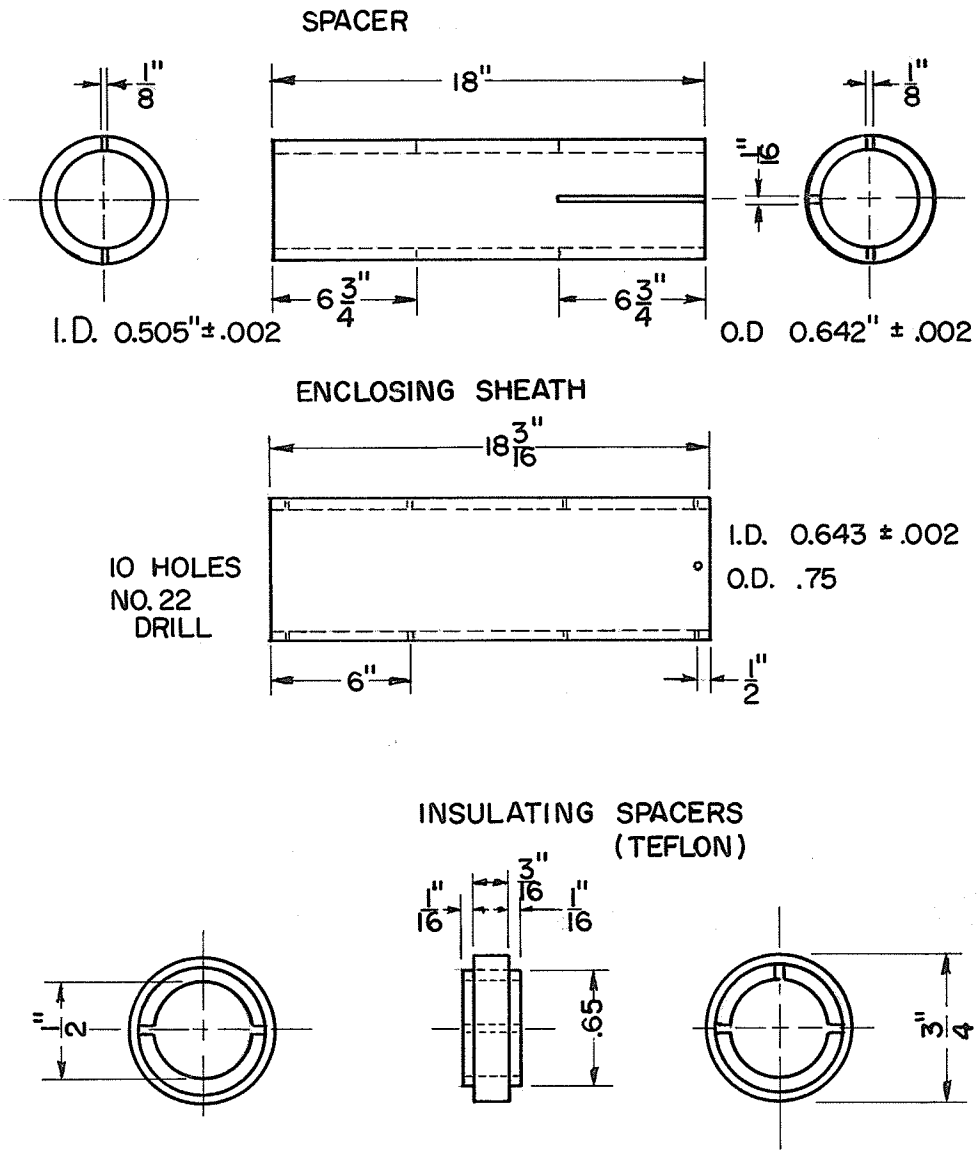

APPENDIX D

THERMISTOR CONSTRUCTION AND CHARACTERISTICS

APPENDIX D

THERMISTOR CONSTRUCTION AND CHARACTERISITCS

The thermistors used were supplied by Fenwal Electronics, Inc., with characteristics as follows:

Probe Thermistor

Code number - GB41P2

Resistance at 25°C - 10,000 ohms ±20%

Resistance at 0°C/resistance at 25°C = 7.5

Time constant - 25 seconds

Dissipation constant - 1 milliwatt

Lead wire 0.012" diameter dumet

Probe diameter - 0.10"

Bead Thermistor

Code number - GB41J1

Resistance at 25°C - 10,000 ohms ±20%

Resistance 0°C/resistance at 25°C = 7.5

Time constant - 2 seconds

Dissipation constant - .7 milliwatts

Lead wire - 0.004" Pt - Ir

Bead diameter - 0.043"

The first and most critical step was the connection between the thermistors and the initial lead wire. This wire was #32 stranded, tinned copper wire with a teflon insulating covering,

and was used to withstand the high cell temperatures which ordinary plastic covered wire could not withstand. The connection was made difficult because of the size of the thermistor lead wire; the probe connections being relatively easy as compared to the bead connections because the lead wires were so much larger. The apparatus used for the connection was a mercury pool welder, FIGURE D-1. A power-stat was used to give the correct voltage, so that when the twisted wire connection was touched to the mercury the electrical current heated the connection enough to weld the wires together and did not generate enough heat to melt the thermistor lead wires. The voltages were 12 volts for the 0.004" Pt-Ir wire and 30 volts for the 0.012"dumet wire. An oil layer was used above the mercury to stop the mercury from splashing and to protect the thermistor and thermistor lead wire from the heat produced when the connection was welded. The welded connection and the bare thermistor lead wires were covered with a clear synthetic (Glyptal) air-drying varnish* for strength purposes and for electrical insulating purposes.

The teflon covered wire ended at the cell end plate where it was soldered to #24 stranded, tinned copper multicore wire which made the connection to the thermistor switch box and bridge. This connection was soldered to facilitate ease of assembly since the wires were disconnected at this point when the outside glass cylinder was exchanged. The layout is shown schematically in FIGURE D-2.

The different positioning techniques for the thermistors are shown in FIGURE D-3.

FIGURES D-4 and D-5 show typical thermistor calibration curves.

---

*General Electric Insulating Varnish #G1202

FIGURE D-1

Mercury Pool Welder

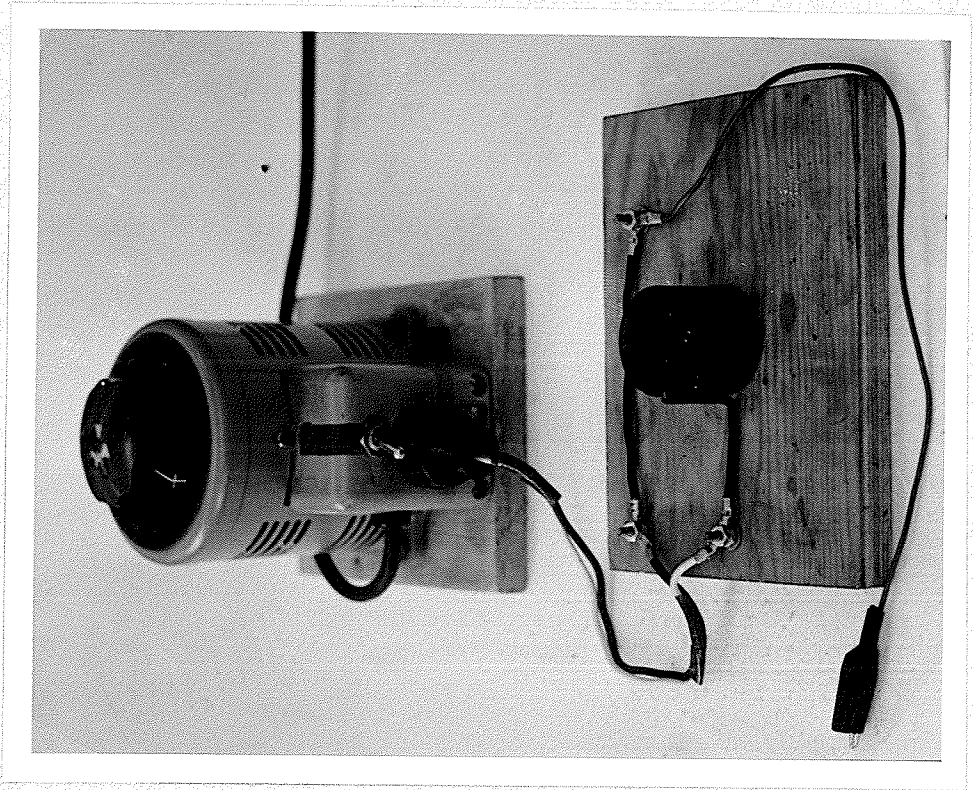

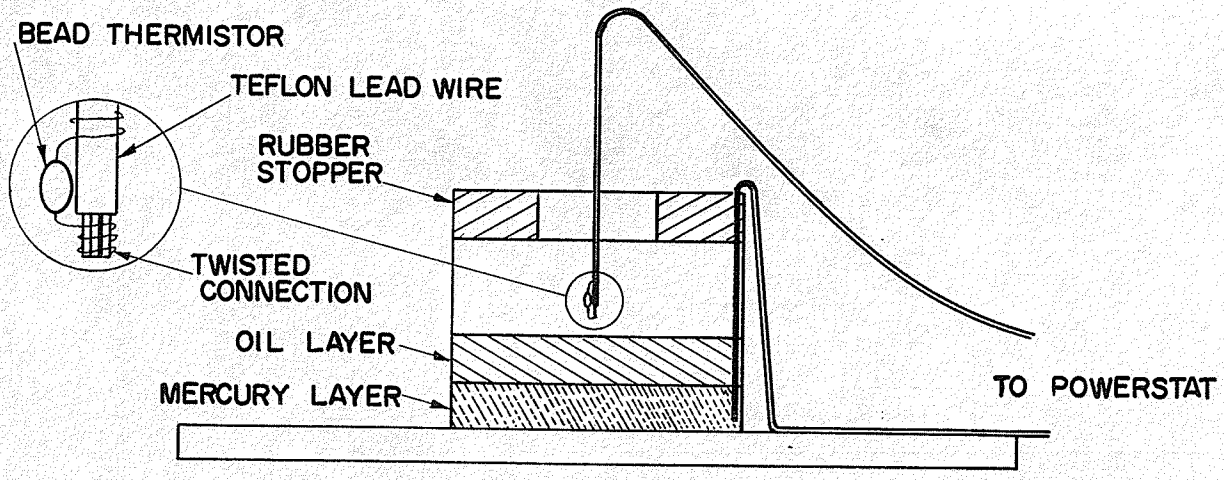

FIGURE D-2

THERMISTOR LEAD WIRE LAYOUT

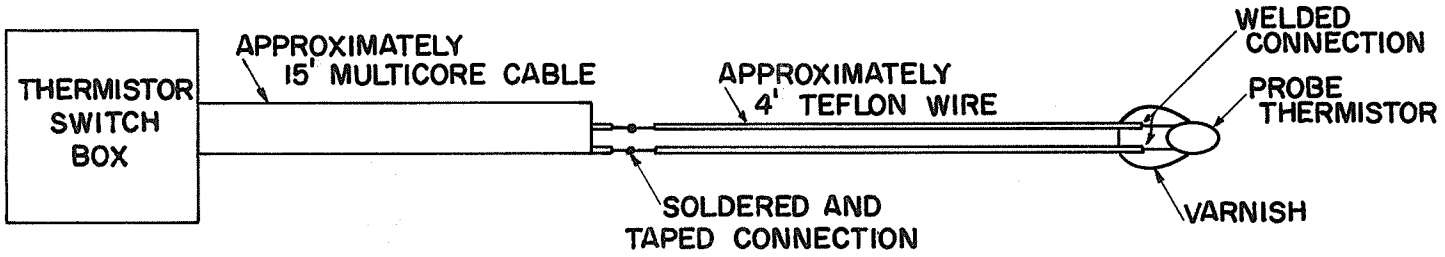

FIGURE D-3

THERMISTOR INSTALLATION

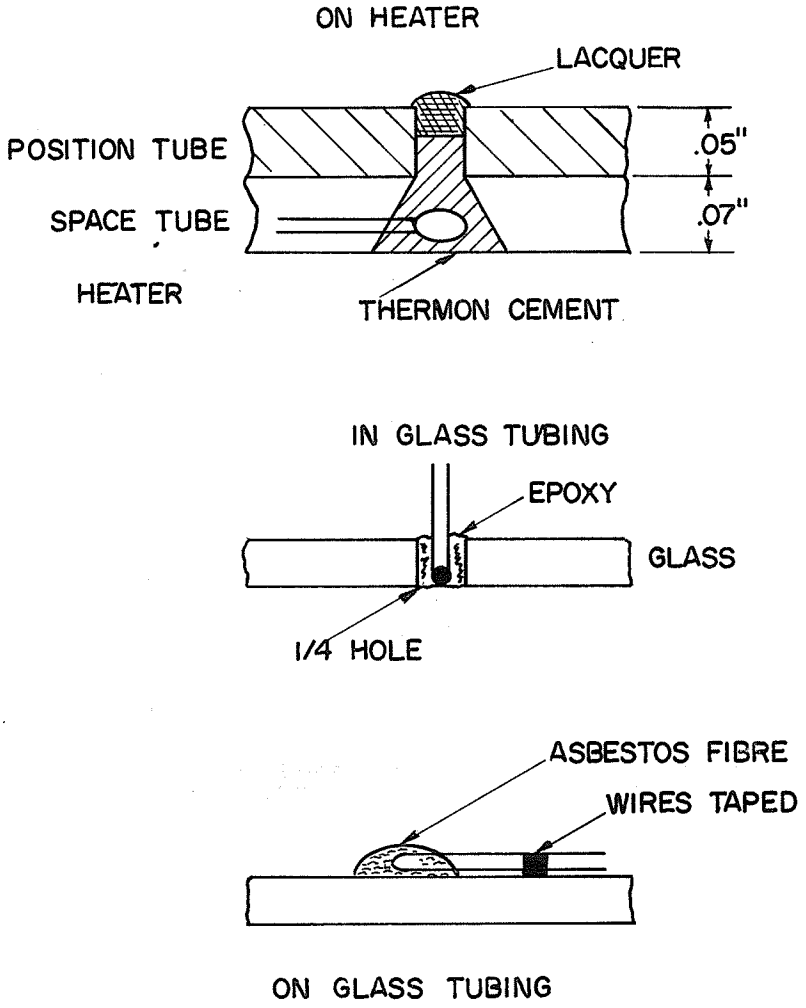

FIGURE D-4
TYPICAL THERMISTOR CALIBRATION CURVE
125°F - 150°F

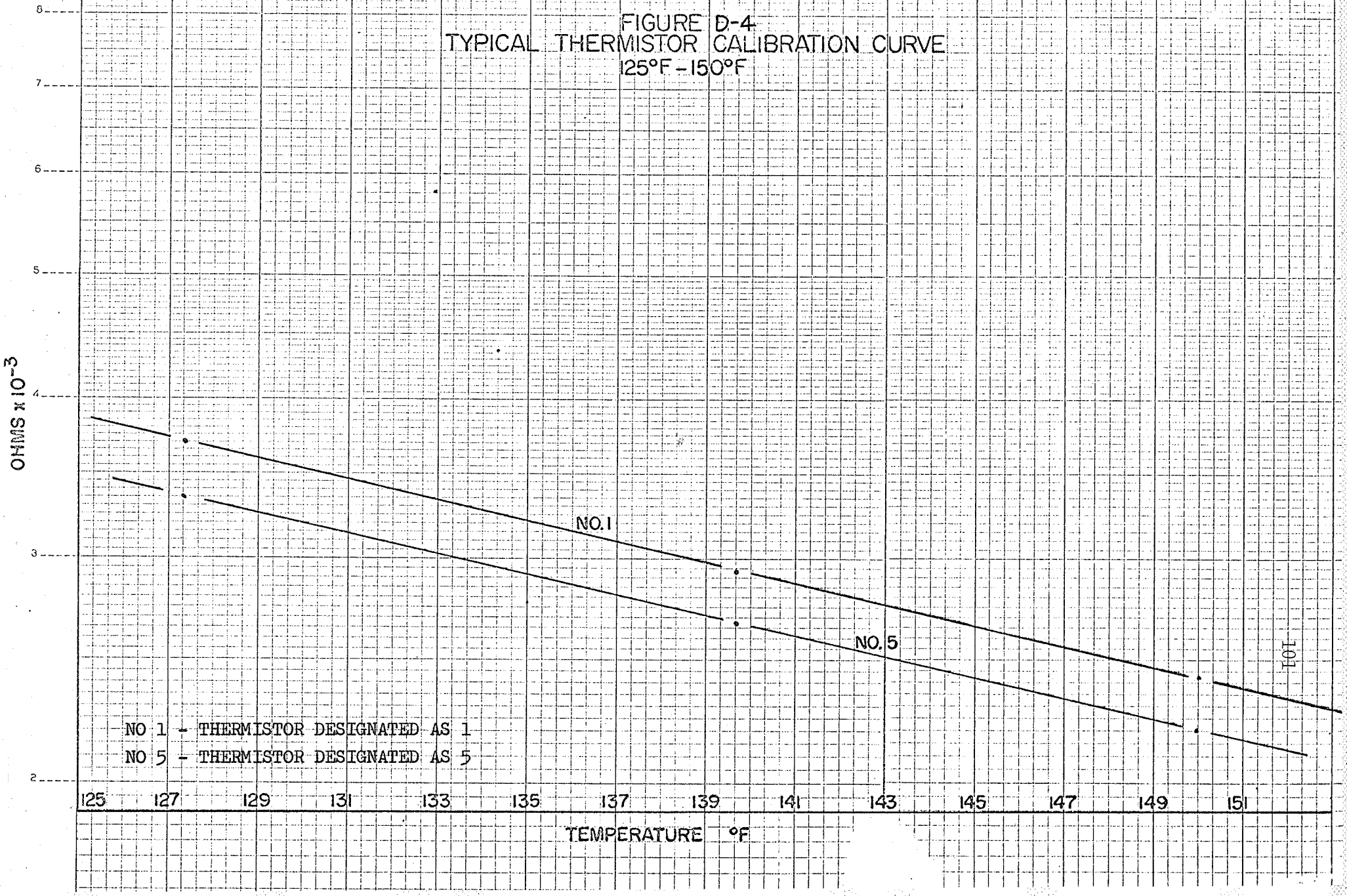

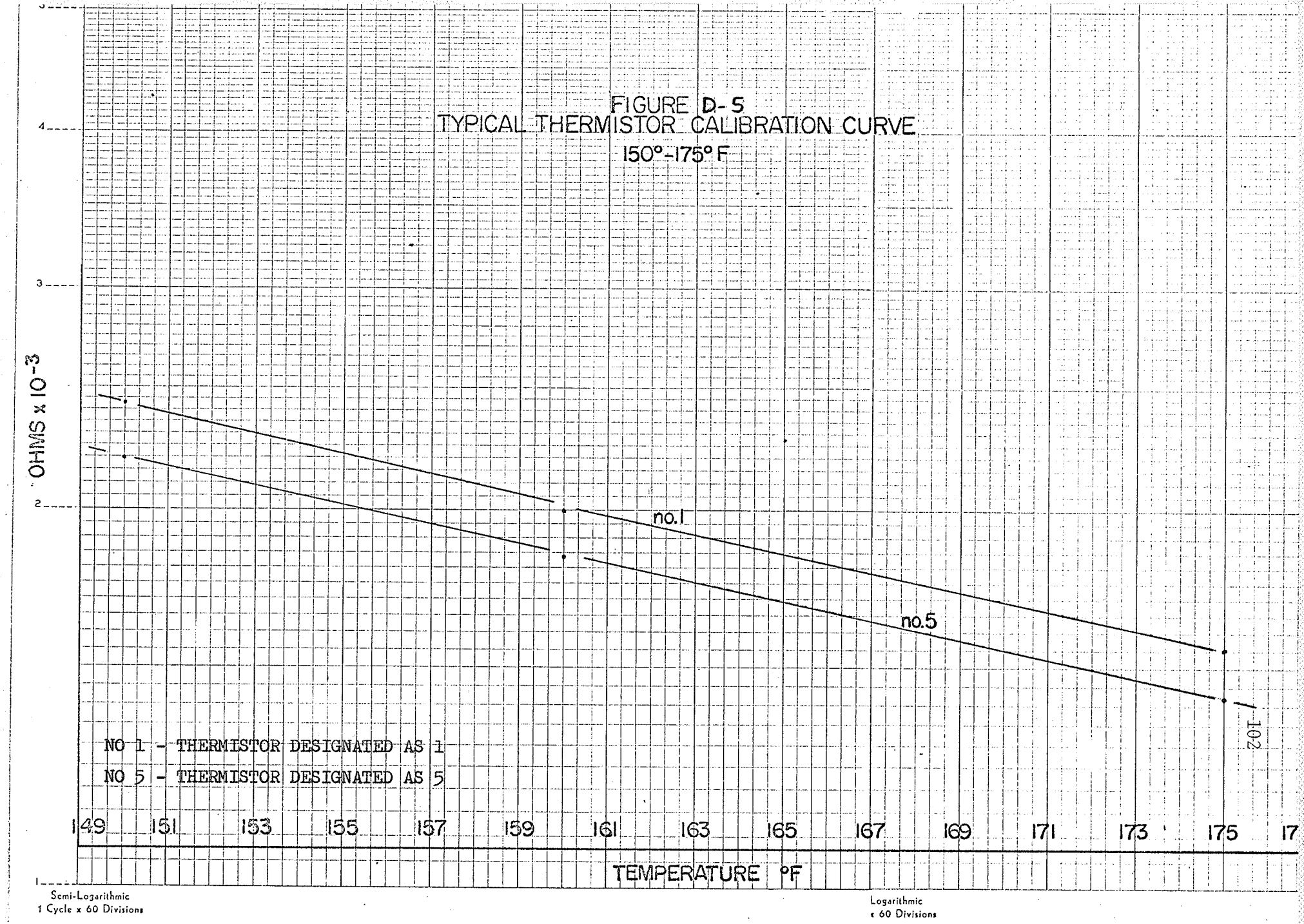
FIGURE D-5
TYPICAL THERMISTOR CALIBRATION CURVE
150°-175° F
OHMS x 10-3
4
3
2
1
no.1
no.5
NO 1 - THERMISTOR DESIGNATED AS 1
NO 5 - THERMISTOR DESIGNATED AS 5
149
151
153
155
157
159
161
163
165
167
169
171
173
175
17
TEMPERATURE °F
102
Semi-Logarithmic
1 Cycle x 60 Divisions
Logarithmic
x 60 Divisions

APPENDIX E

INSTRUMENTATION CALIBRATION

TABLE E-1

VOLTMETER CALIBRATION

Weston 0-30 Volts

NO. IDJI

Standards Reading *	Meter Reading *	Error *	% Error
5.89	6.0	-0.11	1.8
9.995	10.0	-.005	0.05
11.81	12.0	-0.19	1.6
13.80	14.0	-0.20	1.4
15.85	16.0	-0.15	1.0
17.85	18.0	-0.15	1.0
19.80	20.0	-0.20	1.0
21.7	22.0	-0.20	1.4
23.75	24.0	-0.25	1.0
25.70	26.0	-0.30	1.0

Error in Standard $\pm$0.1%

* Units Volts

TABLE E-2

AMMETER CALIBRATION

Weston 0-3 Amp.

NO. DC2

Standards Reading *	Meter Reading *	Error *	% Error
2.375	2.40	-0.025	1.0
2.170	2.20	-0.03	1.4
1.950	2.00	-0.05	2.5
1.775	1.80	-0.025	1.4
1.555	1.60	-0.045	2.4
1.385	1.40	-0.015	1.0
1.185	1.20	-0.015	1.3
0.970	1.00	-0.03	3.0

Standards error $\pm$ .1%

* Units Amperes

TABLE E-3

WATTMETER CALIBRATION

Weston # 27222

Standards Reading *	Meter Reading *	Error *	% Error
50.0	50	-	-
100.0	100	-	-
150.5	150	+0.5	0.3
201.0	200	+1.0	0.5
250.5	250	+0.5	0.2
300.0	300	-	-

Standards errors $\pm$0.2%

* Units Watts

APPENDIX F

TEST FLUID PROPERTIES

FIGURE F-1

'Z' FOR GLYCERINE vs TEMPERATURE

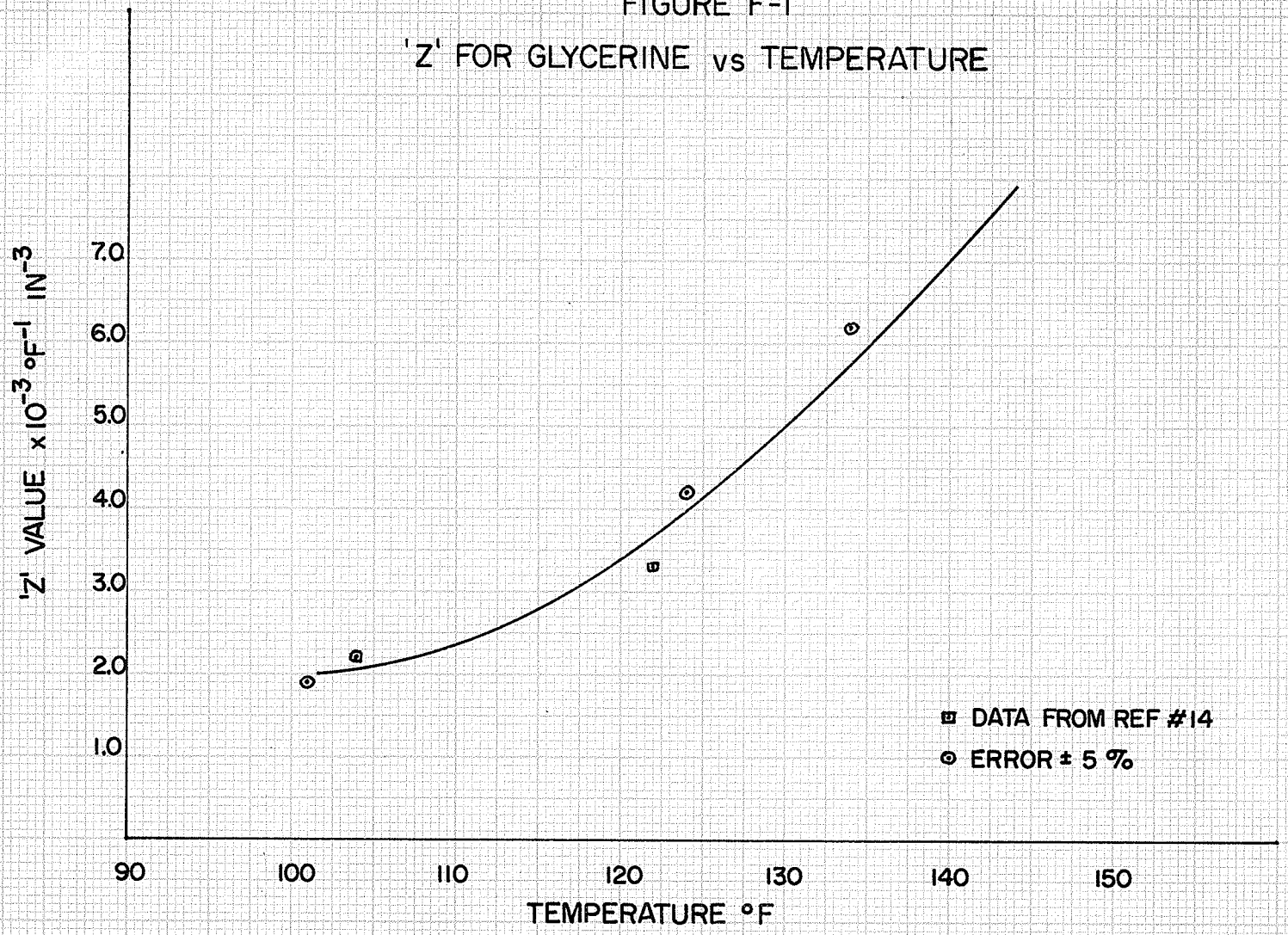

FIGURE F-2

THERMAL CONDUCTIVITY
VS
TEMPERATURE FOR GLYCERINE

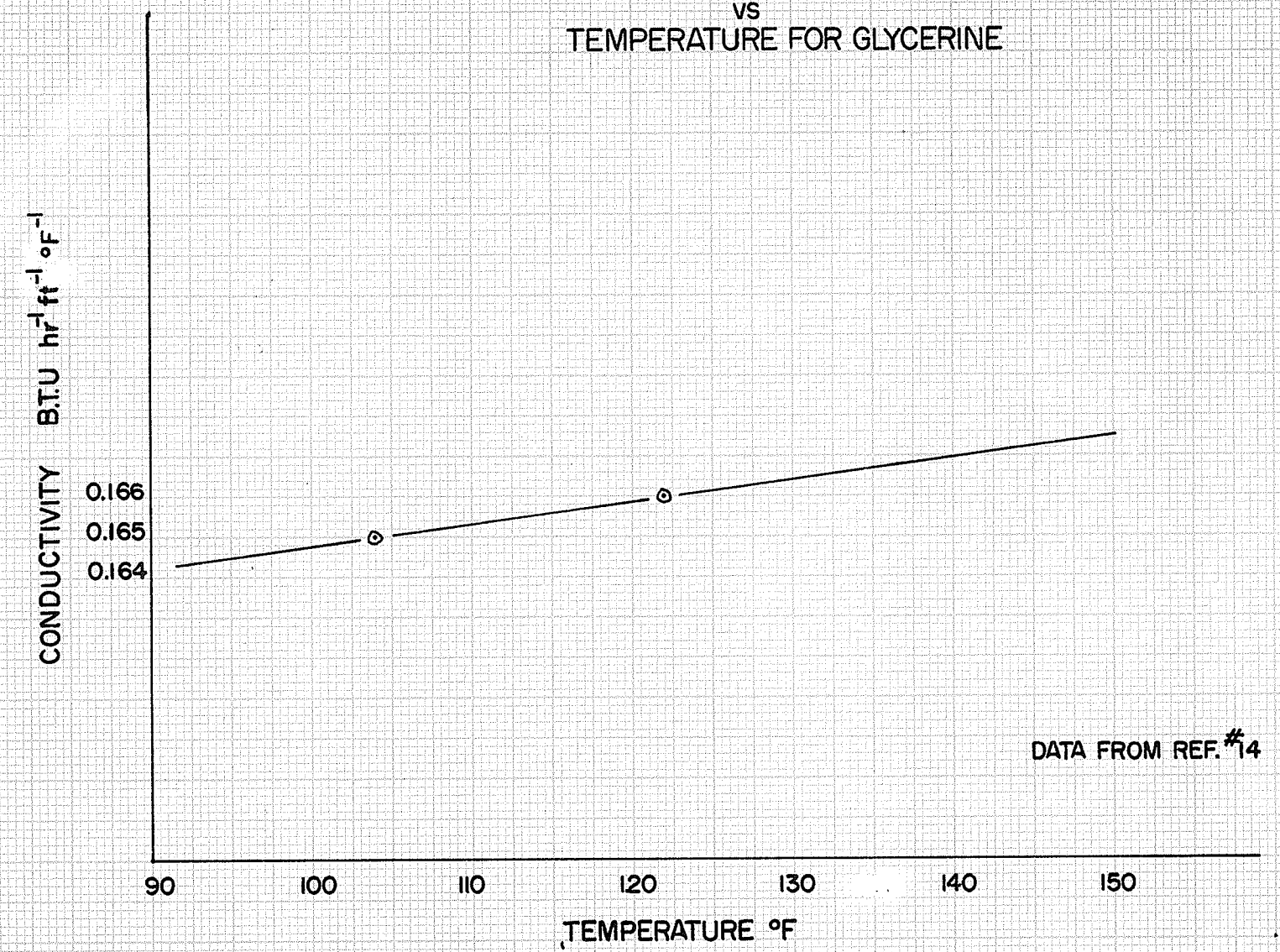

FIGURE F-3

'Z' FOR WATER vs TEMPERATURE

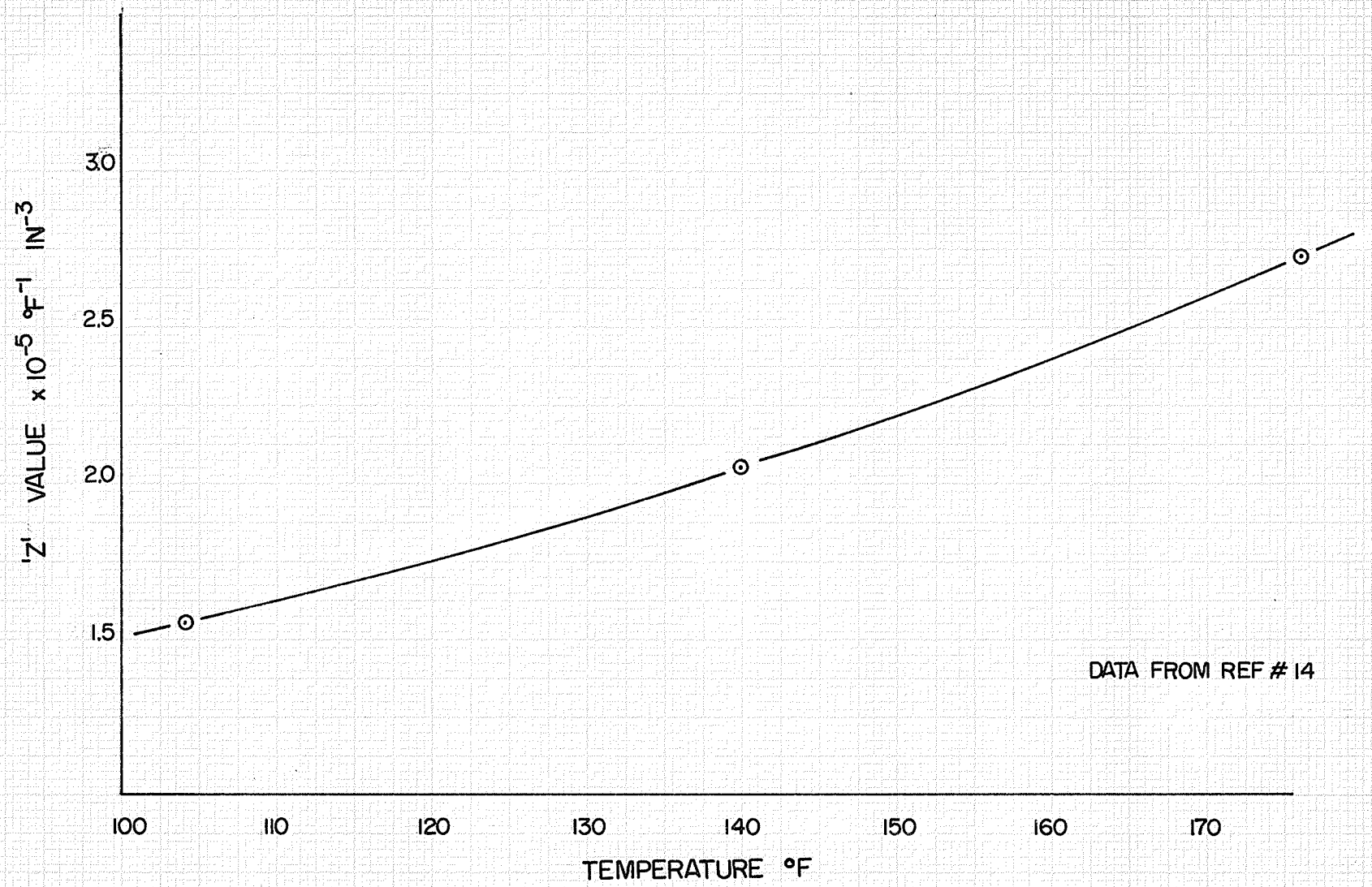

FIGURE F-4

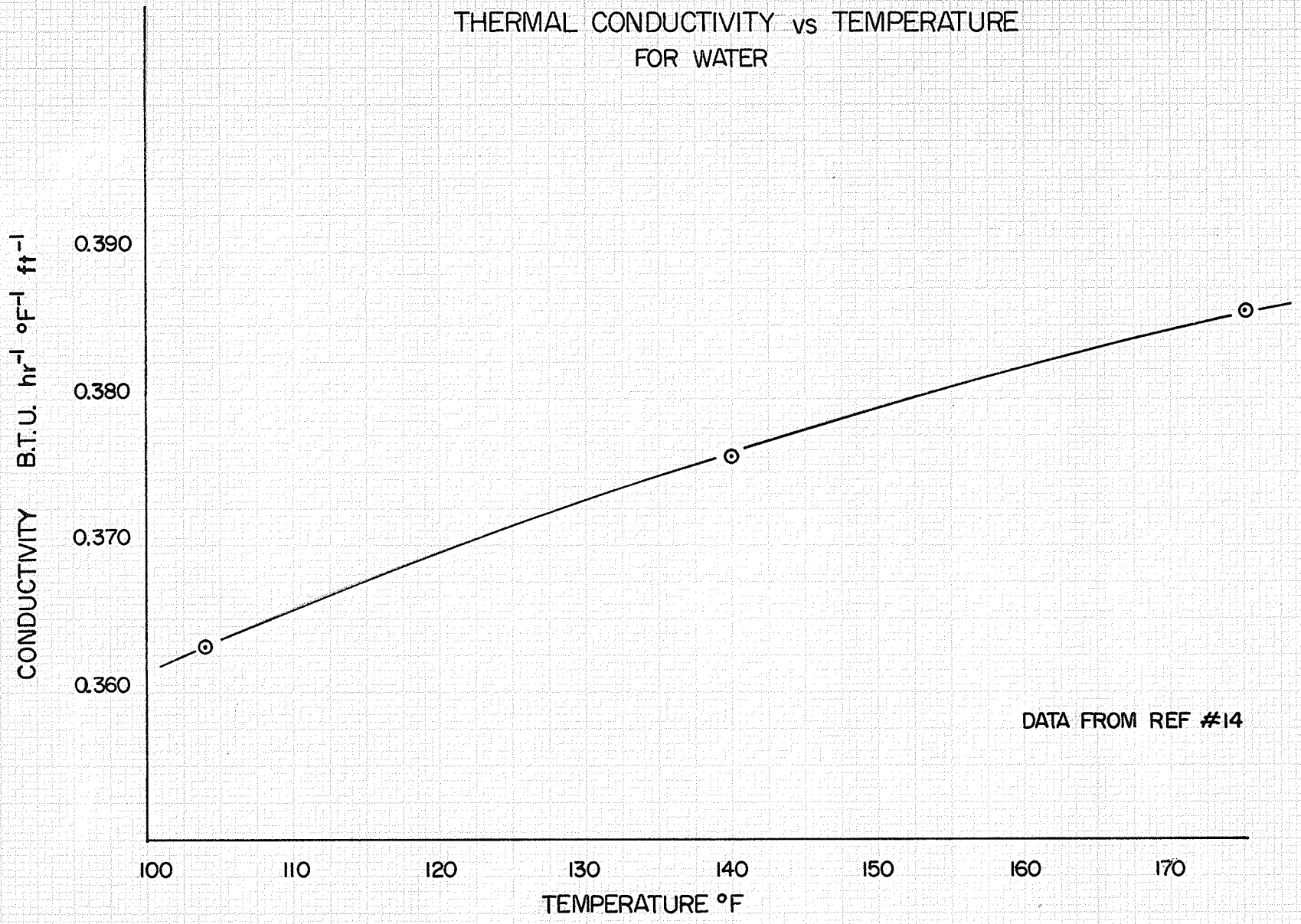
THERMAL CONDUCTIVITY vs TEMPERATURE
FOR WATER
CONDUCTIVITY B.T.U. hr⁻¹ °F⁻¹ ft⁻¹
0.390
0.380
0.370
0.360
DATA FROM REF #14
100
110
120
130
140
150
160
170
TEMPERATURE °F

FIGURE F-5

'Z' FOR AIR vs TEMPERATURE

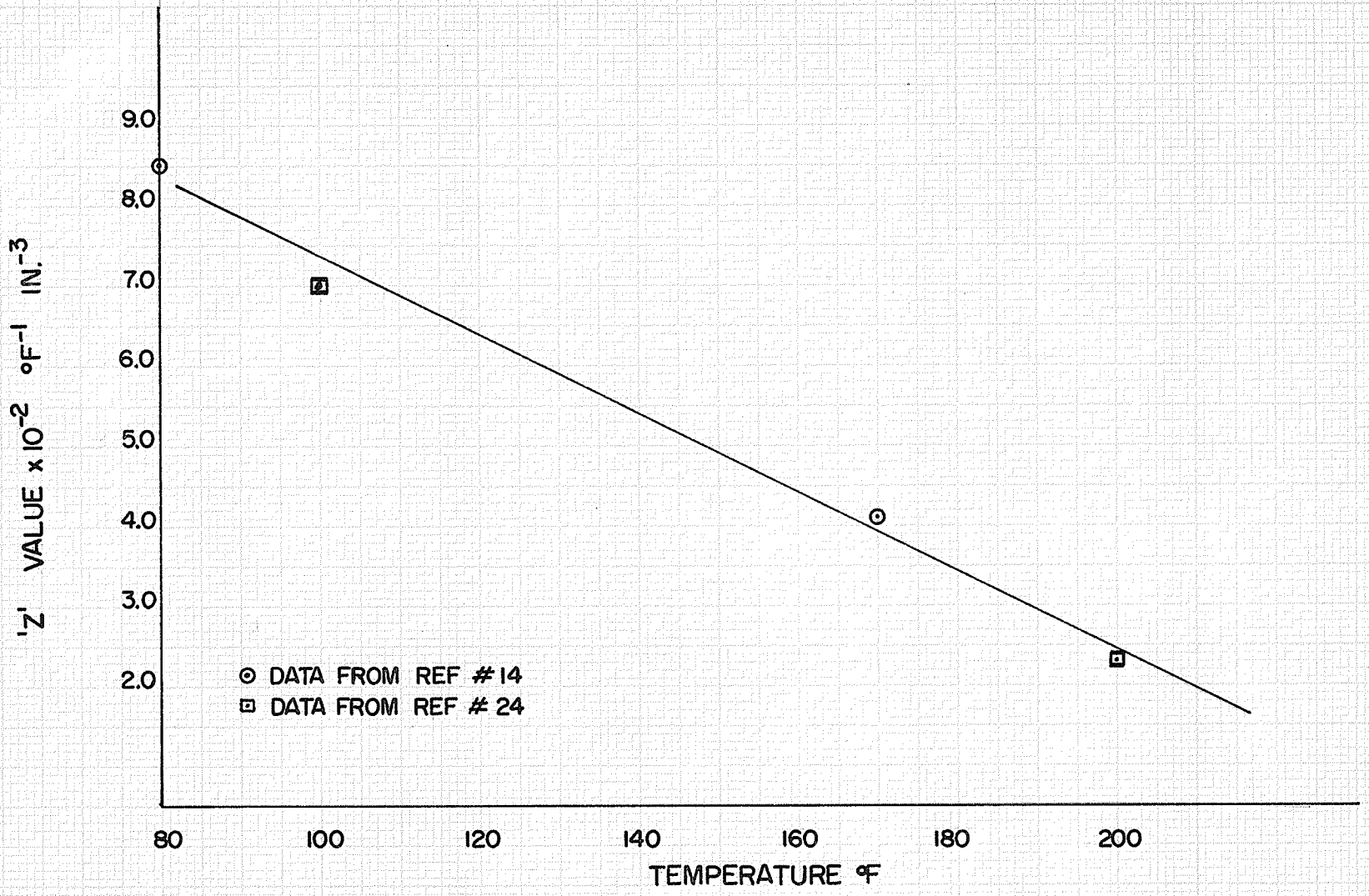

FIGURE F-6

THERMAL CONDUCTIVITY vs TEMPERATURE
FOR AIR

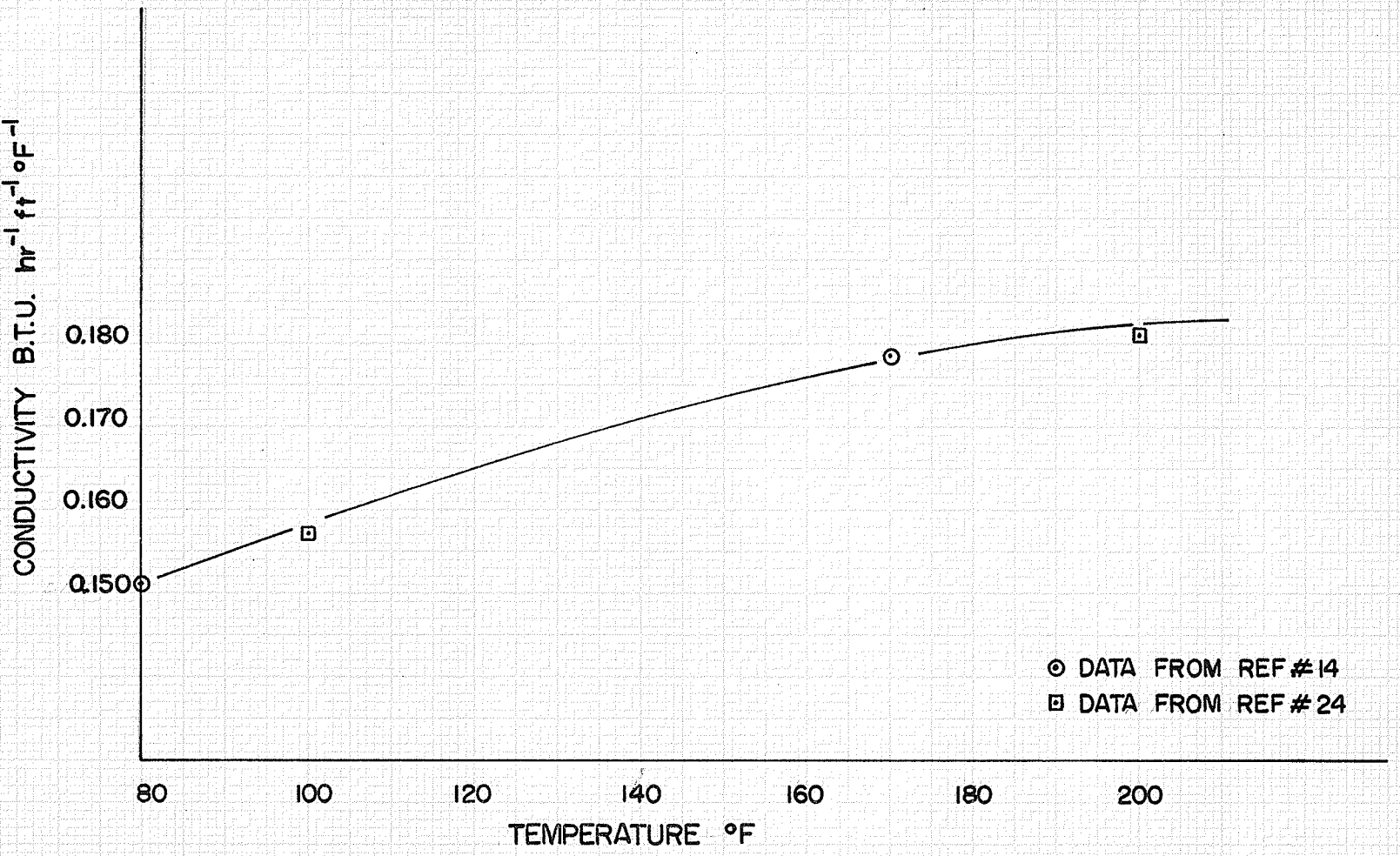

APPENDIX G

CALCULATION OF ERRORS

APPENDIX G

CALCULATION OF ERRORS

The reliability estimates or error estimates will be calculated using the method described by S. J. Kline and F. A. McClintock* for single-sample experiments which is the following:

$$\omega_R = \left[\left(\frac{\partial R}{\partial V_1}\omega_1\right)^2 + \left(\frac{\partial R}{\partial V_2}\omega_2\right)^2 + \text{-----} \left(\frac{\partial R}{\partial V_n}\omega_n\right)^2\right]^{1/2}$$

R - function of n independent variable each of which is normally distributed.

ω_1 - interval of the variable.

ω_R - interval of the result. (The uncertainty in ω_R is the same as in ω_1 and for the following errors will be assumed to be 10 to 1 or 90% certainty).

The above equation may be manipulated to give the fractional error directly:

$$\frac{\omega_R}{R} = \left[\left(\omega_1 \frac{\partial}{\partial V_1}(\ln R)\right)^2 + \left(\omega_2 \frac{\partial}{\partial V_2}(\ln R)\right)^2 + \text{-----} \left(\omega_n \frac{\partial}{\partial V_n}(\ln R)\right)^2\right]^{1/2}$$

1.0 Thermal Conductivity Error

The formula used to calculate the thermal conductivity was $\frac{V\ I\ \ln(D_o/D_i)}{L\ 2\pi\ \Delta t}$. The equation for error estimation is as follows:

$$\frac{\omega_K}{K} = \left[\left(\frac{\omega_V}{V}\right)^2 + \left(\frac{\omega_I}{I}\right)^2 + \left(\frac{\omega_{D_o}}{D_o\ \ln(D_o/D_i)}\right)^2 + \left(\frac{\omega_{D_i}}{D_i\ \ln(D_o/D_i)}\right)^2 + \left(\frac{\omega_L}{L}\right)^2 + \left(\frac{\omega_{\Delta t}}{\Delta t}\right)^2\right]^{1/2}$$

* Kline, S. J. and McClintock, F. A., "Describing Uncertainties In Single-Sample Experiments", Mechanical Engineering, 75 (1953) p.3

** Symbols defined in Nomenclature.

Heat Input Error

The combined calibration and reading error was ±1% in both the ammeter and the voltmeter.

$$\frac{\omega_V}{V} = 0.01$$

$$\frac{\omega_I}{I} = 0.01$$

Dimensional Error

Length 35.1 inches ±0.2"

$$\frac{\omega_L}{L} = \frac{0.2}{35.1} = 0.006$$

For 0.28" annular layer

Inside diameter = 0.750 inches ±0.004"

$$\frac{\omega_{D_i}}{D_i \ln(D_o/D_i)} = \frac{0.004}{0.750 \ln(1.315/0.750)} = 0.0095 = 0.010$$

Outside diameter = 1.315 inches ±0.020"

$$\frac{\omega_{D_o}}{D_o \ln(D_o/D_i)} = \frac{0.020}{1.315 \ln(1.315/0.750)} = 0.027$$

For 0.125" annular layer

Inside diameter = 0.750 inches ±0.004"

$$\frac{\omega_{D_i}}{D_i \ln(D_o/D_i)} = \frac{0.004}{0.750 \ln(1.000/0.750)} = 0.0185 = 0.019$$

Outside diameter = 1.000 inches ±0.002"

$$\frac{\omega_{D_o}}{D_o \ln(D_o/D_i)} = \frac{0.002}{1.000 \ln(1.000/0.750)} = 0.007$$

Temperature Difference

The largest error in the temperature measurement was caused by the thermistor wander during a half-hour test. The maximum wander was ±10% of the temperature difference on theglass surface and ±5% of the temperature difference on the heater cylinder surface. The calibration error of ±0.1°F which gave an error of ±1% on the smallest temperature difference was insignificant in the presence of the thermistor wander.

$$\left(\frac{\omega_{\Delta t}}{\Delta t}\right)^2 = (0.10)^2 + (0.05)^2 = 0.0125$$

The error can be further reduced because the temperature difference is an average of six Δts in the 0.28 annular layer and four Δts in the 0.125 annular layer.

For 0.28" annular layer

$$\frac{\pm 11\%}{\sqrt{6}} = \pm 4.5\%$$

For 0.125" annular layer

$$\frac{\pm 11\%}{\sqrt{4}} = \pm 5.5\%$$

Error in the Thermal Conductivity Calculation

For 0.28 annular layer

$$\frac{\omega_K}{K} = \left[(0.01)^2 + (0.01)^2 + (0.01)^2 + (0.027)^2 + (0.006)^2 + (0.045)^2\right]^{1/2}$$

$$= \pm 0.055 = \pm 5.5\%$$

For 0.125" annular layer

$$\frac{\omega_K}{K} = \left[(0.01)^2 + (0.01)^2 + (0.019)^2 + (0.007)^2 + (0.006)^2 + (0.055)^2\right]^{1/2}$$

$$= \pm 0.061 = \pm 6.1\%$$

Other Errors

Because the thermal conductivity measurement was a secondary aim, the errors were not thoroughly investigated. One important source of error is due to the eccentricity in the cylinders. From the formula used by L. Cox[28]:

$$\text{Percent error} = \left[\frac{\ln (r_o/r_i)}{\cosh^{-1} (y_i/r_i) - \cosh^{-1} (y_o/r_o)}\right] \times 100$$

$$y_i = \frac{r_o^2 + r_i^2 - a^2}{2a}$$

$$y_o = \frac{r_o^2 + r_i^2 + a^2}{2a}$$

where r_o - outer radius

r_i - inner radius

a - eccentricity

a = eccentricity (This case ± 0.020 inches.)

Error in 0.28" layer $\pm$ 2.0%

Error in 0.125" layer $\pm 4.0\%$

Also, since the formula did not contain the layer width as a measured quantity, this error should be taken into account:

0.28" layer $\pm 4.3\%$

0.125" layer $\pm 2.4\%$

The largest calculation of the error would be addition of the separate errors giving:

0.28" layer - 5.5 + 2.0 + 4.3 = $\pm 11.8\%$

0.125" layer - 6.1 + 4.0 + 2.4 = $\pm 12.5\%$

From the thermistor readings on each side of the insulating washers at the ends of the test section, the heat loss axially from the test section was found to be less than 0.1 watts or less than 1% of the test section heat input. Another error is in the thermistor placement; that is, the temperature error introduced because the thermistors were not reading the cylinder surface temperature. These errors are small and should be relatively constant for all tests and not affect the continuity of the experimental points.

2.0 Rayleigh Number Error

The formula used to calculate the Rayleigh number was $Z\ \Delta t \left(\frac{D_o - D_i}{2}\right)^3$* with Δt and $\left(\frac{D_o - D_i}{2}\right)^3$ measured quantities and Z calculated from references, Appendix F. The equation for the error estimation is as follows:

$$\frac{\omega_R}{R} = \left[\left(\frac{\omega_Z}{Z}\right)^2 + \left(\frac{\omega_{\Delta t}}{\Delta t}\right)^2 + \left(\frac{3\omega_{D_i}}{D_o - D_i}\right)^2 + \left(\frac{3\omega_{D_o}}{D_o - D_i}\right)^2\right]^{1/2} *$$

Dimensional Error

For 0.28" annular layer

$$\frac{3\omega_{D_i}}{D_o - D_i} = \frac{3(0.004)}{0.565} = 0.021$$

$$\frac{3\omega_{D_o}}{D_o - D_i} = \frac{3(0.020)}{0.565} = 0.105$$

* Symbols defined in Nomenclature.

For 0.125" annular layer

$$\frac{3\omega_{D_i}}{D_o - D_i} = \frac{3(0.004)}{0.250} = 0.048$$

$$\frac{3\omega_{D_o}}{D_o - D_i} = \frac{3(0.002)}{0.250} = 0.024$$

Temperature Difference

As in the calculation of the thermal conductivity error, the temperature difference error is as follows:

0.28" layer = $\pm$4.5%

0.125" layer = $\pm$5.5%

Fluid Property Error

Mean temperature error $\pm$3%. Error in fluid property (Appendix F) $\pm$10%.

$$\frac{\omega_Z}{Z} = 0.10$$

Error in the Rayleigh Number Calculation

For 0.28" annular layer

$$\frac{\omega_R}{R} = \left[(0.01)^2 + (0.045)^2 = (0.021)^2 + (0.105)^2\right]^{1/2}$$

$$= 0.115 = 11.6\%$$

For 0.125" annular layer

$$\frac{\omega_R}{R} = \left[(0.01)^2 + (0.055)^2 + (0.048)^2 + (0.024)^2\right]^{1/2}$$

$$= 0.078 = 7.8\%$$

However, the eccentricity is a significant error and must not be ignored; although, because of the geometry, the eccentricity affects only a small portion of the cell, and any error calculation is only an estimation.

For 0.28" annular layer

$$\frac{3\omega_E}{D_o - D_i} = \frac{3(0.02)}{0.565} = 0.105$$

For 0.125" annular layer

$$\frac{3\omega_E}{D_o - D_i} = \frac{3(0.02)}{0.250} = 0.24$$

Total Rayleigh number error calculation is as follows:

For 0.28" annular layer

$$\frac{\omega_R}{R} = \left[(0.116)^2 + (0.105)^2 \right]^{1/2}$$

$$= 0.157 = 15.7\%$$

For 0.125" annular layer

$$\frac{\omega_R}{R} = \left[(0.078)^2 + (0.24)^2 \right]^{1/2}$$

$$= 0.252 = 25.2\%$$

3.0 Significant Error (Precision)

A more practical approach of determining the experimental error is to calculate the error causing scatter. This approach eliminates the geometrical error since this error is constant (may be slightly dependent on fluid motion). Also, for an absolute measurement of thermal conductivity the apparatus may be calibrated

with a liquid of known thermal conductivity in order to determine the correction for geometrical irregularities; eccentricity, thermistor mounting, heater placement, and end heat losses.

The contributing factors to the scatter of the apparent thermal conductivity measurements would be the heat input error and the temperature error giving the following errors (with a 90% certainty):

0.28" layer - $\pm$4.7%

0.125" layer - $\pm$5.7%.

APPENDIX H

TEST RESULTS

TABLE H-1

TEST RESULTS

Glycerine in 0.28" Horizontal Annular Layer

Test No.	Power Watts	Δts ^oF	Δt_L ^oF	Δt_m ^oF	t_m ^oF	$Z_m \times 10^{-3}$ $^oF^{-1}in^{-3}$	K_{CAL} Btu/^oF hr.ft.	K_{error}	Ke Btu/^oF hr.ft.	Ke/K	N_{RAY}	Motion
100	60.7	26.7	39.0	32.8	124	4.17	0.192	1.10	0.212	1.26	3300	yes
101A	46.8	24.0	33.9	29.0	125	4.26	0.168	1.10	0.186	1.12	2880	yes
101B	47.1	22.8	33.5	28.2	125	4.26	0.174	1.11	0.194	1.17	2700	yes
102	40.6	22.4	28.8	25.6	117	3.32	0.165	1.08	0.179	1.075	1900	yes
103	37.4	20.5	27.1	23.8	120	3.62	0.164	1.09	0.178	1.07	1940	yes
104A	32.6	18.0	24.5	21.3	116	3.20	0.160	1.09	0.174	1.05	1530	yes
104B	33.0	16.8	25.5	21.2	120	3.62	0.162	1.08	0.174	1.06	1720	yes
105A	26.4	14.5	20.7	17.6	110	2.60	0.156	1.06	0.166	1.00	1030	yes
105B	26.4	15.9	19.7	17.8	109	2.50	0.154	1.06	0.164	0.98	1000	yes
106A	18.5	9.6	14.4	12.0	104	2.11	0.161	1.12	0.181	1.09	570	slight
106B	16.3	9.8	12.8	11.3	102	1.91	0.150	1.055	0.159	0.96	480	no
106C	18.8	10.5	14.1	12.3	105	2.17	0.153	1.08	0.165	0.99	600	slight
108A	78.0	27.7	47.2	37.5	144	7.0	0.217	1.15	0.249	1.50	5900	yes
108B	78.0	29.8	47.5	38.7	145	7.0	0.210	1.14	0.242	1.46	6100	yes
109	21.6	13.4	16.3	14.9	100	1.76	0.161	1.04	0.157	0.95	600	no
110	23.9	13.0	17.7	15.4	112	2.80	0.161	1.07	0.177	1.065	970	yes

Symbols defined in Nomenclature

TABLE H-2

TEST RESULTS

Glycerine in 0.28" Vertical Annular Layer

Test No	Power Watts	Δts ^oF	Δt_L ^oF	Δt_m	t_m ^oF	$Z_m \times 10^{-3}$ $^oF^{-1}in^{-3}$	K_{CAL} Btu/^oF hr.ft.	K_{error}	Ke Btu/^oF hr.ft.	Ke/K	N_{RAY}	Motion
1	16.6	11.5	13.5	12.5	102	1.90	0.139	1.05	0.146	0.88	530	no
2	23.7	13.8	18.7	16.0	115	2.60	0.154	1.055	0.163	0.98	930	yes
3	25.4	15.5	18.5	17.0	116	2.70	0.156	1.055	0.164	0.99	1000	yes
4	29.3	19.5	20.5	20.0	123	4.05	0.157	1.02	0.160	0.96	1770	yes
5A	32.3	22.0	24.0	23.0	122	3.90	0.146	1.01	0.148	0.89	2000	yes
5B	32.3	21.9	24.2	23.0	122	3.90	0.146	1.015	0.149	0.90	2000	yes
5C	32.3	21.0	22.2	21.6	123	4.05	0.157	1.01	0.160	0.96	1950	yes
6A	35.0	25.1	25.5	25.3	126	4.40	0.144	1.00	0.144	0.87	2500	yes
6B	34.8	23.1	24.5	24.0	131	5.20	0.151	1.02	0.154	0.93	2800	yes
7	34.2	23.2	25.6	24.0	131	5.20	0.149	1.03	0.153	0.92	2800	yes
8	41.1	26.5	27.5	27.0	133	5.60	0.159	1.01	0.160	0.97	3420	yes
9	60.1	35.2	35.2	35.2	150	8.0	0.180	1.00	0.180	1.08	6500	yes
10A	38.8	24.5	28.5	26.5	130	5.00	0.153	1.05	0.160	0.97	2980	yes
10B	38.8	25.0	26.1	25.5	132	5.38	0.158	1.01	0.160	0.97	3100	yes
10C	39.2	25.3	26.1	25.7	133	5.63	0.159	1.01	0.162	0.98	3250	yes
11	44.4	26.5	29.5	28.0	127	4.50	0.165	1.035	0.171	1.03	2830	yes
12	19.2	13.3	14.6	13.9	108	2.45	0.144	1.03	0.148	0.89	760	slight
13A	13.2	8.6	12.0	10.5	102	1.90	0.131	1.10	0.144	0.87	450	slight
13B	12.8	8.5	10.0	9.3	102	1.90	0.144	1.055	0.152	0.91	400	slight
13C	12.8	8.3	10.0	9.2	103	2.05	0.145	1.055	0.153	0.92	420	slight

Symbols defined in Nomenclature

TABLE H-3

TEST RESULTS

Glycerine in 0.28" 45^{o} Annular Layer

Test No	Power Watts	Δts ^{o}F	Δt_L ^{o}F	Δt_m	t_m ^{o}F	$Z_m \times 10^{-3}$ $^{o}F^{-1}in^{-3}$	K_{CAL} Btu/^{o}F hr.ft.	K_{error}	Ke Btu/^{o}F hr.ft.	Ke/K	N_{RAY}	Motion
200A	24.2	15.8	16.0	15.9	110	2.65	0.159	1.00	0.159	0.96	950	yes
200B	23.9	15.8	15.9	15.9	106	2.23	0.156	1.00	0.156	0.94	800	yes
200C	23.6	14.2	17.3	15.8	110	2.65	0.155	1.04	0.162	0.97	950	yes
201A	12.6	7.7	8.8	8.3	103	2.05	0.159	1.04	0.165	0.99	380	yes
201B	12.4	7.5	8.8	8.2	101	1.83	0.158	1.045	0.165	0.99	340	yes
203A	11.0	7.0	7.5	7.3	99	1.70	0.156	1.02	0.160	0.96	280	yes
203B	10.8	6.2	7.4	6.8	100	1.75	0.166	1.055	0.175	1.05	270	yes
205A	50.3	29.4	32.3	30.8	122	3.85	0.170	1.03	0.175	1.05	2670	yes
205B	50.1	28.2	34.2	31.2	124	4.17	0.167	1.06	0.177	1.08	2930	yes
205C	50.3	29.0	32.0	30.5	125	4.25	0.172	1.03	0.177	1.08	2900	yes
206A	33.8	20.0	25.2	22.6	113	2.90	0.156	1.07	0.167	1.00	1470	yes
206B	33.4	21.0	24.7	22.8	112	2.80	0.153	1.05	0.160	0.97	1440	yes
207A	39.1	25.0	25.4	25.2	118	3.45	0.162	1.00	0.163	0.98	1950	yes
207B	38.5	22.4	27.8	25.1	118	3.45	0.161	1.075	0.172	1.04	1950	yes
207C	38.7	22.1	28.8	25.4	119	3.50	0.159	1.10	0.176	1.06	2000	yes

Symbols defined in Nomenclature

TABLE H-4

TEST RESULTS

Glycerine in 0.125" Annular Layer

Test No	Position	Power Watts	Δt_m ^oF	t_m ^oF	$Z_m \times 10^{-3}$ $^oF^{-1}in^{-3}$	K_{CAL} Btu/^oF hr.ft.	K_{error}	Ke Btu/^oF hr.ft.	Ke/K	N_{RAY}	Motion
1	Vertical	32.2	11.0	126	4.83	0.154	1.00	0.154	0.92	105	
2A	Vertical	55.6	18.3	172	10.00	0.162	1.00	0.162	0.96	350	
2B	Vertical	53.3	18.8	144	7.00	0.151	1.00	0.151	0.90	250	
2C	Vertical	57.7	19.6	150	9.00	0.157	1.00	0.157	0.93	330	
4	Vertical	29.4	10.6	120	3.60	0.147	1.00	0.147	0.88	75	no
5	Vertical	37.6	13.5	137	5.60	0.148	1.00	0.148	0.88	150	slight
10	Vertical	71.0	23.0	180	11.00	0.192	1.00	0.192	1.14	500	yes
11	Vertical	86.0	24.6			0.187	1.00	0.187	1.11		
400A	Horizontal	34.6	11.0	130	5.10	0.168	1.00	0.168	1.00	105	no
400B	Horizontal	36.1	11.5	133	5.50	0.167	1.00	0.167	1.00	120	no
400C	Horizontal	33.7	10.9	130	5.10	0.165	1.00	0.165	0.98	100	no
401	Horizontal	57.9	16.9	160	10.00	0.183	1.00	0.183	1.09	300	no
1000	45^o	61.6	17.4	160	10.00	0.189	1.00	0.189	1.12	300	
1001	45^o	71.0	19.2	180	11.00	0.197	1.00	0.197	1.29	350	slight

Symbols defined in Nomenclature

TABLE H-5

TEST RESULTS

Water in 0.125" Annular Layer

Test No	Position	Power Watts	Δt_m ^oF	t_m ^oF	$Z_m \times 10^{-5}$ $^oF^{-1}in^{-3}$	K_{CAL} Btu/^oF hr.ft.	K_{error}	Ke Btu/^oF hr.ft.	Ke/K	N_{RAY}	Motion
3A	Vertical	41.0	6.0	123	1.90	0.37	1.00	0.37	0.98	2200	yes
3B	Vertical	41.2	6.0	126	1.95	0.37	1.00	0.38	0.98	2300	yes
3C	Vertical	40.6	5.5	127	1.95	0.39	1.00	0.39	1.05	2100	yes
4A	Vertical	48.3	7.1	135	2.07	0.36	1.00	0.36	0.96	2900	yes
4B	Vertical	48.8	6.9	138	2.10	0.38	1.00	0.38	1.00	2800	yes
5A	Vertical	59.9	8.9	154	2.35	0.36	1.00	0.36	0.94	4100	yes
5B	Vertical	59.6	7.7	153	2.32	0.41	1.00	0.41	1.07	3500	yes
7A	Vertical	85.0	10.3	157	2.40	0.44	1.00	0.44	1.14	4800	yes
7B	Vertical	83.0	8.5	160	2.45	0.52	1.00	0.52	1.28	4050	yes
100A	45^o	63.9	7.1	155	2.36	0.48	1.00	0.48	1.25	3300	yes
100B	45^o	59.7	6.4		2.20	0.50	1.00	0.50	1.30	2750	yes
101A	45^o	85.0	8.5		2.54	0.53	1.00	0.53	1.38	4200	yes
101B	45^o	86.0	9.0		2.58	0.51	1.00	0.51	1.31	4500	yes
200A	Horizontal	78.0	7.1	159	2.42	0.59	1.00	0.59	1.53	3350	yes
200B	Horizontal	81.0	7.7	170	2.58	0.57	1.00	0.57	1.47	3900	yes
200C	Horizontal	84.0	7.4	172	2.60	0.61	1.00	0.61	1.56	3750	yes

Symbols defined in Nomenclature

TABLE H-6

TEST RESULTS

Air in 0.125" Annular Layer

Test No.	Position	Power Watts	Δt_m ^oF	t_m ^oF	$Z_m \times 10^{-2}$ $^oF^{-1}in^{-3}$	H_r* Watts	K_{CAL} Btu/^oF hr.ft.	Ke/K Btu/^oF hr.ft.	N_{RAY}	Motion
1	Vertical	35.8	111	185	2.9	4.3	0.154	0.86	90	no
2	Vertical	35.4	112	185	2.9	4.4	0.150	0.84	90	no
3	Horizontal	34.8	90	180	3.9	3.2	0.189	1.07	70	no
4	Horizontal	34.5	83	180	3.9	2.9	0.208	1.18	65	no
5	45^o	35.6	92	180	3.9	3.3	0.190	1.07	70	no
6	45^o	35.6	93	180	3.9	3.3	0.188	1.07	70	no

*H_r - Heat transferred by radiation

Other symbols defined in Nomenclature